ዘይሮ

የኢትዮጵያ መሐንዲሶችና አርኪቴክቶች መጽሔት

ISSN (Print): 0514-6216
ISSN (Online): 2731-2968

Indexed on
AJOL & EJOL

zede

Journal of Ethiopian Engineers and Architects

42 ሐምሌ ፳፻፲፮
July 2024

Annual Publication of the Addis Ababa Institute of Technology
Addis Ababa University

ዘዴ
የኢትዮጵያ መሐንዲሶችና አርኪቴክቶች መጽሔት

Zede
Journal of Ethiopian Engineers and Architects

የተቋቋመው ፲፱፻፶፫ Established 1963	ሐምሌ ፳፻፲፯ July2024	42	ፖ.ሣ.ቁ አዲስ አበባ P.O. Box 385 Addis Ababa

Publisher
Addis Ababa University
Addis Ababa Institute of Technology
P.O. Box 385
Addis Ababa
Ethiopia

Postal Address
Addis Ababa University, AAiT
P.O. Box 385
Addis Ababa
Ethiopia

Email: zede@aait.edu.et

CONTENTS **Page**

Website: http://www.aait.edu.et/zede-journal-engineers-architects

Guide to Authors

ZEDE is a scientific journal on engineering science and application, produced under the auspices of the Addis Ababa Institute of Technology, Addis Ababa University. The main objective of the journal is to publish research articles, findings and discussions on engineering sciences, technology and architecture thereby assisting in the dissemination of engineering knowledge and methodologies in solving engineering problems. Technical Notes of significant contribution may be considered for publication. Zede is an open access journal. It is published annually in both PRINT and ONLINE versions.

Original papers for publication in the journal should be submitted by email at zede@aait.edu.et or using the online submission system at **http://ejol.aau.edu.et/index.php/ZEDE/** in both pdf and MS word (2007 or later). All articles submitted for publication in the journal should comply with the following requirements:

1. Title of Paper: The title of the paper should be phrased to include only key words and must have a length of not exceeding *80* characters including spaces.

2. Format of Manuscript: The manuscript should be written with MS word 2007 or later using A4 size, double-spaced, single column with 25 mm margin on all sides.

3.Length of Article: The length of the article should not exceed word equivalent of 6000 words, or *20* pages, double spaced using font size *12* typed in Times New Roman.

4. Author's Affiliation: The author's full name and institutional affiliation and rank, must appear on the article.

5. Abstract: The abstract must not exceed 200 words. It should not contain any undefined abbreviations or unspecified references.

6. Keywords: All articles submitted must include Keywords not exceeding 6 in number.

7. Style of Writing: It is recommended that third person pronoun/s be used when referring to author/s.

8. Illustrations: Figures should be drawn in black, at a size with a *50%* reduction to fit in *160 mm* width of journal for the print version and in color for the online version. Explanations and descriptions must be placed in the text and not within figures. All figures must include numbered captions. See example:

Figure 1 Typical creep strain versus time curve

9. Tables: Tables must be numbered in the same order as cited in the text. Explanations of tables must appear in the text and all tables must include numbered captions. See example:

Table 1 Basic water supply system data

10. Equations: Equations numbers should be right-justified. See example:

$$u(x, y) = -y\theta(x) \qquad (1)$$

11. References: References in the body of the Article should be cited at the end of the paper by placing a reference number in square brackets and should be arranged sequentially as they appear in the text. Ethiopian names may be given in direct order, i.e. given name followed by father's name. All main words in titles (papers, books, reports) should be initialized by capital letters. Items in citations should be separated by commas. Page numbers should be included whenever applicable

.**Examples:**

1. ***References to Journal Articles and Proceedings***

   Spillers,W.R. and Lefeochilos, E., "*Geometric Optimization Using Simple Code Representation*", Journal of the Structural Division, ASCE, vol. 106, no. ST5, 1980, pp. 959-971.

2. ***References to Books and Reports***

   Korsch, H.L. and Jodl, H. –J., "*Chaos: A Program Collection for the PC*", Springer-Verlag, 1994.

***12. Units*:** *SI* units must be used.

13. Conclusions: A set of conclusions must be included at the end of the paper.

14. Submission of Paper: Any paper submitted for publication in ZEDE must not have been published previously, or submitted for publication elsewhere; and if accepted for publication by ZEDE, the author/s shall transfer the copy right to ZEDE.

Zede Journal of Ethiopian Engineers and Architects Editorial Policy

This policy describes guidelines in the publication process of Zede Journal.

Authorship

An author is an individual who has significantly contributed to the development of a manuscript. Zede recommends that authorship be based on the following four criteria:

Substantial contributions to the conception or design of the work; or the acquisition, analysis, or interpretation of data for the work; AND

Drafting the work or revising it critically for important intellectual content; AND

Final approval of the version to be published; AND

Agreement to be accountable for all aspects of the work in ensuring that questions related to the accuracy or integrity of any part of the work are appropriately investigated and resolved.

Changes in authorship

Whenever there is a need to make changes in the authorship of a manuscript or a published article, the changes will be implemented according **Zede** specification. Only corresponding authors can make request for a change in authorship. Request should be made to the Editor- in Chief.

Editor-in-chief

The editor-in-chief is the journal's editorial leader who has final responsibility for its operations and policies. He is the lead editor who acts as the chief executive officer of the Journal.

Associate Editor

The journal will have an associate editor assigned by the Institute based on qualification/experience. The associate editor supports the chief editor in terms of editing, identifying appropriate reviewers for submitted manuscripts.

Advisory Board

The Journal has an advisory board. The members are selected from Ethiopia and abroad. Members of the advisory board are expected to contribute to the quality, coverage, and publicity of the Journal nationally and internationally.

Acknowledgements

Individuals who participated in the development of a manuscript but do not qualify as an author should be acknowledged. Organizations that provided support in terms of funding and/or other resources should also be acknowledge.

Submission of Manuscript

Authors should read the "Authors Guideline" on the **Zede** journal's page before making a submission. Manuscripts should be prepared according to the style and specifications of the journal's policy. Authors listed on the manuscript should have met the requirements for authorship specified above. Where possible, contributions of each author may be specified at the end of the paper. All authors should approve the final version of the manuscript prior to submission. Once a manuscript is submitted, it is therefore assumed that all authors have read and given their approval for the submission of the manuscript. Contact information of all authors should be stated on the manuscript.

Conflict of Interest

Authors should disclose financial or any other interest that may have influenced the development of the manuscript. Reviewers should disclose any conflict of interest and if necessary decline the review of any manuscript they perceive to have a conflict of interest.

Confidentiality

A submitted manuscript is a confidential material and will not be disclosed to anyone except to individuals who partake in the processing and preparation of the manuscript for publication (if accepted).

Correction and retraction of articles

Corrections may be made to a published article with the authorization of the Editor-in-Chief of the journal.

Submission of Paper

Any paper submitted for publication in ZEDE must not have been published previously, or submitted for publication elsewhere; and if accepted for publication by ZEDE, the author/s shall transfer the copyright to ZEDE.
Manuscript submissions should be made using the online submission platform at **http://ejol.aau.edu.et/index.php/ZEDE/** or by Email at: **zede@aait.edu.et.**

Advisory Board Members

Evaluation of Public Bus Stops Location and Spacing: The Case of Selected Routes of *Anbessa* City Bus Service Enterprise

Getachew Bahiru[1,*], Bikila Teklu[1], and Tamru Tilahun[1]

[1]School of Civil and Environmental Engineering, Addis Ababa Institute of Technology, Addis Ababa University, Addis Ababa
**Corresponding author's E-mail address: getachewbahiru12@gmail.com*

DOI: https://doi.org/10.20372/zede.v42i.10178

ABSTRACT

Currently, the primary challenges in Addis Ababa include traffic accidents, comfort issues, travel delays, and productivity problems for travelers. To address these issues, it is recommended to enhance public services by incorporating suitable geometric features, particularly for bus stops. This study focused on evaluating existing bus stop locations and spacing and put remedial measure for any existing drawbacks on public transport Road networks particular on Anbessa City Bus Service Enterprise (ACBSE) routes. Observation, field measurement, GPS method tracking location of bus stops and GIS method produced point mapping were the methodologies used for the study. Travel speed, bus stop location, its configuration and service coverage radius data were acquired. The maximum travel speed that was determined during the study period was 26km/hr. Based on the analysis result, 29% of Mid-Block pullout bus stops should be changed to mid-block curb-side and mid-block bus bulb bus stops on-street having vehicle parking. Generally, 8% of bus stop locations needs future modification. From the research finding, the final bus stops location and spacing depend on the combined effect of location with respect to the nearest intersection, travel speed, service coverage radius, topographical limitation, safety issues and passenger loading of the surrounding area.

Keywords: *Anbessa* City Bus Service Enterprise Bus stop location; Bus Stop Optimization; Passenger loading; Public Bus Transport Routes; Spacing.

1 . INTRODUCTION

Transportation infrastructure, as a complex network, connects cities and accommodates human activities coupling the social, economic and environmental systems with the urbanization and population growth. Additionally, the transportation network contributes to the socioeconomic development and the increased quality of life through generating inter- or intra-city connections [1].

Due to the economic growth of the community, the number of car ownerships increase through time which results in increasing of fuel consumption, traffic accident, congestion and reduction of the mobility of the city. Mass transport facilities are efficient ways to address these problems with less cost in the developed world.

It serves the public at a cheaper operating cost, with less amount of fuel, safe and environmentally friendly as compared to the private cars, small and collective taxicabs [2, 3].

A bus stop is the first point of contact between the passenger and the bus service which define as a designated place where buses stop for passengers to get on or off from bus. According to Bachoket et al. [4] bus stop is defined as a linear curbside area that is specially designated for buses stopping to board and alight passengers. It is usually implemented on the right side of urban streets. Buses usually travel in the

curbside traffic lane and make frequent stops to pick up and drop off passengers. Therefore, it is important to keep these areas clear of potential obstructions [5, 6]. To tackle the huge transportation demand and to provide a sustainable environment, there is a need for the provision of better public transportation facilities. To fulfill the high demand for better public transport system, there is a need to establish attractive, safe and highly sophisticated public transport systems. In this regard, it is essential to conduct a detailed evaluation of public transport modes [7].

Providing and improving urban public transport service is becoming highly important to meet the demand of rapidly growing mass mobility due to high population growth. However, Transportation system has gained very fast growth in recent decades; still now we cannot address the accident, congestion and mobility problems in the capital city of Addis Ababa.

Even though, there are small number of public transport services which cannot accommodate the current demand, there is no standard and consistent bus stops and terminals on the given road networks. In addition to that the total travel time and at what time the bus reach at the bus stop (cycle time) are not briefly explained.

Limited research has been conducted on the performance evaluation of public transportation in Addis Ababa, focusing on the quality of service using efficiency measures, special analysis, and improvement strategies. Recent studies, such as the research by Demelash Abate [8] in 2007, analyzed the efficiency of *Anbessa* city bus transport service and identified deficiencies in the bus route network to ensure equitable service for all societal groups in Addis Ababa, Ethiopia. Another study by Muktar Husein in June 2021 evaluated the performance of *Anbessa* City Bus on the Bethel to *Merkato* route based on quality of service. Additionally, studies like the one by Mesfin Tsegaye [9] in 2018 have proposed modes for evaluating the quality of service in public bus transportation and improvement strategies in Addis Ababa, specifically focusing on *Sheger* Mass Transport Enterprise, considering factors such as Level of Service (LOS) and passenger loading parameters.

However, as previously mentioned, there is a significant lack of research focusing on the impact of efficient public bus stop location and spacing on the quality of public transport, specifically analyzing the performance of public transport in terms of public bus transport quality.

Furthermore, these studies have not explored the correlation between public bus quality and the location of public bus stops, nor have they examined the combined effect of these factors on evaluating public bus transport performance. Additionally, these studies have not addressed the influence of public bus stop location and spacing quality in alignment with the demand for public buses and international design guidelines. Therefore, the primary objective of this study was to consider the impact of public bus stop location and spacing on public bus transport quality.

The aim of this paper is to describe, characterize and evaluate the existing bus stop locations, spacing and put an engineering remedial measure for the defects according to the international design guideline by taking into account the local context. The study is based on the following initial assumption:

Anbessa public bus transport network of Addis Ababa offers a territorial coverage which differs between the various areas of the city. This implies improper lay out and unequal conditions of accessibility to public

transport services for different surrounding areas.

Improper location and spacing of public bus stops have versatile impact on performance of public bus transport. This situation alters the efficiency and spatial coverage of the public transport network.

To supplement the study questions of a desk study and address the study objective three ACBSE operational routes that have representative characteristic were selected. Travel speed, bus stop location with respect to the intersection, bus stop configuration and service coverage radius data were acquired.

2 MATERIALS AND METHODS

In order to obtain the applicable data both primary and secondary sources were used to address the specific details under the study. The primary data were obtained through Observation, field measurement, GPS method of tracking and identifying co-ordinate of bus stop locations. Secondary data were obtained from published and unpublished documents, different relevant research papers, books, journals, internet sources and archival documents such as design guide- line of bus stop location, reports, and principles of locating, placing and spacing of bus stops [10]. These were collected from different organization such as: ACBSE, Addis Ababa city Road Authority (ACRA) [11], different literatures, and relevant documents collected from different websites. Observation, field measurements, GPS method tracking location of bus stops and GIS method produced point mapping were the methodology used for the study.

2.1 Type and Data Sources

Quantitative and Qualitative data were collected from primary and secondary sources.

The data collection mechanism of primary data was Observation, Felid measurement, GPS method of tracking identifying co-ordinate of bus stop locations. Sufficient information was acquired and achieved through the subject routes by observations, field measurement and GPS tracking methods and identifying the coordinates of bus stops (Figure 1).

During site observation, there were chances to communicate with passengers and staff members on prevailing service provisions and operational problems of *Anbessa* city bus routes related with bus stop locations and spacing. Data acquired by site observations were bus stop locations with respect to the nearest intersections (near-side, far-side and mid-block), bus stop configuration (curb-side, turnout, bus bulb, on-street transfer center and shared cycle), direction of travel of buses (on street travel, Right or left turn at the intersection), conveniences of bus stop placement upstream or downstream of the intersection [12, 13].

Data acquired by field measurements were bus stop distance from nearest intersection, pedestrian crosswalk and parking area, dimension of deceleration and acceleration zone, travel distance and travel time. In relation to this, the data recorded and measured should be taken in consideration the type of bus stop locations and its configuration. Travel distance between terminal points of bus routes, travel time, distance between two consecutive bus stop and coordinate of bus stops locations (x, y, z) data were recorded from GPS navigation system. In parallel with this, along the GPS survey Passenger loading (number of passenger boarding and alighting) data count were conducted through administered routes at each bus stop points.

Figure 1 Routes Selected for the study[11]

i. On-board survey

During the on-board survey for the purpose of observing the bus route, enumerators identified the name and the distance between bus stops or other points of bus stops.

Since *Anbessa* city buses have one door for passengers to embark and disembark, therefore only one enumerator is required to be located at the front door of the bus to record the number of passengers' boarding or alighting at or between bus stops, excluding him/herself as a passenger. Another enumerator was assigned to read and record the GPS co-ordinate of passengers' access and egress points. The enumerator traveled in different buses in the morning and the afternoon at peak hours in both directions of flow. Travel time and travel distance were recorded using the GPS apparatus that was harmonized with the mobile satellite. Three bus routes were navigated with GPS on both directions of travel. Track points were recorded and the bus stops were marked as way points.

ii. Plotting of GPS points using GIS

The main purpose of the GPS survey was to identify co-ordinates of bus-stops locations, travel distance and travel time. The GPS data were then converted into shape files as way points and tracks whereas GIS software was used to make a point map for the spatial analysis.

iii. Bus stop locations and configurations

The types of bus stop locations in relation to the intersections were Near-side (upstream) of the intersection, Far-side (downstream) of the intersection and Mid-block (midway between intersections) [14, 15]. These locations were evaluated and selected based on site observation of facilities on segment, passenger volume of the surrounding area, traffic volume at the upstream and downstream of the intersection and direction of the travel bus (Figure 2).

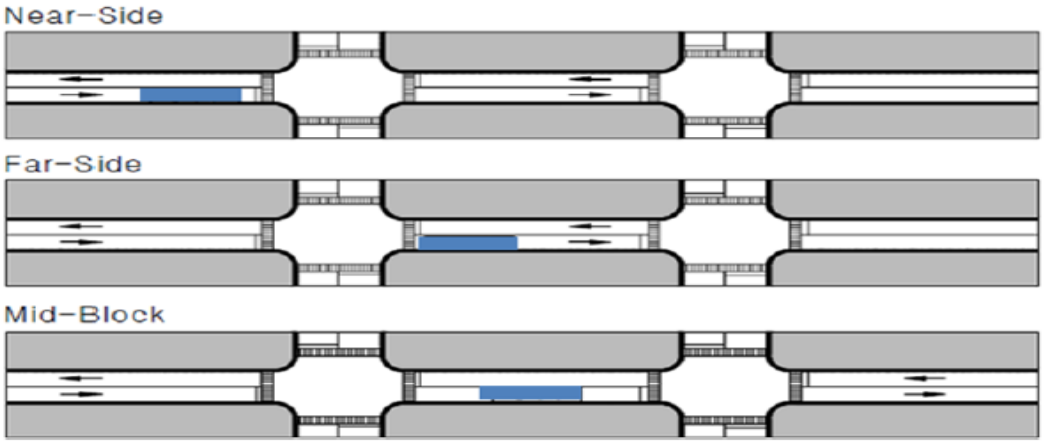

Figure 2 Bus stops location with respect to intersection [15]

According to SEPTA Bus Stop Design Guideline [16], the preferred configuration is based on the local site condition and the bus network conditions. There are six bus stop configurations (curb-side, pullout, bus bulb, shared cycle track stop, Boarding Island, on-street transfer center), each characterized and selected based on the travel speed and the existence of on-street vehicle parking. These bus stops are either inline or off-line with respect to the traffic lane.

Figure 3 Bus stops configuration [16]

iv. Service Coverage at Stop Level

The general process described below for calculating service coverage at a system level can also be used to calculate coverage at an individual stop level. The objective of this level of analysis was to identify how much of the area within theoretical walking distance of the stop could actually access the stop. According to Transit Capacity Quality Service Manual [17], the optimized bus stop location can be determined using equation (1) at each stop ends up with an individual service radius;

$$r = ro * fsc * fpop * fpx \quad (1)$$

where:

r= transit stop service radius (mi, m)
ro= ideal transit stop service radius (mi, m), 0.25 mi (400 m) for bus stops. When accurate bus stop location data are not available,
f_{sc}= street connectivity factor, When GIS software is used path-tracing functionality, fsc = 1.0
f_g= grade factor;
f_{pop}= population factor
f_{px}= pedestrian crossing factor

Table 1 Corresponding grade factor for average grade

Average grade	Grade Factor, fg
0-5%	1
6-8%	0.95
9-12%	0.8
12-15%	0.65

This factor assumes that pedestrians will have to walk uphill either coming or going. If the transit route network provides service on parallel streets, such that a person could walk downhill to one route on an outbound trip and downhill from another route back to

one's origin on the return trip, use a grade factor of 1.00 is used.

$$fpx = \sqrt{\frac{-0.0005(dec)^2 - 0.1157dec + 100}{100}} \quad (2)$$

where:

f_{px} = pedestrian crossing factor, and

d_{ec} = pedestrian crossing delay exceeding 30 s (s).

The factor is 1.00 whenever pedestrian crossing delay on the street with transit service is less than or equal to 30 s. When d_{ec} exceeds 345 s, fpx should be automatically set to 0.0 which describes from the curves below [17].

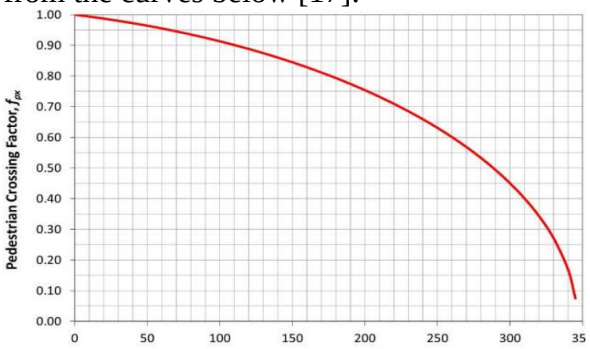

Figure 4 Pedestrian crossing delay Vs. Pedestrian crossing factor

At signalized pedestrian crossings, average crossing delay is based on the cycle length and the amount of time available for pedestrians to begin crossing the street (Eq. (3)).

$$dp = \frac{(\mathbf{c} - \text{gwalk})^{\mathbf{2}}}{\mathbf{2c}} \quad (3)$$

where:

d_p = average pedestrian delay (s),

C = traffic signal cycle length (s) = and

G_{walk} = effective green time for pedestrians (WALK time+ 4 s of flashing DON'T WALK) (s).

For transit stops where 20 % more of the boarding volume consists of elderly pedestrians (65 years or older), a population factor, F_{pop}= 0.85.

2.2 Method of analysis

The research methodology applied has intended to answer the research questions and objectives. The research was designed to address evaluation of the existing urban public bus stops location and spacing as per the specified standard. Observation, field measurement and Global Positioning system are the methods used to collect the impute data of the study. The collected GPS co-ordinates were tracked at GIS software to make a point map of bus stops. Finally, the existing bus stop location and spacing parameters such as distance from origin/destination to the bus stops, bus stop location with respect to the nearest intersection, parking area, pedestrian cross walk and bus stop configuration, accessibility, safety and appropriateness of passengers boarding and alighting points, average travel speed and its geometric lay out were analyzed and an engineering remedial measure were outline for any exiting problems.

2.2.1 Assessment of bus stop location with respect the intersection

Bus stop locations with respect to the intersection were assessed by comparing the traffic volume of the road in relation to the downstream, upstream and at the mid of the intersection area, facility on the road segment and direction of travel bus at the intersection such as left turn, right turn and on – street direction, This method is simply understood by field observation which bus stop location has less traffic interruption for placing bus stop on the near-side, far-side and mid-block with respect to the intersection.

Based on SEPTA Bus Stop Design Guideline, far-side bus stop is recommended when Primary trip generator is upstream from the intersection, existing pedestrian facility greater than the near-side, Vehicular

traffic is heaver on the near-side and when the route requires left turn.

Near-side bus stop location is efficient alternative when Primary trip generator is downstream of the intersection, existing pedestrian facility greater than the far-side, vehicular traffic is heaver on the far- side and the route requires right turn.

Mid-block bus stop is mostly recommended when major trip generator is at the mid-block and existing pedestrian facility is safe at the mid-block than the far-side and the near-side of the intersection.

2.2.2 Assessment of bus stop configuration

The major parameters for evaluation of the existing bus stop configuration (curb-side, pullout, bus bulb, shared cycle track stop, boarding island, on-street transfer center) are travel speed and existence of on-street vehicle parking. As stated on highway capacity Manuel the travel speed for the facility is the ratio of facility length to facility travel time [18] as shown by equation (4).

$$VT = \frac{DT}{tT} \quad (4)$$

where:

V_T=facility travel speed,

D_T = facility travel length and

t_T= facility travel time

In-line bus stop is the best option of bus stop configuration for streets that are at or near vehicle capacity, with long traffic signals and having no vehicle parking [18]. Pullout bus stop is the second option for streets with vehicle parking next to bus bulb and on-street when travel speed exceeds 70 km/hr. Bus bulb is most effective for streets that have vehicle parking, moderate traffic volume and for travel speeds lower than 48 km/hr [18]. On-street transfer center is designed to better organize bus stops on busy downtown areas and congested areas with many bus routes serving the same street.

After determining and evaluating travel speed of specified road segment, the right type of bus stop configuration was recommended by incorporating existence of on-street vehicle parking as one evaluation criterion.

2.2.3 Bus stop location with respect to parking area and pedestrian crosswalk

As recommended by SEPTA Bus Stop Design Guideline, the minimum required distance between the bus stop and the pedestrian cross walk is 3 m and its distance with respect to the parking area depends on the type of bus stop configuration (Table 2).

Table 2 Bus stop location from parking area

Bus Stop configuration	Bus stop location	Distance from vehicle parking (m)
Pull out	Far-side pull out	7
	Near-side pull out	15
	Mid- block pullout	15
In-line	Far-side in-line	Vehicle parking is not allowed
	Near-side pull out	
	Mid- block pullout	
Boarding bulb stop	Far-side Boarding bulb	No need additional spacing; the bulb by itself is enough
	Near-side Boarding bulb	
	Mid- block Boarding bulb	7

2.2.4 Determination of passenger loading

During the on- board surveys, the bus route enumerators have identified the name and the distance between bus stops. The main purpose of the GPS survey was to identify coordinates of bus stops location, recorded travel distance and travel time. The GPS data were then converted into shape files as

way tracks points. The sum of passengers' boarding or alighting at each bus stop was taken as passenger loading.

GIS software was used to make a point map of bus stops for spatial analysis to apply bus stop modification such as keep on the existing situation, required additional infrastructure for the passengers such as shelter and seat bench, adding bus stops, relocation bus stop, increase the trip rate removing or used as it is based on time peak hour volume of the day.

3 RESULTS AND DISCUSSION

3.1 Location of bus stop with respect to the intersection

Out of the three representative selected routes, 52 bus stops were taken for the evaluation from which 13 (25 %) were near-side, 20 (38 %) far-side and the remaining 19 (37 %) were mid-block bus stops.

From these bus stops, BS3 on *Legehar to Jemo 3* and BS4 on *Megenagna to Piasa* road segment near-side bus stops are located on high traffic volume at the downstream direction, the travel buses make left turn at the intersection, high passenger's volume at the upstream direction. Due to this, it is more appropriate to change to Far-side bus stop location. On *Gurara to Merkato* a road segment, BS10 (on St. Georgas) mid- block bus stop has no minimum required space to accommodate the arriving public bus and has heavier vehicular traffic at the mid-block. Hence, it is preferable if it changes to near-side bus stops since near-side has enough facility to install the bus stop and less vehicular traffic.

Totally, 8% of the bus stops throughout the selected routes need further modification on their location. Traffic marking of the bus stops, distance from parking area and pedestrian crosswalk were continued as a general problem throughout the road segments.

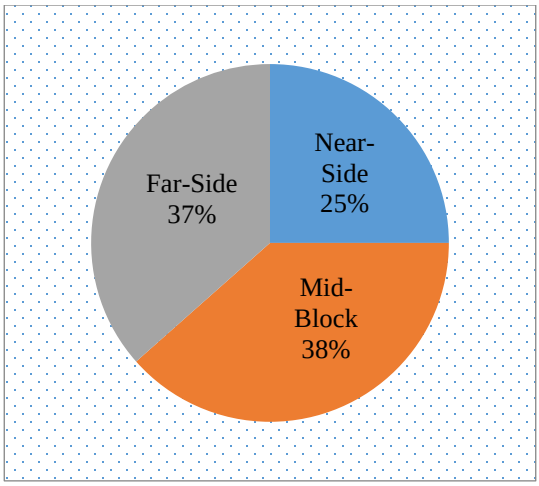

Figure 5 Bus stops location with respect to the intersection

3.2 Bus stops configuration

As stated above the major parameters for evaluation of the existing bus stop configurations were travel speed and existence of on-street vehicle parking. The determined value of travel speed on *Legehar-Jemo3*, *Gurara-Merkato* and *Megenagna-Piasa* road segments were 10.64 km/hr-20 km/hr., 13km/hr-26km/hr. and 12km/hr-16km/hr. respectively. The maximum travel speed that was determined during study period was 26 km/hr. on *Gurara-Merkato* road segment.

Based on the analysis result, 29 % of Mid-Block pullout bus stops should be changed to mid-block curb-side bus stops and mid-block bus bulb bus stops on-street that has vehicle parking.

Table 3 Bus stop configuration on three routes

Bus Stop Configuration	Number of Bus stop	Percent (%)
Pull-out/Turnout	15	29
Crub-side	29	56
Bus-Bulb	0	0
Boarding Island	0	0
Shared Cycle	0	0
On-street Transfer	8	15
Sum	**52**	100

3.3 Passenger Loading

Passenger loading data were recorded by local time. Based on the analysis result of passenger loading, relatively the total number of passengers loading at the intermediate bus stops was low as compared to the starting and ending point bus stops.

At the starting and ending point bus stops on both direction of travelling, passenger

loading was high which needs provision of special infrastructure that accommodates waiting passengers such as seating bench, shelter, minimum optimized distance, safe from climate change impact, and security issue.

Passengers at the intermediate bus stops did not get on time service as the bus grasped to its capacity at the starting point. To counter balance this effect providing enough bus frequency is the best option.

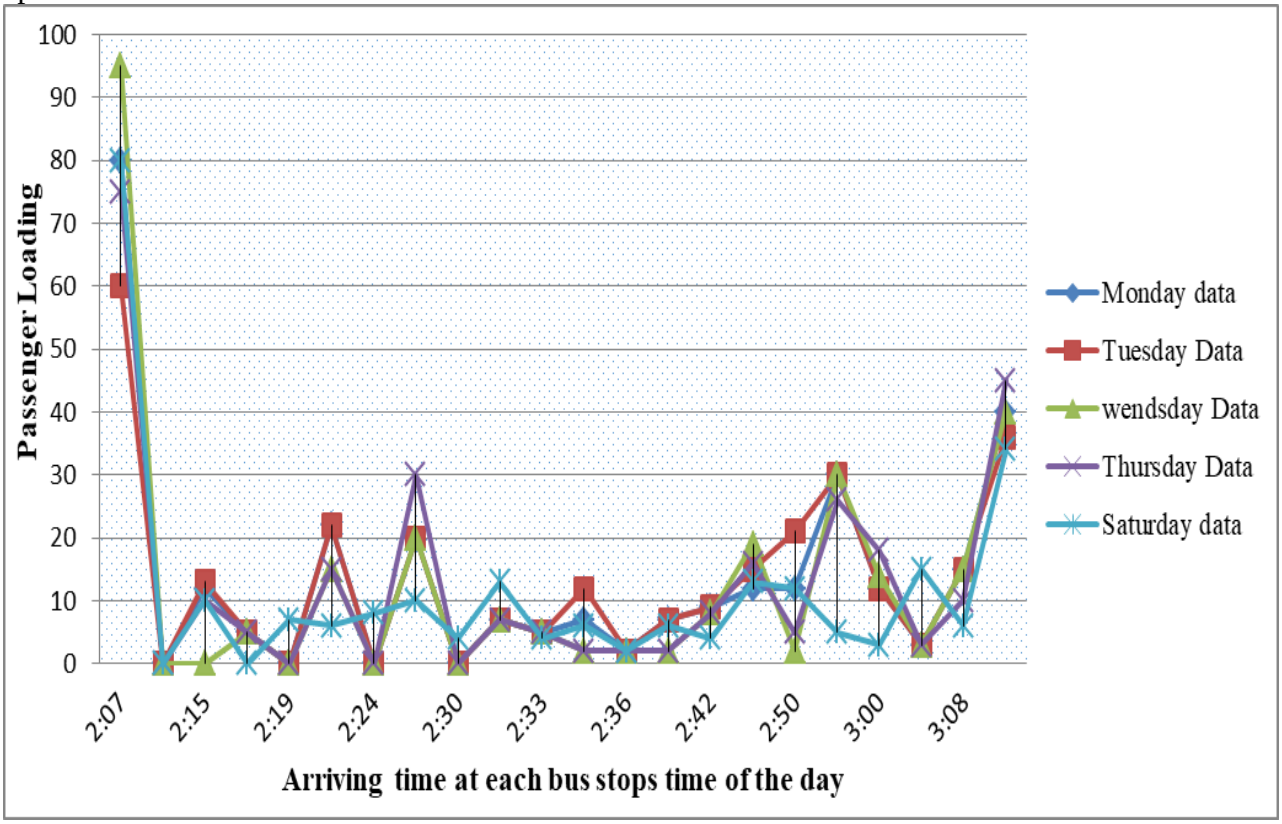

Figure 6 Passenger loading at bus stops morning peak hour from *Jemo* 3 to *Legehar*

According to the field observation during data collection and the passengers loading analysis result, most of the residential areas are located at the periphery and large institutions and economic activities are found in the central parts of the city.

Hence, special attention and remedial measure should be given by government officials to counter balance the passengers demand and location of institutions and economic activity zones.

3.4 Bus stop optimization

As per the analysis result from the data obtained from hand GPS recorded, some bus stops have large spacing that may be due initial consideration of parameters for bus stop spacing or due to topographical limitation and security issues. The minimum

and maximum bus stop spacing were 200m and 1300 m at *Jemo-Legehar* and *Megenagna- Piasa* bus routes, respectively.

Based on the analysis result, the final optimized bus stops spacing is between the interval of (170 m-1 km), which shows that the minimum and the maximum service radius are 170m and 1km respectively. Transit Capacity Quality Service Manual acquired that in order to maintain operating speed; bus stops, normally, should not be placed closer than 200 m apart. Hence, the result is more preferable which guided by Transit Capacity Quality Service Manual.

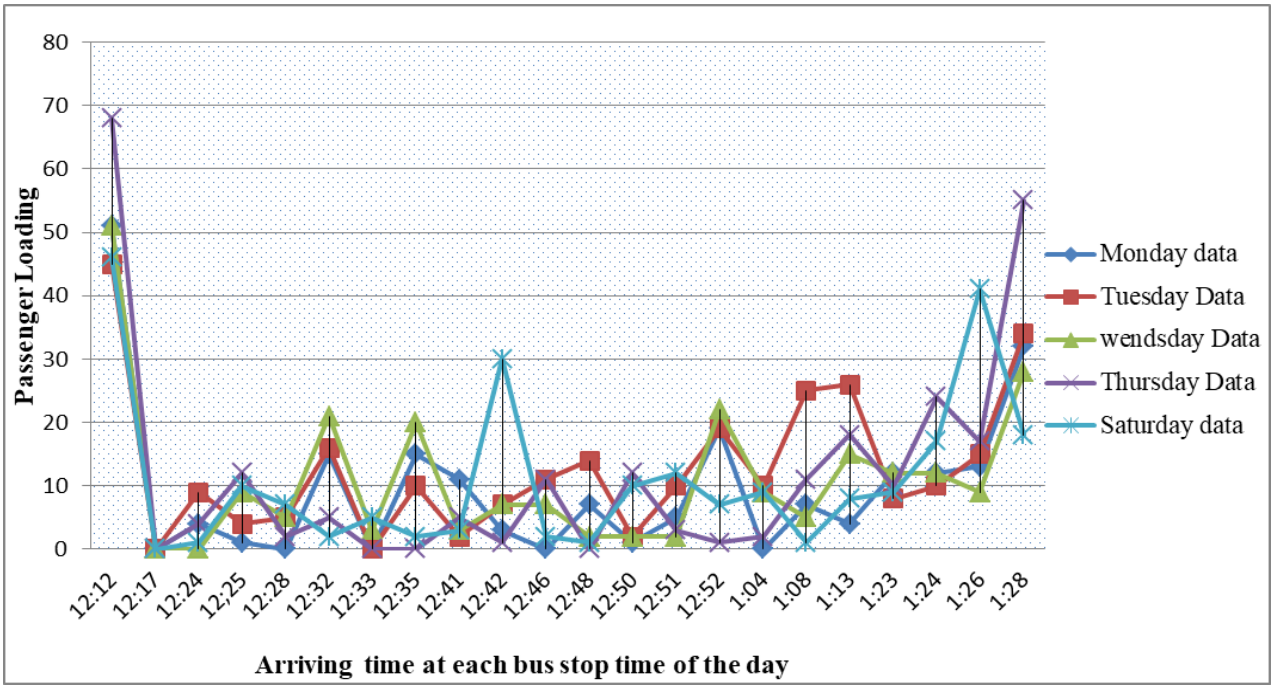

Figure 7 Passenger loading at afternoon peak hour from *Legehar* to *Jemo* 3

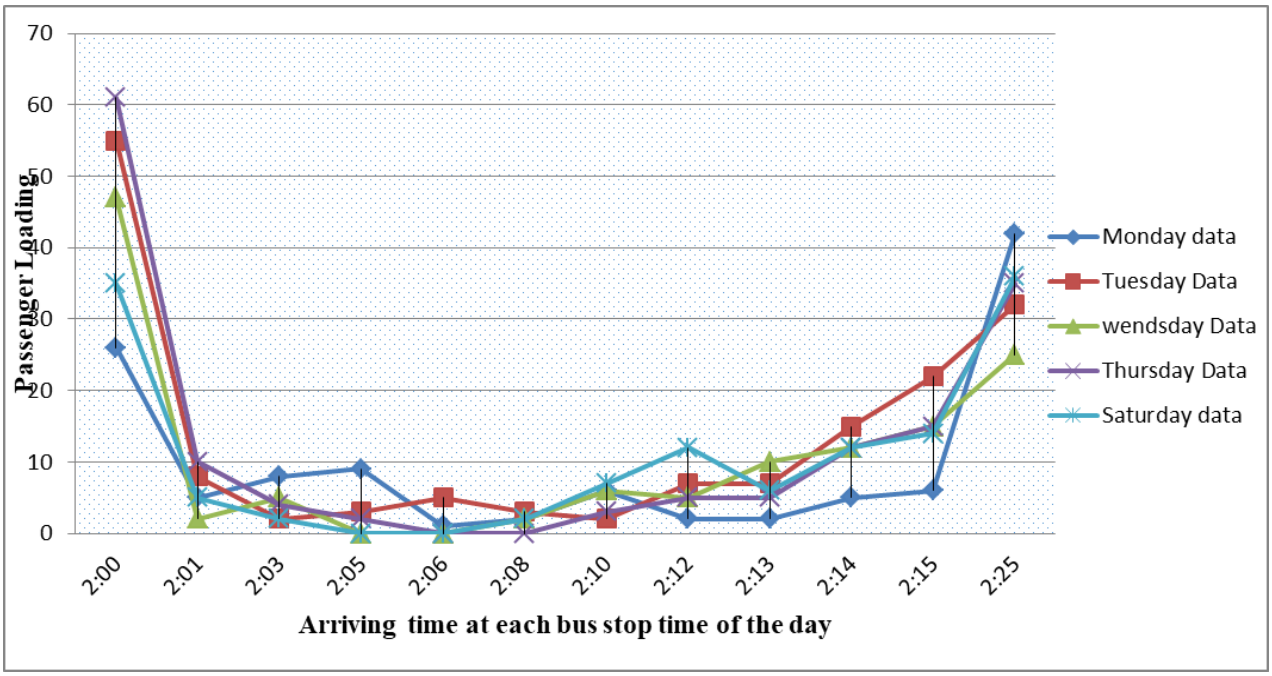

Figure 8 Passenger loading at bus stops at morning peak hour *Megenagna* to *Piasa*

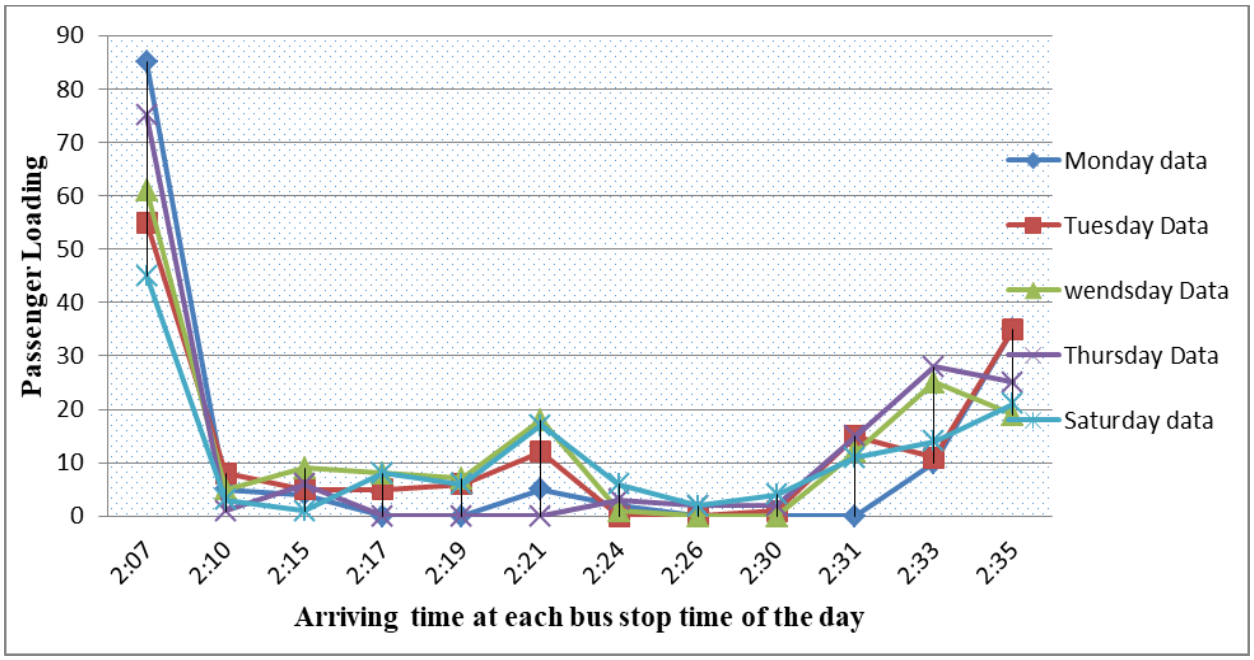

Figure 9 Passenger loading Gurara- Merkato road segment at the morning peak hour

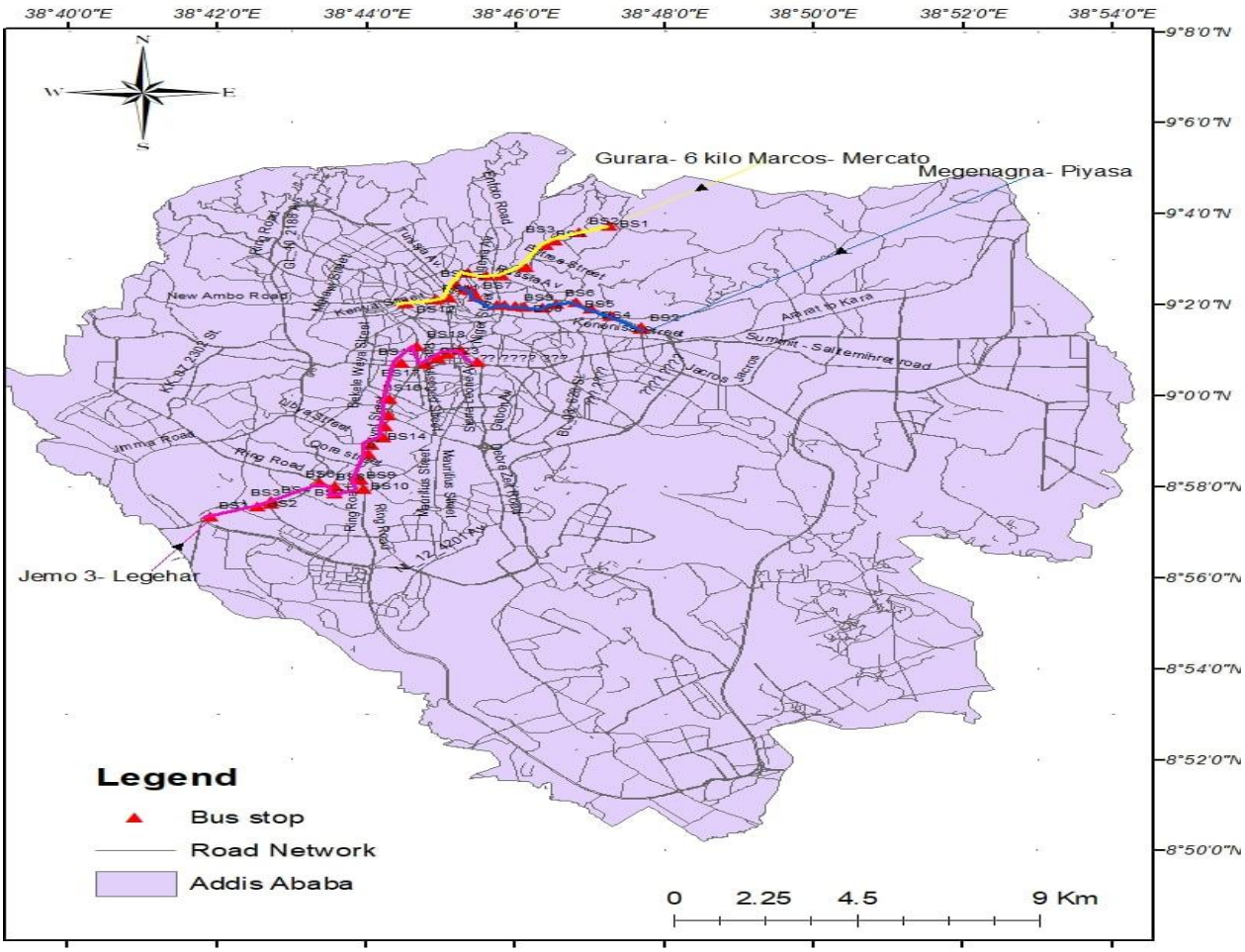

Figure 10 Existing bus stops location on the three routes

4. CONCLUSIONS

The study has evaluated ACBSE bus stop location and spacing using Passenger loading, configuration, service radius and existing bus stop location evaluation parameters. From the findings of the study, it can be concluded that both bus stop location and spacing of ACBSE, as compared to the standard, are relatively low in some of the evaluation parameters. In case of bus stop configuration, though the overall average exhibits very low, 29% of Mid-Block pullout bus stops should be changed to mid-block curb-side bus stops and mid-block bus bulb bus stops on-street that has vehicle parking which shows the existing bus stop configuration needs further improvement.

Based on the result of bus stop location with respect to the intersection evaluation, 8% of the bus stops throughout the selected routes need further modification on their location. Traffic marking of the bus stops, distance from parking area and pedestrian crosswalk were general problems throughout the road segments.

From the study finding, bus stops location and spacing depend on the combined effect of their distance with respect to the nearest intersection and bus stop, their configuration, direction and speed of travel bus, traffic volume and passenger loading of the surrounding area, appropriateness of the area for locating bus stops, service radius, topographical and security issue of the road segments.

CONFLICT OF INTEREST

The authors declare that they have no conflict of interest.

ACKNOWLEDGEMENTS

The authors are grateful to Addis Ababa Institute of Technology (AAiT) and *Anbessa* City Bus Service Enterprise (ACBSE) for their fruitful support and open-handed all the necessary data that related with my research work.

REFERENCES

[1]. Jian, Z., Zhibin, L. and Fangwei, Z. *"Evaluating the impact of bus stop design and bus dwelling on operation of multiple Road users",* Journal of Advanced Transportation, vol. 2018, 2018, pp. 1-10, doi.org/10.1155/2018/4702517.

[2]. Jean-Paul R., Claude C. and Brian S., "*The Geography of Transport Systems*", UK, 2016, pp. 13-15, doi.org/10.4324/9781315618159

[3]. Xiaodong, L., Yao, Y., Meng, M. and Andreas, R., "*Impact of different bus stop designs on bus operating time components*", Journal of Public Transport, vol. 20, no.1, 2017, pp. 104-118, doi.org/10.5038/2375 0901.20.1.6

[4]. Syahriah, B., Zakiah, P., Mariana, M. and Zulfadly, A., "*GPS/GIS identification of potential bus stop location and passengers assess for egress points*", Kulliyah of Architecture and Environmental Design, International Islamic University Malaysia, Nagoya, Japan, 2013, pp. 409-474.

[5]. Sruthi, S. and Arpan, M. "*Capacity drop at the bus stop on multilane divided urban roads under mixed traffic conditions*", vol. 48, 2024, pp. 14-26, doi.org/10.1016/j.iatssr.2023.12.005

[6]. Delaware Valley Regional Planning Commision (DVRPC), "*SEPTA Bus Stop Design Guideline*", 2019, pp. 1-55.

[7]. Dilrukshi, H. "*Factors Affecting Service Quality in Public Bus Transportation*", Proceedings of 8th International Research Conference, Srilanka, 2015, pp. 103-109.

[8]. Demelash Abate, "*Analyzing Public Transport Performance Using Efficiency Measures and Spatial Analysis The case of Addis Ababa, Ethiopia*", International Institute for Geo-information Science and

Earth Observation, Netherland, 2007, pp. 1-95.

[9]. Mesfin Tagagne, "*Evaluating Quality of Service on Public Bus Transportation and Improvement*", M. Sc. Thesis, Addis Ababa Institute of Technology, 2018, pp. 1-131.

[10]. Luigi, D., Angel, I. and Patricia, C., "*The quality of service desired by public transport users*", vol. 18, 2011, pp. 217-227.

[11]. Addis Ababa City Road Authority AACRA, "*Draft Route Rationalization Report*", Addis Ababa, vol. 4, 2020, pp.1-159.

[12]. Agarwal P. and Singh A., "*Performance Improvement Urban Bus System"*, International Journal of Engineering Science and Technology, vol. 2, No. 9, 2010, pp. 4759-4766.

[13]. Kelbesa, K., Susan, K. and Delwar, A., "*Accessibility of anbessa city bus service in Addis Ababa*", Australasian Journal of Regional Studies, vol. 23, no. 1, 2017, pp. 48-67.

[14]. Maryland Department of Transportation (MDOT), "*Bus Stop Design Guideline*", 2019, pp. 1-122.

[15]. Riverside Transit Agency (RTA), "*Bus Stop Guideline*", 2015, pp. 1-52.

[16]. Delaware Valley Regional Planning Commission (DVRPC), "*SEPTA Bus Stop Design Guideline*," Pennsylvania and New Jersey: SEPTA, 2012, pp. 1-54.

[17]. Transportation Research Board of National Academies, "*Transit Capacity Quality Service Manual (TCRC)*", third Edition, Washington, D.C, 2013, pp. 299-434.

[18]. Transport Research Board, "*Highway Capacity Manual*," Washington DC, 2010.

Reliability-Based Numerical Modeling for Investigation of the Impact of Printing Parameters on Buildability of 3D Printed Concrete Structures

Meron Mengesha[1, 3,*], Abrham Gebre[3], Albrecht Schmidt[2], Luise Göbel [2],TomLahmer[1,2]

[1]*Bauhaus-Universität Weimar, Germany, Institute of Structural Mechanics*
[2]*Materials Research and Testing Institute (MFPA) at Bauhaus-Universität Weimar, Germany*
[3] *School of Civil and Environmental Engineering Addis Ababa Institute of Technology, Addis Ababa University, Addis Ababa, Ethiopia*
⁎*Corresponding author's E-mail address: meron.wondafrash@gmail.com*

DOI: https://doi.org/10.20372/zede.v42i.10179

ABSTRACT

The significance of 3D concrete printing (3DCP) as an additive manufacturing technology has increased over the past few years. Both academic research studies and large-scale industrial realizations of 3DCP have shown that it represents a viable alternative to traditional concrete mold casting. The key reason for this rapid development is that urgent challenges of the construction sector, in particular sustainability and productivity, are addressed. However, previous studies on technological progress have mainly been experimentally driven. The introduction of appropriate numerical modeling techniques would, therefore, further foster the success of 3DCP by providing insight into the structural behavior, which is beyond experimental possibilities. The present study introduces a numerical modeling technique for the analysis of 3DCP wall structures using a time-dependent reliability analysis. Uncertainties occurring throughout the printing process and time-dependent properties of printable concrete are considered. In addition, sensitivity analysis of random variables is done, which could be used as indicative preference for future process optimizations. The results yield valuable insight into the influence of printing process parameters on the failure of 3D printed concrete structures. The numerical model predicts build ability of a 3D printed concrete wall structure as it is in very good agreement with experimental results of similar studies.

Keywords: Buildability; 3D-Concrete printing; Numerical modeling; Random variables; Sensitivity analysis; Time-dependent reliability.

1. INTRODUCTION

Additive manufacturing refers to a procedure in which a product is created in layers using a computer-controlled positioning process based on a digital 3D model. Additive manufacturing and digital fabrication open up new possibilities in the production of concrete structures [1]. In contrast to traditional subtractive or forming production methods, additive manufacturing techniques allow for a design-driven manufacturing process, enabling the construction of structures with a high degree of complexity, design freedom, and functionality.

Among the different additive manufacturing technologies for concrete, extrusion-based techniques are supposed to be the most popular ones with a stringent entry into everyday construction processes [2-4] which offer material and labor savings, increased production speed, and complex geometries [1, 5-7].

The reduced construction waste because of the accurately controlled manufacturing process of 3D printing and optimized material consumption may be estimated at 30 to 60 % [8]. The ability to construct concrete structures without the need for formwork has a significant economic and productivity benefit; as indicated by Perrot

et al., formwork accounts for 35 to 60% of the total material costs in the construction industry [1].

Several challenges have been recognized that hamper the extension of 3DCP to a larger number of structural applications and to open its full potential with a load-bearing capacity. Fresh concrete undergoes time-dependent chemical reactions and rapid phase changes during the extrusion-based printing process. The material must be fluid in the first stage to be easily pumped towards the printing unit [3]. It is also commonly understood that the bonding strength of two consecutive layers reduces as the time gap between them increases [9].

Besides, variations in the properties of the raw materials, printing parameters, such as printing velocity, nozzle size, nozzle height from the printing platform, layer interval time, layer thickness, temperature and concrete mixture have a substantial effect on the overall performance of 3DCP [10-13]. Disturbances during printing may lead to inconsistencies and impair the quality of the product [14]. So-called cold joints should be avoided [15-17] by the appropriate setting of the printing process parameters. Insufficient strength, or stability may cause the 3DCP wall structure to fail during the process of printing, either by plastic yielding of the concrete (a strength mechanism) or due to elastic buckling of the printed height (a stability mechanism).

Several numerical modeling strategies to either simulate the extrusion process or estimate the printability of concrete objects have been developed. A first, finite element (FE) analysis of a 3D printed concrete shell construction was performed by Feng et al. [18]. Wolfs et al. [19] proposed a FE approach for a 3D printed concrete structure. A time-dependent Mohr-Coulomb failure criterion and a linear stress-strain behavior up to failure were used to investigate the failure mechanism of the structure. Elastic buckling and plastic collapse were the two failure mechanisms investigated, as well as three different wall layouts (i.e., boundary conditions). As a result, the wall that was simply supported showed global buckling, but the wall that is entirely clamped exhibits local buckling.

Comminal et al. [20] provided a computational fluid dynamics (CFD) model of 3DCP. The cross-sectional shape of 3D printed segments was predicted using numerical simulation. For a single layer printed on a planar build surface, the CFD approach can reliably model material extrusion and deposition.

The previously developed approaches for numerical models of the printing process have in common that they are deterministic in their nature. However, there are inherent uncertainties in the models' input parameters, mainly the elastic properties of the material phases due to raw materials or measurement uncertainties [21]. Large scatter on experimentally investigated freshly printed concrete specimens were observed [19, 22]. Therefore, a reliability-oriented model should account for both temporal changes and the randomness of material properties.

As a straight free wall buckles, it loses its stability and under goes large deformation necessitating for further investigation. Hence, in this study, modeling of a straight free wall with different layer thicknesses and wall widths is considered. Moreover, the findings of experimental tests are primarily focused on straight walls [8, 19, 23] and in this paper, these test data are used for validation. The present study introduces a numerical modeling approach for the assessment of the buildability of 3D printed concrete wall structures, in which a time-dependent reliability analysis is inserted. Various types of uncertainties throughout the printing process are taken into account by including the variability of printing process parameters. In addition, sensitivity analysis is used to evaluate the impact of various printing process

parameters on the 3D printed concrete structures.

2. METHODS

2.1. Numerical Modeling

The 3D printed wall configuration used in this numerical model is the straight free wall. The defined boundary conditions are fixed at the bottom of the wall due to friction on the printed bed [19]. As the printing progresses, the loading consists of the increasing self-weight caused by the layer-wise production process.

2.1.1. Specifics about the modeled concrete wall structure

Mechanical properties of 3DPC, such as Young's modulus and compressive strength, exhibit considerable variations throughout the manufacturing process [19, 22]. During printing process, such variations on the properties of fresh concrete may result in geometrical imperfections [24]. Further uncertainties are related to the printing process itself, e.g., different printing velocities, varying time gaps between consecutive layers, and changing nozzle heights and pressures. Besides, interruptions during the printing process may occur, resulting in further irregularities.

As a result, a simplified uncertainty approach is presented in this contribution in which Young's modulus and compressive strength of freshly pumped concrete are modeled using log-normally distributed random processes [25]. Furthermore, random variables are used to represent printing process parameters such as printing velocity, wall length, width, thickness of each layer, and density. The statistical models of the random variables, as well as their corresponding distribution functions, are shown in Table 1. The mean and standard deviations of Young's modulus and compressive strength are obtained from Wolfs et al. [19]. An exponentially decaying correlation function with a layer-wise correlation structure with a correlation length of 30mm was assumed [25, 26]. The mean values and coefficients of variation of the other parameters have been obtained from recent studies [8, 13, 22, 27, 28]. The numerical simulation was realized by generating independent random numbers according to the considered distribution type and parameters [29-33].

Table 1 Statistical distribution of the random variables

Random variables	Mean values	CoV (%)	Min. value	Max. value	Distribution type
Young's modulus, $E(t)$ (kPa)	1.2t+78	15	0.60t+39.5	1.80t+115.5	Lognormal [29]
Compressive strength, $\sigma_y(t)$, (kPa)	0.14t+5.98	14	0.08t+3.22	0.20t+8.73	Lognormal [30]
Printing speed, v_p(cm/s)	10.42	1.0	10.07	10.76	Normal [31]
Model Uncertainty, N_R	1.00	4.6	0.84	1.15	Lognormal [32]
Length, L (mm)	1000	0.5	983.5	1,016.4	Normal [33]
Wall width, δ (mm)	55	3.0	49.57	60.5	Normal [33]
Thickness of each layer, h (mm)	9.5	5.0	7.95	11.06	Normal [33]
Density, ρ (kg/m^3)	2033	0.56	1,994	2,072	Normal [32]

2.1.2. Consideration of the time-dependent mechanical properties

Because of the nature of the printing material and the specific process, some variations in the rheological properties of fresh concrete and the mechanical behavior of the product must be accounted for [25]. This was also observed by [19, 22]. The time-dependent Young's modulus and compressive strength of concrete are given in Eqs. (1) and (2), respectively [19].

$$E(x,t) = E_0(x)+E_1t \quad (1)$$

$$\sigma_y(x,t) = \sigma_{y,0} + \sigma_{y,1}\ t \quad (2)$$

where:

$E_0(x)$ is the initial Young's modulus when it leaves the printing nozzle
E_1 is the gradient of temporal increment
$\sigma_{y,0}$ is the initial compressive strength of the printable concrete when it leaves the printing nozzle
$\sigma_{y,1}$is the gradient of temporal increment
t is the cycle time at a certain location x

The time it takes to print a single layer is referred to as the layer cycle time. In an extrusion-based additive manufacturing of the wall, as shown in Figure1, the minimum layer cycle time for the i^{th} layer is determined using Eq. (3) [34].

$$t_i = H(x,t)/h \times (L/v_p) \quad (3)$$

where:

v_p is the printing velocity
$H(x,t)$is the total height at time t_i and a specific location x
L is the total travel length of the print head to extrude a single layer
h is the thickness of a single layer

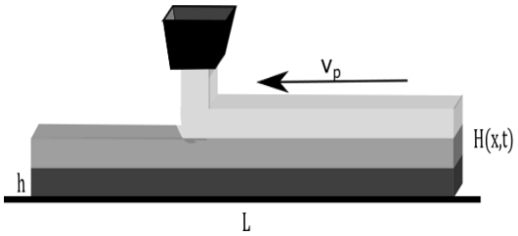

Figure 1 Extrusion-based additive manufactu-ring of a wall of height H(x,t)

A gradient of strength is formed over the height of the structure (Eqs. (1) to (3) [35]. This gradient is caused by the different layer cycles and hydration-induced micro-structural evolution of the concrete material after each layer is deposited [36]. In Figure 1, the strength gradients are represented by shades of gray.

This gradient in strength was included in the proposed numerical model to investigate the stability of the extrusion-based printed wall structure at any moment during the printing process. Regarding the temporal evolution of the compressive strength, Figure 2 provides an example of the resulting strength gradient.

Following Wolfs et al. [19], an increase of $\sigma_{y,1}$=0.147 kPa/min for the compressive strength, a printing velocity of 1cm/s is chosen for a concrete wall with a length of 500m, a width of 40mm, and a layer thickness of 9.5mm. Considering these variables, the gradient of the 3D printed concrete wall's strength produced by extrusion-based additive manufacturing is plotted and shown in Figure 2 [26].

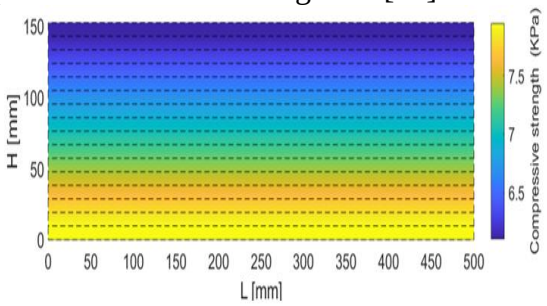

Figure 2 Gradient of the strength of extrusion-based additive manufacturing of the concrete wall

2.2. Buildability in 3DCP Structures

The number of layers or the height at which the printed wall structure collapses is used to measure buildability [8]. Buildability depends upon the rheological properties of concrete; therefore, the simulation of the 3DCP process necessitates a choice of suitable material models. Buildability failure of printed wall structures has been described elsewhere [19,23] due to plastic collapse (a strength mechanism) and elastic buckling (a stability mechanism).

2.2.1. Elastic buckling

Another possible failure mode is the overall buckling of a slender vertical structure under its own weight, $E_c(x,t)$, can then be determined using Eq. (4) [37-39]. For the printed wall structure to be stable, the elastic Young's modulus has to stay higher than the critical value.

$$E_c(x,t) = H(x,t)^3 \rho\, g\, A / 8\, I \quad (4)$$

where:

I is the second moment of area
A is the cross-sectional area

2.2.2. Plastic collapse

The plastic collapse of a 3D printed concrete wall structure is studied by comparing the stresses caused by concrete as expressed in Eq. (5)[34]:

$$\sigma_y(x,t) \leq \sigma_p(x,t) \quad (5)$$

where:

$\sigma_y(x,t)$is the compressive yield strength

$\sigma_p(x,t)$is the gravity-induced stresses

$\sigma_p(x,t)$depends on the height of the wall to be printed and it can be written as expressed in Eq. (6) [36]:

$$\sigma_p(x,t) = \rho g H(x,t) \quad (6)$$

where:

$\rho$is the density of the material

g is the gravity

Another method for calculating gravity-induced stress is to use the printing elevation rate r as shown in Eq. (7) [34, 36, 37].

$$\sigma_p(x,t) = \rho g r t \quad (7)$$

The printing velocity and geometry of the wall structure to be printed (see Figure 1) define the elevation rate, Eq. (8) [34]:

$$r = v_p\, h/L \quad (8)$$

2.3. Reliability-based Assessment

Herein, a probability-based procedure is applied to ensure an appropriate safety margin. One advantage of using a probabilistic approach is that uncertain variables may be considered jointly and their effects may be separated systematically, which allows for a more systematic determination of structural reliability [33].

The numerical model developed is able to estimate if a layered structure can support its self-weight and anticipate when it will collapse. The theoretical framework is based on comparing the vertical stress $S(t)$ acting on the deposited layer to the critical stress $R(t)$associated with the material yield stress as described in section 2.2. The developed framework ensures that vertical stress does not reach critical stress [1].

In this study, a MATLAB algorithm was developed to compute the time-dependent vertical stress $S(t)$, critical stress $R(t)$, and design margin utilizing the statistical random variables mentioned in Table 1. As the printing progressed at each layer, 5000 combinations of random Latin Hypercube Sampling (LHS) variables were tested for reliability assessment.

2.3.1. Time-dependent reliability

The material properties of the printed structure are functions of the hydration process. As a result, a time-dependent reliability assessment was used in the numerical simulation. The vertical stress gradually increases as successive layers are deposited in the extrusion-based additive manufacturing of concrete walls, and material strength properties evolve over time [10]. In order to assess reliability on a temporal scale, a straightforward idea is to utilize a generalization of the reliability equation in the time domain [29, 40-47]. As a result, the generalized reliability problem can be represented in Figure 3 for the 3DPC wall structure.

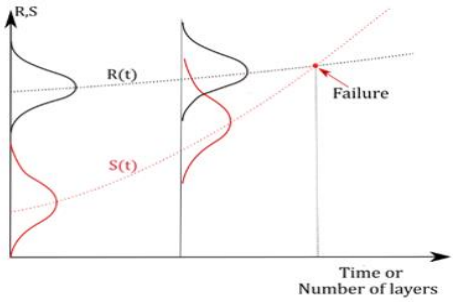

Figure 3 Time-dependency of both the resistance $R(t)$ and load $S(t)$ [40-44]

Whenever, at any point t, in the printing process, the safety margin $M(t)$ is violated if the condition given in Eq. (9)is less than zero [29, 47].

$$M(t)=R(t)-S(t)<0 \quad (9)$$

In this study, the reliability index was computed using the Rackwitz-Fiessler approach. As shown in Table 1, the resistance has a log-normal distribution

and the load has a normal distribution. In these circumstances, the reliability index and the measure of the shift away from the mean value can be expressed by Eq. (10) [48].

$$\beta = \frac{\mu_R\left(1-k\frac{\sigma_R}{\mu_R}\right)\left[1-ln\left(1-k\frac{\sigma_R}{\mu_R}\right)\right]-\mu_s}{\sqrt{\left(\mu_R\left(1-k\frac{\sigma_R}{\mu_R}\right)\left(\frac{\sigma_R}{\mu_R}\right)\right)^2+\sigma_S^2}} \quad (10)$$

where:

β is the reliability index

μ_R and σ_R are mean and standard deviation for the resistance, respectively

$\mu_s$and σ_S are mean and standard deviation of total-load effect, respectively

$\bar{R}^e$, $\sigma_R^e$are mean and standard deviation for the resistance of the approximating normal distributions (equivalent normal parameters), respectively

k is a multiplication factor of the standard deviation

The multiplication factor, k was computed using Eq. (11). The solution was determined iteratively by assuming a value for the design point and continues the iteration until β and x^* converge [48].

$$\mathrm{k} = \frac{\mu_R - x^*}{\sigma_R} \quad (11)$$

where:

x^* is the design point on the failure boundary.

Since no formwork was used to build the wall, failure was initiated if the safety margin tended to zero. In this case, the factor of safety to be considered for the assessment of the buildability of the wall was fixed to one which is the condition where the critical stress R (t) and the vertical stress $S(t)$ are equal. In this study, the minimum safety margin computed using Eq. (10) was considered zero. This resulted in a reliability index of zero which satisfied the minimum requirement to build the 3DPC wall. The reliability of the process decreased as the reliability index decreased.

Based on the concept of Eq. (9), the safety margins $M(t)$ for elastic buckling and plastic collapse were computed according to Eq. (12) and Eq. (13), respectively.

$$M_E(t) = E(x,t) - N_R E_c(x,t) \quad (12)$$

$$M_p(t) = \sigma_y(x,t) - \sigma_p(x,t) \quad (13)$$

where:

N_R is model uncertainty

2.3.2. Sensitivity analysis

Sensitivity analysis is the study of how the variation in the output of a statistical model can be attributed to different variations in the inputs of the model [49]. As there is a built-in MATLAB function [50], the sensitivity of the model to each of its input variables was assessed in this study using the Monte-Carlo based standard regression coefficients (SRC) [51, 52]. In this method, the models given in Eq. (12) and Eq. (13) are approximated by a linear regression given in Eq. (14), with constants of b_o and b_i.

$$Y = M(X) \approx b_0 + \sum_{i=1}^{n} b_i X_i \quad (14)$$

The SRC indices are given in Eq. (15):

$$SRC_i = b_i \frac{\sigma_i}{\sigma_Y} \quad (15)$$

where:

σ_i and σ_Y denote the standard deviation of the model input X_i and the model output Y, respectively.

UQLab, an open-source scientific module for uncertainty quantification was used for the sensitivity analysis. For such tasks, a MATLAB built-in function for sensitivity analysis with a fixed Monte-Carlo sample size of 10,000 was used [50].

3. RESULTS AND DISCUSSION

3.1. Time-Dependent Reliability Analysis Results

The time-dependent reliability analysis is used to assess the structure's susceptibility

to failure during printing for the two types of failure mechanisms.

3.1.1. Elastic buckling result

The critical Young's modulus at which buckling is expected to occur can be found by rearranging Eq. (4) for the considered one linear meter of a wall with a width (δ) and it is expressed by Eq. (16).

$$E_c(x,t)=3\,\rho\,g\,H(x,t)^3\,/2\,\delta^2 \quad (16)$$

Figure 4 depicts the probability distributions of $R(t)$ and $S(t)$ for the overall buckling behavior of 3D printed concrete at each layer as a result of the time-dependent reliability analysis.

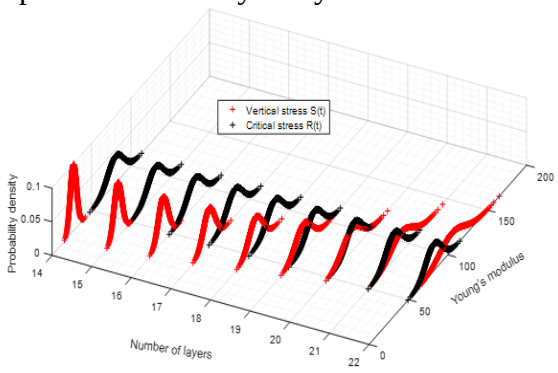

Figure 4 Probabilistic distribution of $R(t)$ and $S(t)$ for elastic buckling at different layers

The vertical stress as well as the critical stress, increases as the printing process progresses. As shown in Figure 4, the vertical stress due to self-weight is lower than the critical stress below layer 20, resulting in a safety margin of $M(t) > 0$, whereas after this layer, the vertical stress is greater than the critical stress, resulting in a safety margin of $M(t) < 0$, indicating that the printed wall begins to buckle.

Furthermore, Figure 5 provides the time-dependent reliability index graph for elastic buckling of a 3D concrete printed wall at each layer. As shown in Figure 5, as the number of layers increases, the reliability index decreases accordingly.

According to the time-dependent reliability analysis result, the maximum number of layers that can be printed without elastic buckling was found to be 20, as shown in Figures 4 and 5. This is in very good agreement with other experimental results of the research on 3D printing concrete [19, 23, 29, 53].

As shown in Figure 5, the reliability index declines steadily for the first 10 layers before rapidly reducing to zero beyond that. This is due to the fact that the elastic Young's modulus requirement (Eq. (16)) scales with the third power of height.

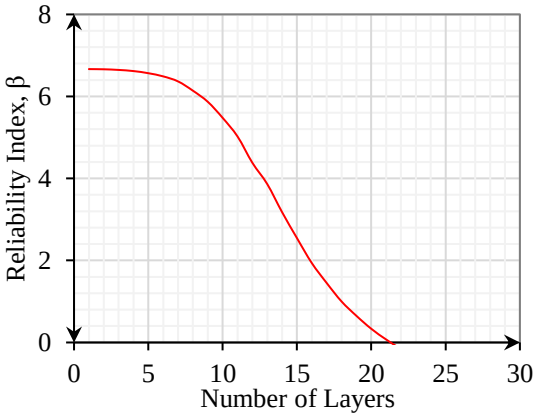

Figure 5 Time-dependent reliability index for elastic buckling of the 3DCP wall

3.1.2. Plastic collapse result

Similarly, the time-dependent reliability index was determined for the plastic collapse using the inputs in Table 1. As shown in Figure 6, after printing layer 36, the vertical stress is greater than the yielding stress, resulting in a safety margin $M(t) < 0$, indicating that the printed wall begins to collapse.

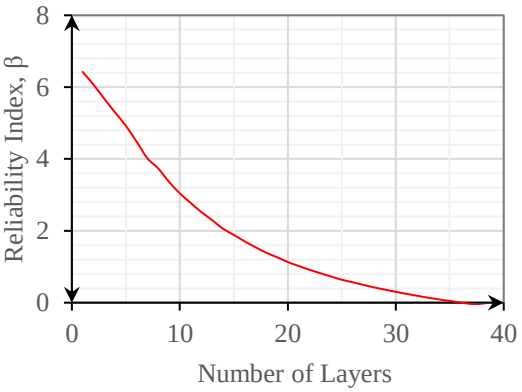

Figure 6 Time-dependent reliability index for plastic collapse of the 3DCPwall

The findings show that 3DPC wall printing is more prone to elastic buckling than plastic collapse due to self-weight, as various other studies have observed [8].

3.2. Sensitivity Analysis

As described before, the printing process parameters, in addition to the material composition, have significant impact on the final performance of 3DPC [12, 13,54]. Printing process control and printing parameter selection are significant components that define the final printing quality of concrete, and they are also important linkages in the development of concrete 3D-printing structures [10].

Sensitivity analysis was carried out in order to identify the most sensitive parameter influencing the buildability of a 3D concrete printed wall. Furthermore, for the two types of failures, influential factors were identified and a parameter study was conducted. The relevant reliability indexes are computed as well.

3.2.1. Sensitivity analysis for the elastic buckling

Sensitivity analysis of the printing process parameters on the elastic buckling safety margin function (Eq. (12)) in terms of sensitivity indices were computed at 5,10,15, and 20layers. The first printed layer was referred to as layer 1, and so on.

The comparison of the sensitivity indices of printing process parameters is shown in Figure 7. In the early stages, variations in the printing speed have the largest impact on the stability. In contrast, later on, the variability of width and layer thickness have a greater impact on the buildability of 3D printed concrete. The important effect of the width on buildability has also been illustrated in [37]. The influence of the printing speed reduces after the tenth layer, as seen in Figure 7. After the fifteenth layer, the wall width and layer thickness have the most significant influences on the stability of the 3DPC wall structure.

Variability in the layer thickness has negative effects on the wall's stability, whereas variation in the width has positive consequences. This means that increasing the layer thickness reduces the elastic buckling resistance and increasing the wall width increases elastic buckling resistance. The length and density variables, in particular, exhibit lower significance and low sensitivity, implying that, if necessary, these variables might be considered constants in the elastic buckling analysis.

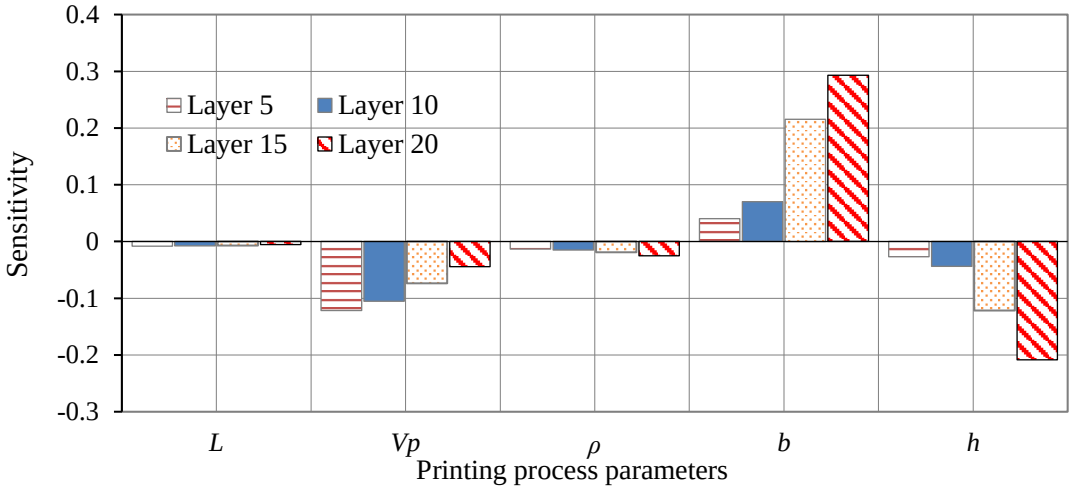

Figure 7 Sensitivity of printing process parameters on the elastic buckling safety margin function

3.2.2. Sensitivity analysis for the plastic collapse

Similarly, at selected layers 5, 10, 15, 20, 25 and 30, sensitivity analysis of printing process parameters on the plastic collapse safety margin function (Eq. (13)) in terms of sensitivity indices were computed. The variations of the printing speed as well as

the layer thickness contribute more to the plastic collapse in the early and later stages compared to the elastic buckling analysis, as shown in Figure 8. Variability in both printing parameters has an adverse influence on the plastic collapse resistance, implying that raising these printing process parameters reduces the resistance to plastic collapse. The reason for this may be that increasing the printing velocity decreases the layer cycle time while raising the layer height increases the wall's self-weight. The length and density variables are less influential input parameters in the plastic collapse analysis, contributing less to the variability of the results.

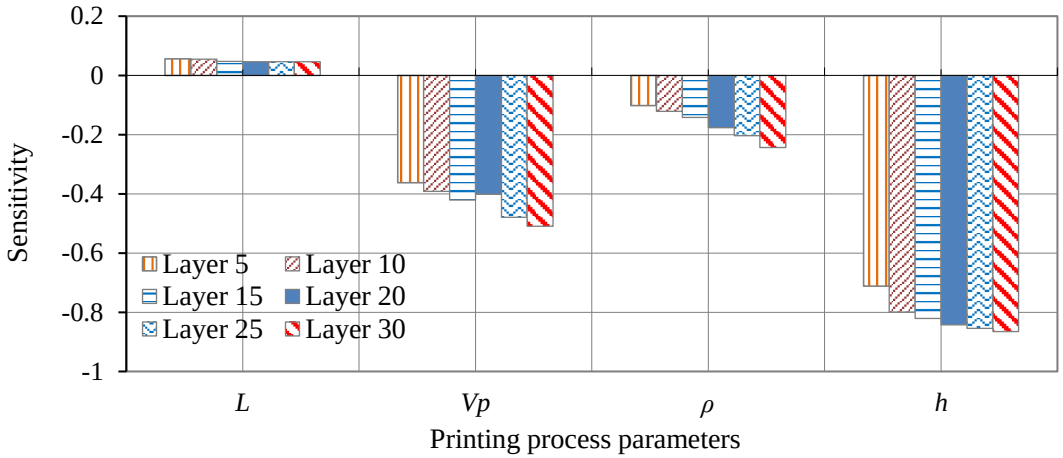

Figure 8 Sensitivity of printing process parameters on the plastic collapse safety margin function

3.3. Parametric Study

The influence of printing process parameters on the contribution to the variability of the stability of 3DPC walls is investigated further. Based on the sensitivity analysis results, the wall width and layer thickness for the case of elastic buckling, as well as the printing velocity and layer thickness for plastic collapse, were chosen for the following parameter study.

3.3.1. Elastic buckling

i. Effect of layer thickness

The MATLAB algorithm was used to conduct the time-dependent reliability study, and the layer thicknesses chosen were based on a majority of studies done on the 3DCP projects [53]. Figure 9 shows the effect of layer thickness on β. In the analysis, other parameters were considered as deterministic values (i.e., v_p=10.42 cm/s, b=55 mm and L=1000 mm). Lowering the layer thickness increases the buildability height, as seen in Figure 9. For example, a layer thickness of 8 mm increases the wall height by 8.27 % when compared to a layer thickness of 9.5 mm.

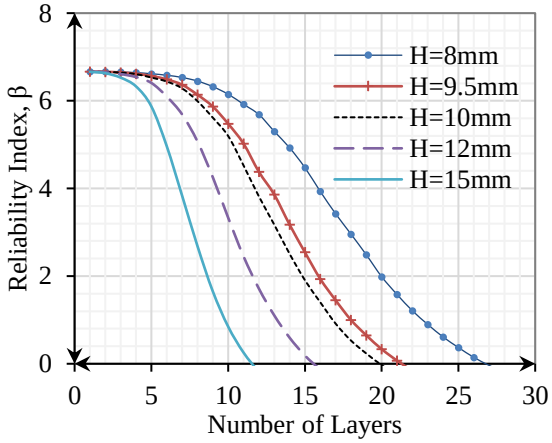

Figure 9 Time-dependent reliability index for 3D printed concrete with different layer thicknesses

This is also expected because lowering the layer thickness increases the overall buildability time (Eq. (3)), which increases the concrete material yielding strength (Eq. (1)). Similarly, increasing the layer thickness reduces the wall's buildability height. For example, a layer thickness of 15 mm reduces the total buildability height

by 13.53 % when compared to a 9.5 mm layer thickness.

i. Effect of wall width

Similarly, to the previous section, ranges of wall width were chosen based on the previously reported values [55]. As demonstrated in Figure 10, increasing the wall width results in a higher buildability height, which is similar to the finding obtained elsewhere [37]. The buildability height increases by more than 80% when the maximum and minimum widths of the selected wall widths (w) are compared. This is because increasing the width of the wall increases its stiffness, which reduces the loss of stability [8].

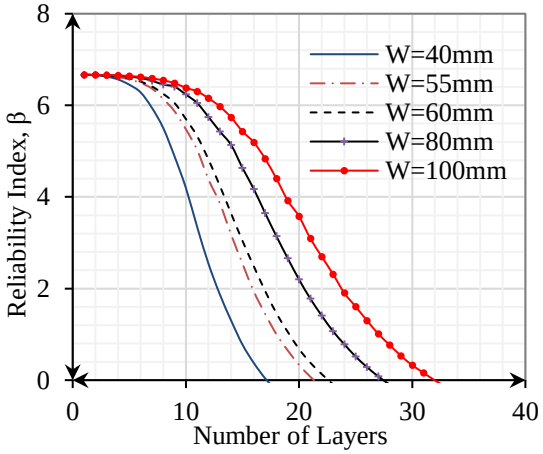

Figure 10 Time-dependent reliability index for 3D printing concrete with different wall widths

3.3.2. Plastic collapse

The printing velocity and the layer thickness are the most influential parameters for the plastic collapse, according to the sensitivity analysis. By keeping the other printing process parameters constant and just altering the printing speed and layer thickness, a parameter study was performed and the results are shown in the next sections.

ii. Effect of printing velocity

The influence of the printing speed on 3D printing plastic collapse is substantial at lower speeds (1.2 cm/s), which can produce concrete with around 80 layers, as demonstrated in Figure 11.

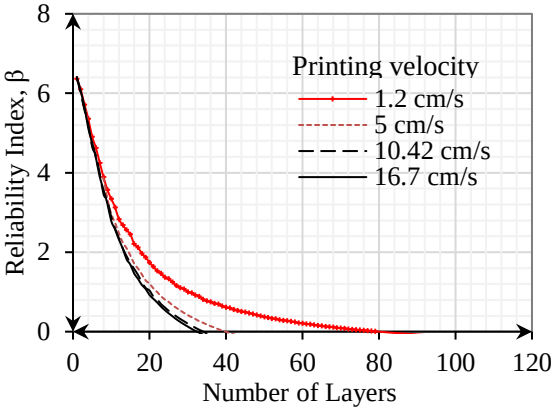

Figure 11 Time-dependent reliability indexes for 3D printing concrete with different printing speeds

Because of the high increase in the layer cycle time (Eq. (3), along with the reduction of the printing speed from 16.7 cm/s to 1.2 cm/s, the height before plastic collapse rises by over 85 %.

iii. Effect of layer thickness

For the next parameters study, the same layer thickness as used in section 3.3.1 was employed. When the layer thickness is reduced from 15 mm to 8 mm, the height of the wall increases by 6.67 % before the plastic collapses, as illustrated in Figure12.

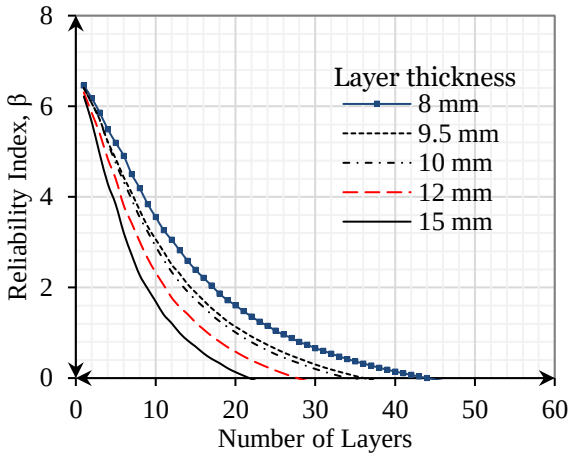

Figure 12 Time-dependent reliability index for 3D printing concrete with different layer thicknesses

The reason for this is that decreasing the layer thickness increases the layer cycle time, which increases the yielding strength. The results revealed that the printing velocity variability has a greater impact on the plastic collapse than layer thickness.

4. CONCLUSIONS

A reliability-based assessment scheme considering the variability of printing process parameters for the buildability of 3D concrete is presented. According to reliability and sensitivity analysis, changes in printing speed, layer thickness, and concrete width are the most influential parameters for predicting the maximum number of printed concrete layers before failure. It is also noted that after the wall tends to buckle, reducing the printing speed of the 3DCP does not have an impact on its buckling stability. The sensitivity results revealed that the printing velocity variability has a greater impact on the plastic collapse than the layer thickness. Furthermore, the elastic buckling is influenced more by the width of the concrete wall than by the thickness of the layers.

Plastic collapse is influenced more by the printing speed than elastic buckling is, and elastic buckling is influenced more by the width of the concrete wall than plastic collapse is.

The length and the density variables, in particular, exhibit lower significance and low sensitivity, implying that, if necessary, these variables might be considered constants in the elastic buckling analysis and plastic collapse.

CONFLICT OF INTEREST

The authors declare that there is no conflict of interest.

ACKNOWLEDGMENTS

The work has been financially supported by different institutions, which is highly acknowledged. Among them are DAAD (Ethiopian - German Exchange of Ph.D. candidates), DFG (German Research Foundation) within the priority program 1886 “Polymorphic uncertainty modeling for the numerical design of structures” and the Federal State of Thuringia, Germany.

REFERENCES

[1] Perrot, A., Rangeard, D., and Pierre, A., “*Structural Built-up of Cement-based Materials used for 3D-Printing Extrusion Techniques*”, Materials and Structures, vol. 49, no. 4, 2016, pp. 1213–1220, doi:10.1617/s11527-015-0571-0.

[2] Valente, M., Sibai A., and Sambucci, M.,“*Extrusion-based Additive Manufacturing of Concrete Products: Revolutionizing and Remodeling the Construction Industry*”, Journal of Composites Science, vol. 3, no. 3, 2019, pp. 1-20, doi:10.3390/jcs3030088.

[3] De Schutter, G., Lesage, K., Mechtcherine, V., Nerella, V. N., Habert, G., and AgustiJuan, I., “*Vision of 3D Printing with Concrete-Technical, Economic and Environmental Potentials*”, Cement and Concrete Research, vol. 112, 2018, pp.25–36, doi:10.1016/j.cemconres.2018.06.001

[4] Albar, A., Chougan, M., Al- Kheetan, M. J., Swash, M. R., and Ghaffar, S. H., “*Effective Extrusion-based 3D Printing System Design for Cementitious-based Materials*”, Results in Engineering, vol. 6, 2020. doi: 10.1016/j.rineng.2020.100135.

[5] Chen, Y., Veer, F., and Copuroglu, O., “*A Critical Review of 3D Concrete Printing as a Low CO_2 Concrete Approach*”, Heron, vol. 62, no. 3, 2017, pp. 167-194. doi: 10.13140/RG.2.2.12323.71205.

[6] Bos, F., Wolfs, R., Ahmed, Z. and Salet, T., “*Additive Manufacturing of Concrete in Construction: Potentials and Challenges of 3D Concrete Printing*”, Virtual and Physical Prototyping, vol. 11, no. 3, 2016, pp. 209-225. doi: 10.1080/17452759.2016.1209867

[7] Hojati, M., Li, Z., Memari, A. M., Park, K., Zahabi, M., Nazarian, S., Duarte, J. P., and Radlińska, A., “3D-*Printable Quaternary Cementitious*

Materials Towards Sustainable Development: Mixture Design and Mechanical Properties", Results in Engineering, vol. 13, 2022. doi: 10.1016/j.rineng.2022.100341.

[8] Kaszyńska, M., Skibicki, S., and Hoffmann, M., "*3D Concrete Printing for Sustainable Construction*", Energies, vol. 13, no. 23, 2020, doi:10.3390/en13236351.

[9] Le, T.T., Austin, S.A., Lim, S., Buswell, R.A., Law, R., Gibb, A.G., and Thorpe, T., "*Hardened Properties of High-Performance Printing Concrete*", Cement and Concrete Research, vol. 42 no. 3, 2012, pp. 558–566.

[10] Fuyan, L., Zhao, D., Hou, X., Sun, L., and Zhang, Q., "*Overview of the Development of 3D-Printing Concrete: A Review*", Applied Sciences, vol. 11, no. 21, 2021. doi: 10.3390/app11219822.

[11] Uzel, S.G., Weeks, R.D., Eriksson, M., Kokkinis, D. and Lewis, J.A., "*Multi-material Multi-nozzle Adaptive 3D Printing of Soft Materials*", Advanced Materials Technologies, vol. 7, no. 8, 2022, pp. 1-10.

[12] Khan, M. S., Sanchez, F., and Zhou, H., "*3-D Printing of Concrete: Beyond Horizons",* Cement and Concrete Research, vol. 133, 2020, doi: 10.1016/j.cemconres.2020.106070.

[13] Rehman, A. U., and Kim, J.H., "*3D Concrete Printing: A Systematic Reviewof Rheology*", In Materials, vol. 14, no. 14, 2021, doi:10.3390/ma14143800.

[14] Buswell, R. , Leal de Silva, W. Jones, S. and Dirrenberger, J., "*3D printing using Concrete Extrusion: A Roadmap for Research*". Cement and Concrete Research, vol. 112, 2018, pp. 37-49, doi: 10.1016/j.cemconres.2018.05.006.

[15] Nerella, V., Hempel, S. and Mechtcherine,V., "*Effects of Layer-Interface Properties on Mechanical Performance of Concrete Elements Produced by Extrusion-Based 3D Printing*", Preprints, 2018. doi.: 10.20944/preprints201810.0067

[16] Panda, B. , Paul, S. C. , Mohamed, N. A. N. ,Tay, Y. W. D. and Tan, M. J., "*Measurement of Tensile Bond Strength of 3D Printed Geopolymer Mortar*", Measurement, vol. 113, 2018, pp. 108-116. doi: 10.1080/17452759.2018.1500420.

[17] Lee, H., Kim, J. J., Moon, J., Kim, W., and Seo, E., "*Evaluation of the Mechanical Properties of a 3D-Printed Mortar*", Materials, vol. 12, no. 24, 2019, pp. 1–13.

[18] Feng, P. , Meng, X.Chen, J.F. and Ye, L., "*Mechanical Properties of Structures 3D Printed with Cementitious Powders*", Construction and Building Materials, vol. 93, 2015, pp. 486-497. doi: 10.1016/j.conbuildmat.2015.05.132

[19] Wolfs, R., Bos, F. and Salet,T., "*Early Age Mechanical Behaviour of 3D Printed Concrete: Numerical Modelling and Experimental Testing*", Cement and Concrete Research, vol. 106, 2018, pp. 103-116, doi:10.1016/j.cemconres.2018.02.001.

[20] Comminal, R., Leal da Silva, W. R., Andersen, T. J., Stang, H., and Spangenberg, J., "*Modelling of 3D Concrete Printing based on Computational Fluid Dynamics*", Cement and Concrete Research, vol. 138, 2019. doi.org/ 10.1016/j.cemconres.2020.106256

[21] Göbel, L., Lahmer, T., & Osburg, A., "*Uncertainty Analysis In Multiscale Modeling of Concrete based on Continuum Micromechanics*", European Journal of Mechanics, A/Solids, vol. 65, 2017, pp. 14–29, doi.org/10.1016/j.euromechsol.2017.02.008.

[22] Casagrande, L., Esposito, L., Menna, C., Asprone, D., and Auricchio, F., "*Effect of Testing Procedures oo Buildability Properties Of 3D-Printable Concrete*", Construction and Building Materials, vol. 245, 2020, doi.org/10.1016/j.conbuildmat.2020.118286.

[23] Suiker, A. S. J., "*Mechanical Performance of Wall Structures in 3D Printing Processes: Theory, Design Tools and Experiments*", International Journal of Mechanical Sciences, vol. 137, 2018, pp. 145-170. Doi.org/10.1016/j.ijmecsci.2018.01.010.

[24] Buswell, R. , Kinnell, P. , Xu, J. , Hack Kloft. H, Maboudi, M. , Gerke, M., Massin, P. Grasser, G. , Wolfs, R.J.M., and Bos, F.P., "*Inspection Methods for 3D Concrete Printing*", 2nd RILEM International Conference on Concrete and Digital Fabrication: Digital Concrete 2020, vol. 28, 2020, pp. 790–803.

[25] Schmidt, A., Mengesha, M., Göbel, L., Könke, C., Lahmer, T., "*Numerical Modeling of an Extrusion-based Concrete Printing Process Considering Spatially and Temporarily Varying Material and Process Parameters*", 18th International Probabilistic Workshop, vol. 153, 2021, pp. 531-538.

[26] Mengesha, M., Schmidt, A., Göbel, L., Lahmer, T., & Könke, C., "*Numerical Simulation for 3D Printed Wall Structure During the Process of Printing Considering Uncertainty",* 4th International Conference on Uncertainty Quantification in Computational Sciences and Engineering, 2022, pp. 100–111, doi.org/10.7712/120221.8025.18985.

[27] Wolfs, R. J. M., and Suiker, A. S. J., "*Structural Failure During Extrusion-based 3D Printing Processes*", International Journal of Advanced Manufacturing Technology, vol. 104, 2019, pp. 565–584. Doi.org/ 10.1007/s00170-019-03844-6.

[28] Wolfs, R. J. M., Bos, F. P., and Salet, T. A. M., "*Triaxial Compression Testing on Early Age Concrete for Numerical Analysis of 3D Concrete Printing*". Cement and Concrete Composites, vol. 104, 2019, doi.org/10.1016/j.cemconcomp.2019.103344.

[29] Gordon A., Fenton ,D. and Griffiths, V., " *Risk Assessment in Geotechnical Engineering*", John Wiley & Sons, 2008.

[30] Baji, H., and Yang, W., "*Probabilistic Model for Time to Cover Cracking due to Corrosion*". Structural Concrete, vol. 21, no. 4, 2019, pp. 1408-1424, doi.org/ 10.1002/suco.201900341.

[31] Pradalier, C. , Hermosillo, J. , Koike, C., Braillon, C., Bessire, P. and Laugier, C., "*Safe and Autonomous Navigation for a Car-Like Robot among sPedestrian*", Int. Workshop on Service, Assistive and Personal Robots, Madrid (ES), 2003.

[32] NCHRP REPORT 292, "*Strength Evaluation of Existing Reinforced Concrete Bridge*s", Transportation Research Board, Washington DC, 1987.

[33] JCSS "*Probabilistic Model Code, Part 1-Basis of Design*", Joint Committee on Structural Safety, 2000, pp. 64.

[34] Perrot, A. and Rangeard, D., "*3D Printing in Concrete: Techniques for Extrusion/Casting, State of the Art and Challenges of the Digital Construction Revolution"*, 2019, pp. 41-72, Doi.org/ 10.1002/9781119610755.

[35] Mengesha, M., Schmidt, A., Göbel, L., Lahmer, T., "*Numerical Modeling of an Extrusion-based 3D Concrete Printing Process Considering a*

Spatially Varying Pseudo-Density Approach, 2nd RILEM International Conference on Concrete and Digital Fabrication, 2020, doi.org/10.1007/978-3-030-49916-7_33.

[36] Perrot, A., "*3D Printing of Concrete",* ISTE Ltd and John Wiley & Sons, Inc, Great Britain and the United States, 1st ed. 2019, doi.org/10.1002/9781119610755.

[37] Roussel, N., "*Rheological Requirements for Printable Concretes*", Cement and Concrete Research, vol. 112, 2018, pp. 76-85, doi.org/10.1016/j.cemconres.2018.04.005.

[38] Esposito, L., Menna, C., Asprone, D., Rossino, C., Marchi, M.., "*An Experimental Testing Procedure to Assess the Buildability Performance of 3D Printed Concrete Elements*". 2nd RILEM International Conference on Concrete and Digital Fabrication. vol 28. Springer, 2020, https://doi.org/10.1007/978-3-030-49916-7_24.

[39] Greenhill, A., "*Determination of the Greatest Height Consistent with Stability that a Vertical Pole or Mast can be Made, and of the Greatest Height to which a Tree of Given Proportions can Grow",* In Proceedings of the Cambridge Philosophical Society, vol. 4, 1881.

[40] Wang, C., "*Structural Reliability and Time-Dependent Reliability*", Springer Nature, Switzerland, 2021, doi: doi.org/10.1007/978-3-030-62505-4

[41] Wen, Y. K., and Chen, H. C., "*On Fast Integration for Time Variant Structural Reliability*", Probabilistic Engineering Mechanics, vol. 2, no. 3, 1987, pp. 156–162.

[42] Baingo, D. A., "*Framework for Stochastic Finite Element Analysis of Reinforced Concrete Beams Affected by Reinforcement Corrosion*", (Doctoral dissertation), University of Ottawa, 2012.

[43] Rostam, S., "*Reinforced concrete Structures - Shall Concrete Remain the Dominating Means of Corrosion Prevention*?", Materials and Corrosion, vol. 54, no. 6, 2003, pp. 369–378, doi.org/10.1002/maco.200390086.

[44] Siemes, T., and Rostam, S., "*Durable Safety and Serviceability: A Performance based Design Format*", IABSE Colloquium, 1996, pp. 41–50.

[45] Stewart, M. G., and Rosowsky, D. V., "*Structural Safety and Serviceability of Concrete Bridges Subject to Corrosion*", Journal of Infrastructure Systems, vol. 4, no. 4, 1998, pp.146–155.

[46] Animesh, D., and Sankaran, M., "*Reliability Estimation with Time-Variant Loads and Resistances*", Journal of Structural Engineering, vol. 126, 2000, pp. 612–620.

[47] Melchers, R. E., and Beck, A. T., "*Structural Reliability-Analysis and Prediction*", 3rd ed., John Wiley & Sons Ltd. 2018.

[48] Ghasemi, S. H., and Nowak, A. S., "*Reliability Index for Non-Normal Distributions of Limit State Functions*", Structural Engineering and Mechanics, vol. 62, no. 3, 2017, pp. 365–372, doi.org/10.12989/sem.2017.62.3.365

[49] Saltelli, A., Tarantola, S., and Campolongo, F., "*Sensitivity Analysis as an Ingredient of Modeling*", Statistical Science, vol. 15, no. 4, 2000, pp. 377–395.

[50] Marelli, S., Lamas, C., Konakli, K., Mylonas, C., Wiederkehr, P. and Sudret, B., "*UQLab User Manual-Sensitivity Analysis*", *Report UQLab-V1*, 2019, pp. 2-106.

[51] Saltelli, A., and Marivoet, J., "*Non-Parametric Statistics in Sensitivity Analysis for Model Output: A Comparison of Selected Techniques*",

Reliability Engineering and System Safety, vol. 28, no. 2, 1990, pp. 229–253.

[52] Borgonovo, E., and Plischke, E., "*Sensitivity Analysis: A Review of Recent Advances*", European Journal of Operational Research, vol. 248, no. 3, 2016, pp. 869–887.

[53] Suiker, A. S. J., "*Effect of Accelerated Curing and Layer Deformations on Structural Failure during Extrusion-based 3D Printing*", Cement and Concrete Research, vol. 151, 2022, doi: https://doi.org/10.1016/j.cemconres.2021.106586.

[54] Li, Z., Hojati, M., Wu, Z., Piasente, J., Ashrafi, N., Duarte, J. P., Nazarian, S., Bilén, S. G., Memari, A. M., and Radlińska, A., "*Fresh and Hardened Properties of Extrusion based 3D-Printed Cementitious Materials: A Review*", Sustainability, vol. 12, no. 14, 2020, pp. 1–33. doi: doi.org/10.3390/su12145628.

[55] Kruger, J., Cho, S., Zeranka, S., Viljoen, C., and van Zijl, G., "3D *Concrete Printer Parameter Optimisation for High Rate Digital Construction Avoiding Plastic Collapse*", Composites Part B: Engineering, vol. 183, 2020, doi: doi.org/10.1016/j.compositesb.2019.107660.

The Performance of Private Residential Real Estate Developers in Ethiopia: The Case of Addis Ababa

Selam Yohannes[1,*] and Abebe Dinku[1]

[1]School of Civil and Environmental Engineering, Addis Ababa Institute of Technology, Addis Ababa University, Addis Ababa, Ethiopia
**Corresponding author's Email address: seleyoh@gmail.com*

DOI: https://doi.org/10.20372/zede.v42i.10181

ABSTRACT

The issue of providing adequate housing to the general public is critical in both developed and developing nations. This requires continuous monitoring of performance in the provision of housing as a fundamental approach to enhance efficiency and establish a strategic framework for achieving better productivity. This study focuses on the performance evaluation of real estate firms in Addis Ababa and identifies the obstacles encountered that would influence their construction operations and management. The primary goal of this research is to introduce the concept of project performance, identify the factors influencing performance and propose strategies for enhancing performance in real estate firms. The qualitative research methodology employed involved non-random sampling. The methodology involved preliminary investigation and a pilot study, to refine and explore the research areas. Through the data analysis process; the study underscored the significance of focusing on customer satisfaction, cost overruns and other financial aspects when considering performance metrics. Furthermore, among the factors impacting performance; material price fluctuations, exchange rate variations and construction material shortages ranked highest in their order of appearance.

The study's findings culminate in essential recommendations for improvement strategies. In conclusion, it emphasizes the necessity of a collaborative effort among all stakeholders to notably elevate the real estate sector.

Keywords: Housing demand and supply, Key Performance Indicators; Performance measurement; Real estate developer.

1. INTRODUCTION

It is estimated that Africa could potentially have up to 1.2 billion urban residents by the year 2050, with 4.5 million new inhabitants settling in informal areas annually. The majority of these individuals are unable to afford basic formal housing or secure mortgage loans [1]. The rise in population leads to an increased demand for various resources, such as natural resources, job opportunities and housing. The growth in population can create challenges to development; hence, many of the world's most populous nations have endeavored to regulate their annual population growth rates.

The concept of housing, when viewed in the context of services and community, can be described as the provision of living spaces and associated amenities that enhance the well-being and stability of individuals and families within a community. It encompasses not only the physical structures like houses, apartments or shelters but also the array of supportive services and infrastructure that ensures residents have access to secure, affordable and adequate housing. This definition underscores housing as a crucial social service necessary for promoting community unity, economic prospects and the overall quality of life for all community members [2].

Residential real estate developers are expected to play a crucial role in providing housing for the community. To maximize the output from real estate developers, organizations need to be effectively managed. However, the performance and delivery of housing units have been unsatisfactory so far. According to the master plan of Addis Ababa (2003-2010), the actual delivery of residential real estate developers amounts to only 25 % of the promised quantity.

Performance measurement is defined as "the process of quantifying the efficiency and effectiveness of past actions." Performance management holds significance in the construction industry as it enables managers to assess how (and if) employees are contributing to the overall business strategy and project success [3].

The performance of housing developers is multifaceted, covering their responsibilities in supply, quality, affordability, innovation, project management, community influence and financial sustainability within the broader housing market framework. Their choices and activities not only influence the physical environment but also the socio-economic dynamics of the communities they cater for. To accomplish these objectives and ensure that construction work is carried out in the most efficient and organized manner, companies must establish and uphold robust teams, monitor and evaluate progress, and guarantee the smooth execution of construction projects.

To date, there are studies done on real estate's regarding the failure and institutional issues faced by real estate developers but not on performance related matters. This study thus focuses on the factors influencing real estate performance derived from literature reviews and personal interviews. The chosen methodology for exploring performance influencing factors entails conducting a preliminary study as a pilot survey. Based on the findings, a list of parameters for further evaluation was outlined. This evaluation was carried out by formulating a questionnaire aimed at real estate staff, with a few customers consulted to validate the findings. The assessment and rating of performance influencing factors were executed using Minitab to steer the focus of real estate entities, initiate improvement strategies and evaluate the performance index considerations.

Overview on Private Real Estate Developers

Project Life Cycle: The project lifecycle of private real estate developers typically adheres to a structured process from inception to completion and beyond. Here is an outline of the standard stages involved [3]:

i. *Identification and Feasibility Study:* Developers pinpoint potential development opportunities based on market demand, location appeal and zoning regulations.

ii. *Acquisition of Land:* Upon confirming feasibility, developers engage in negotiations and secure the necessary land for the project.

iii. *Planning and Design:* Developers collaborate with architects, engineers and planners to craft the project's design.

iv. *Financing and Investment:* Developers secure funding through a combination of equity investment, loans and potentially government incentives or subsidies.

v. *Pre-Construction Phase:* Preparing the construction site, this may involve demolishing existing structures, clearing the site, securing essential utilities and infrastructure connections.

vi. *Construction:* includes the physical construction of the project involving

coordinating labor, procuring materials, adhering to construction schedules and budgets.

vii. *Marketing and Sales:* As construction progresses, developers launch marketing and sales campaigns to pre-sell or lease units.

viii. *Occupancy and Operation:* Upon completion of construction and obtaining regulatory approvals, units are handed over to buyers or tenants. Developers may oversee property management directly or through property management firms to ensure smooth operation and maintenance.

ix. *Post-Construction Evaluation:* Developers assess the project's performance against initial projections, including financial returns, market reception and operational efficiencies. Insights gained during this phase inform future development strategies.

x. *Asset Management or Disposition:* Depending on the developer's approach, they may retain the property as part of their investment portfolio for long-term income generation (asset management). Alternatively, they may opt to sell the property to realize profits or reinvest capital in new projects.

Real Estate Housing Supply Process: The real estate housing supply process encompasses several fundamental elements that collectively impact the availability, affordability and quality of housing in any given market. Here is an overview of these elements [5]:

i. *Land Availability and Zoning:* The availability of suitable land for development and the zoning regulations governing its use are pivotal factors. Zoning laws dictate the permissible structures in specific areas, influencing the type and density of available housing.

ii. *Development and Construction:* The housing development process involves planning, obtaining permits, construction and infrastructure development. This phase is influenced by factors such as construction costs, labor availability and regulatory compliance.

iii. *Housing Finance and Investment:* Financing plays a crucial role in housing development. Developers secure funding through loans, equity investments or government subsidies. The availability of financing options impacts the feasibility and scale of housing projects.

iv. *Market Demand and Trends:* Housing supply is closely linked to market demand, influenced by demographic trends, economic conditions and consumer preferences.

v. *Government Policies and Regulations:* Government policies, including tax incentives, subsidies and housing regulations, significantly impact housing supply. Policies aimed at promoting affordable housing or sustainable development shape market dynamics.

vi. *Infrastructure and Utilities:* Access to infrastructure such as roads, water supply, sewer systems, and utilities (electricity and internet) is vital for housing development. The adequacy and reliability of infrastructure affect the desirability and feasibility of new housing projects.

vii. *Environmental and Sustainability Factors:* Environmental considerations and sustainability standards increasingly influence housing development. Regulations on energy efficiency, green building practices and environmental impact assessments shape housing supply decisions.

viii. *Community and Stakeholder Engagement:* Local communities and stakeholders, including residents, neighborhood associations and support groups, often influence housing development through public hearings and zoning meetings.

ix. *Market Dynamics and Price Movements:* Housing supply and demand dynamics determine price fluctuations and affordability. Imbalances in supply can lead to price fluctuations, impacting housing affordability and market stability.

x. *Urban Planning and Design:* Urban planning principles influence the layout, density and design of housing developments. Well-designed neighborhoods consider factors such as public spaces and amenities to create livable communities.

In summary, understanding these elements is essential for stakeholders, including developers, policymakers, investors and residents to effectively navigate and influence the housing market.

Construction Performance Measurement

The construction industry has frequently faced criticism for its underperformance attributed to its unique characteristics. Traditional performance evaluation metrics typically encompass cost, time, and quality. In 2010, a research initiative was undertaken to introduce a comprehensive performance measurement model incorporating prioritized BSC (Balanced Scorecard) perspectives and key building project performance indicators (KBPPIs) to assess construction project performance utilizing a multi-criteria decision-making tool like AHP (Analytic Hierarchy Process) [6].

Specifically, within construction projects, real estate performance can be gauged through financial, business and customer perspectives. The financial aspect hinges on stakeholders' perceptions regarding the project's financial aspects, encompassing cash flow projections and cost-benefit analyses. The internal business process perspective concentrates on pivotal process activities, while the customer perspective emphasizes potential customer contentment [6]. Customer satisfaction significantly influences the performance of real estate developers. Three factors from the customer perspective act as performance indicators (housing unit quantity, sales volume impact and occupancy rate impact). Research done in Kenya revealed that an increase in housing unit quantity and occupancy rate impact tends to positively influence performance [7].

A prevalent issue among real estate firms is the delay in delivering housing according to the original contract timeline. The primary causes of delays documented were price hikes, construction material shortages and insufficient financial resources [8].

The theory of real options explains why developers opt to keep land undeveloped for extended periods and how market conditions evolve. There was a remedy proposed for the Real estate developers who were advised to establish a group that enables collaboration agreements endorsed by each developer and by the city [9].

Swedish housing development practices and monitoring lean towards daily planning rather than strict adherence to zoning plans, indicating a swift plan implementation process [10]. It is concurred that a robust political emphasis is necessary to formulate detailed development schemes, ensure efficient coordination to meet milestones and offer incentives to developers for timely project completion.

Regarding institutional enhancement, in Addis Ababa, there are eight primary issues that could boost the construction industry.

By prioritizing and ranking these issues, it was discerned that three of the matters received minimal attention from governmental bodies, thereby contributing to real estate developers' underperformance. These issues encompass land lease allocation, compensation and valuation regulations. The study also highlighted the lack of government oversight or enforceable penalties for real estate companies failing to adhere to customer contracts and granting these companies excessive autonomy. The study further cited data from 2015/16, indicating that out of the total 550ha of leased land given to 120 real estate projects, 119.7 ha remains undeveloped [11]. The prevalent critical failure issues primarily revolve around inadequate feasibility studies, challenges with cost estimation during tendering and construction phases.

Review on Public Sector Housing Strategies, Regulatory and Enabling roles in Addis Ababa

Addis Ababa, the capital city of Ethiopia, is confronted with significant housing challenges attributed to rapid urbanization, population growth and economic advancement. The public sector assumes a pivotal role in shaping housing strategies, regulations and fostering conducive environments to tackle these challenges.

In Addis Ababa, housing strategies encompass affordable housing initiatives, integrated urban development plans, slum upgrades, urban renewal and land use regulations through master plans. The government has initiated various affordable housing programs with the aim of offering housing solutions to low and middle-income households. These programs frequently entail public-private partnerships (PPPs) to expedite housing provision. Efforts are underway to enhance informal settlements and slums, enhancing living conditions and integrating these areas into the formal urban landscape. Urban renewal projects also strive to revitalize older or deteriorated areas [12].

The regulatory frameworks primarily revolve around land tenure and property rights to formalize land ownership, ensuring property rights that influence investment, building codes, safety standards governing construction practices, environmental and sustainability criteria that may involve waste management prerequisites, financial mechanisms and subsidy schemes to facilitate access to mortgage finance that support infrastructure development at reduced construction costs.

Enabling roles encompass enhanced infrastructure development, collaboration between the public and private sectors, community involvement and stakeholder engagement.

Challenges encountered in public sector housing development include addressing informal settlements, land availability, costs in urban areas affecting housing affordability, project feasibility and necessitating effective land management policies. Thus, strengthening institutional capacity and governance frameworks is essential for effective implementation of housing strategies and regulations. Continued efforts in policy innovation, infrastructure investment and community engagement are crucial for achieving sustainable urban development and housing security in the city.

Experience of Different Countries

In the United Kingdom, key performance indicators (KPIs) were programmed for construction projects as early as 1999. These KPIs give information on the range of performance being achieved on all construction activities and they include client satisfaction on the product and service, defects, predictability on cost and

time, profitability, productivity, safety, construction cost and time. On the study done in the United Kingdom; procurement components were challenging the project performance. That is mainly during; building team selection, payment procedures, legal framework, overlap of the building phases and building team organization [13].

In Kuwait, the current market valuation provides strong incentives for private sector developers to expand the supply of dwellings. However, private sector incentives are distorted by the regulatory and tax treatment of real estate due to their high prices on new preconstruction apartment sales and excess capital gains on redevelopment projects [14].

In the United States, local land use regulations have played role in constraining housing supply. While some local regulations have been changed to allow more housing construction in high demand areas, the effects will take time and it remains to be seen whether the increase in supply created by these regulatory changes will be enough to satisfy local demand [15].

South Korea used different procedures and strategies in order to facilitate the housing development. Having a clear policy, signing of collaboration agreement with well-documented strategy between private developers and government projects, having a nationally accepted standard/ legal framework and supervision, having a strong commitment and cooperation by the government are some of the strategies.

India used different housing development strategies. Such as; provision of land as an incentive from the government, government and private developers working together on residential and commercial projects, long term mortgage loan to be arranged, paying half the price of a housing upon purchase and the other half on long term arrangement, developers and end users working cooperatively [16, 17].

The construction industry in Nigeria encounters challenges when it comes to delivering housing efficiently and effectively. There are often reports of inadequate project management, rushed project execution, poor service delivery and instances where facilities are left abandoned or non-operational. It is common to see cost, quality and time overruns in numerous construction projects in Nigeria. These issues could be addressed through careful planning, policy implementation and thorough industry monitoring and supervision [18].

The main strategies used in Vietnam was mainly focused on the project delivery method which is build operate transfer. On those methods, there was a lot of effort regarding the finance as there were initiatives for developer built affordable housing and also conducting a regular audit helped in reforming the standard of housing supply. The audits mainly base on the cost, schedule and delivery of the housing. In addition, the involvement of Public Private Partnership for affordable housing, provident funds and different supporting programs have also contributed positively to the provision of housing in the country [19].

2. METHODOLOGY

In this study, qualitative and quantitative induction methods were employed based on the collected data. Qualitative induction was utilized to generate new ideas regarding subjective experiences and concepts, while quantitative induction was employed to test fixed (deductive) variables.

To pretest certain variables, a pilot study was conducted as an initial investigation. The pilot survey was executed through the utilization of a research instrument, mainly using interviews.

The researchers planned to adopt a non-probabilistic sampling approach, with a preference for the purposive sampling technique based on the results of the pilot study. Given the research's focus on a specific sample, descriptive analysis was applied to the qualitative data produced.

The detailed methodology procedure and sampling technique utilized in this study are outlined in the following section.

2.1. Operational Active Private Residential Real Estate Developers in Addis Ababa

Real estate developers are officially registered by the Ethiopian Investment Commission (EIC) at the Federal level and by the Addis Ababa Investment Agency (AAIA) at the city level. Those registered with the EIC include investors who are either wholly foreign or engaged in a joint venture with domestic investors (Ethiopian and foreign investors as PLC). The primary motivation for investors to undergo registration with the EIC is to establish a legitimate entity within the country for operational purposes. Conversely, individuals registered with the AAIA seek to secure access or priority in acquiring loans from financial institutions and benefit from a 1 % interest rate discount, as revealed in an interview conducted by the EIC. Presently, real estate developers do not receive any incentive in comparison to the manufacturing sector.

In terms of the renewal of investment permits, as stipulated in Proclamation No. 769, Article 17 of 2012, investors who fail to commence the implementation of their project within two years from the date of the investment permit registration risks having their permit revoked unconditionally [20]. Nevertheless, the consistent enforcement of this regulation is not always observed in practice.

The total counts of real estate developers registered with the EIC at the federal level, the AAIA, and through trade license registration and issuing offices is given in Table 1.

Table 1 Real Estate Developers in Ethiopia

Governmental offices approached	**Registered Real estate developers' status**		**Potential Population**	
	Real estate developers' stages	**Number of real estate Developers**		
Ethiopia Investment Commission (EIC)-Invested in Addis Ababa	Pre-implementation	84	**18**	**231**
	Implementation	28		
	Operational	**18**		
AAIA	Implementation	181	**23**	
	Operational	190 totals in RE and other business where 70 are purely working on real estate development but **23 are with 'Real estate' extended naming**		
Business/ trade license office	**Operational on their system/ database**	540 totals in RE but **190 are with 'Real estate' extended naming**	**190**	

The recorded total population of registered real estates is 628; however, only 231 of them bear the specific designation 'real estate' across all offices. For the purpose of this study, the focus was on real estates with the extended designation 'real estate', as those identified by 'individual names' lack organizational structure or a formal company setup that would allow for the application of performance measurement metrics. These entities primarily operate for profit, with half of them having ceased real estate operations.

Analysis of Table 1 reveals inconsistencies in the total count of operational real estates across different offices, casting doubt on the reliability of the compiled list of real estate data sourced from the aforementioned investment and licensing offices.

Moreover, upon closer examination, it was discovered that some of the contacts listed under real estate developers were actually investors not directly engaged in real estate development, many of whom had incorrect or missing contact information. This discrepancy has hindered the feasibility of conducting random sampling. To address this challenge, the researchers conducted a pilot test to validate the chosen sampling methodology and carried out a preliminary investigation to establish the appropriate research procedures.

2.2. Population and Sampling for the Pilot Survey

A pilot study was carried out to examine the critical issues impacting real estate developers in a professional manner. The study involved a set of interview questions for an initial small-scale evaluation of the research. Its purpose was to provide a rationale for the researcher's various decisions and approaches to the main research questions. Furthermore, it would justify the sampling technique employed, identify key factors influencing real estate developers' performance and establish a clear research focus.

The pilot study was conducted in Addis Ababa and deliberately selected only 11 real estate developers. This insightful study was aimed at elevating the research quality by focusing on a limited group of real estate developers, thereby ensuring the viability of the main research. These preliminary investigations delineated and reinforced the objectives, directed the analytical strategy, and gauged the research's effectiveness. The pilot study was structured around specific targeted inquiries to efficiently extract valuable insights. Moreover, the choice of a small sample of real estate developers was intended to streamline the data collection process, avoid redundant efforts and assess the research's feasibility.

The flow chart in Figure 1 illustrates the various stages involved in carrying out the pilot study. The pilot study, as previously mentioned, was conducted as a qualitative inquiry in preparation for the main study.

Data for the pilot study was collected using an interview protocol consisting of both open and closed-ended questions focusing on performance measurement within the real estate development sector. The findings from the pilot study are detailed below:

i. ***Participants and Setting:*** Real estate entities were purposefully selected based on their level of experience categorized into High-level Real Estates, Mid-level Real Estates and New/Minimally Experienced Real Estates in which their corresponding selected samples were 3, 5 and 3 respectively. The classification was primarily based on the longevity of the real estate entities. In total, 11 samples were included, with input from industry professionals to ensure the selection process was robust.

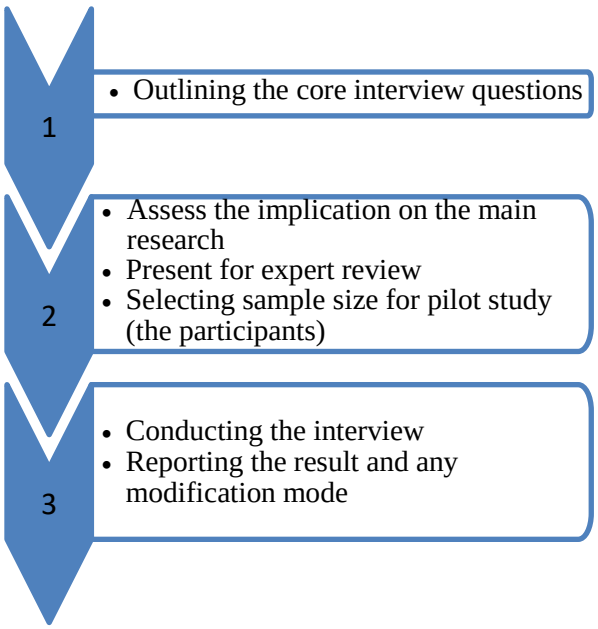

Figure 1 Flow Chart for Pilot Study

ii. ***Purpose of the Pilot Study****:* The pilot study was aimed at validating the chosen sampling method by further exploring Registered and Unregistered Real Estate Developers (REDs), provide insights for the main research design, identify key performance indicators (KPIs) influencing real estate developers' performance, align the research title with its objectives, explore international software technologies for performance management and benchmarking.

2.3. Population and Sampling: for the Main Research Survey

The data obtained shown in Table 1 were obtained from EIC, AAIA and the Trade License Office. It is important to note that, the real estate properties acquired from the Trade License Office are not individually registered under real estate developers but are rather encompassed within other business registries on their roster. This consolidation of data points towards a population size that may exhibit bias.

In the preliminary research evaluation, the population data from EIC was thoroughly analyzed. Conversely, for AAIA and business license offices, only entities explicitly denoted with 'real estate' extension in their company name were selected for further scrutiny, as detailed in Table 2.

The telephone survey was carried out, yielding the subsequent key points identified during the sample screening process.

i. Approximately, 25% of the properties listed were designated for rental purposes.
ii. Close to 50% of the real estate developers included in the list had either ceased operations or have inactive offices, yet remain on the official registry, posing a significant challenge to the sampling procedure.
iii. The presence of duplicate entries of developers on the list was attributed to their involvement in multiple business entities under a single developer.
iv. Some real estate developers featured on the Addis Ababa investment agency's list were actually located in other cities of Ethiopia.
v. A notable portion of the listed real estate properties had inaccurate contact numbers, rendering them untraceable even through online searches.

While there is no specific figure for purposive sampling, a general guideline exists for determining the sample size, suggesting that a sample size exceeding 30 but less than 500 is suitable for most research endeavors [21]. Subsequent to the telephone survey and a thorough examination of their locations, a total of 36 residential real estate developers have been meticulously screened and identified as the final sample size eligible for inclusion in the main questionnaire survey

Table 2 Real estate sample screening

Population from registry	Population size	Real estate with ‘’naming’’ for sample	Sample size after willingness check through phone survey
From EIC	18	18	5
From AAIA	70	23	10
From Trade license office	540	190	12
Others- which are not registered but operational in the real estate sector			9
Total	**628**	**231**	**36**

3. RESULTS AND DISCUSSION

3.1. Findings of the Preliminary/ Pilot Study

The majority of real estate developers surveyed favored traditional performance monitoring methods like reports and scheduling. Three out of the eleven sampled entities employed collaborative tools during the design phase, showcasing effective communication practices.

A significant finding revealed that 70% of the pilot study participants initially operated as contractors before transitioning to real estate developers, making it challenging to establish the total population for random sampling in the main survey. Consequently, purposive sampling will be adopted for the main research. Based on the pilot study, an array of performance affecting factors were identified as detailed in Table 3. The study also highlighted the absence of software applications or benchmarking tools for management purposes.

3.2. Identification of Variables for Further Investigation and Analytical Framework for the Performance Gaps in the Addis Ababa Context

An analytical framework summary based on the performance gaps identified and to be investigated on the upcoming sections are represented in Figure 2.

Figure 2 Analytical frameworks for Performance gaps

The items presented in Table 3 have undergone a thorough review based on the pilot study and existing literature. The pilot study encompassed personal interviews aimed at eliciting specific research insights from respondents. The data obtained, categorized as qualitative data were gathered from a deliberately chosen group of real estate developers central to the primary research investigation.

3.3. Findings of the Main Research

As shown on Table 4; among the 36 sample sizes analyzed, 23 demonstrated full responsiveness by providing all the necessary information, while only 1 partially supplied the requested data. Consequently, the response rate stands at 63.9 %.

Following a comprehensive assessment of real estate developers, specific inquiries were raised during the survey. The findings have been meticulously documented in Table 5, revealing that 39.1% of the participants initially commenced their

professional journey in the realm of real estate development. Interestingly, a significant portion transitioned from other organizational backgrounds to eventually establish them within the real estate industry.

Based on the feedback received, 86.4 % of real estate developers engage in conducting feasibility studies prior to initiating any concept design. The survey results indicate that these developers perceive their performance as moderate, with an approximate 47.8 % likelihood of successfully completing their projects within the scheduled timeframe.

The vast majority of real estate developers did not utilize international benchmarks for performance management; instead, they focused on drawing inspiration from other countries solely in the areas of design and finishing work methodologies. A comprehensive overview of housing delivery is provided in Table 6.

Table 3 Factors affecting performance and measuring indices and representation on analytical framework (Source: literature and interview session during pilot study)

Factors Affecting Performance	**Performance Measuring Indices**
a. Fluctuation of material price	a. Timely completion
b. Exchange rate fluctuation	b. Client satisfaction
c. Shortage of construction materials esp. Cement & Finishing	c. Financial perspectives
d. Lack of adequate finance	d. Overruns
e. Lack of supervision from government institutions	e. Customer satisfaction
f. Technical issue	f. Business perspective
● Improper planning and design	● Number of housings delivered
● Administration and Organization culture	● Impact of sales volume
● Infrastructure	● Impact of occupancy rates
● Project management factors and environment factors	g. Delay in handing over housing
g. Unnecessary rush in project execution	h. Community satisfaction
h. Policy implementation issue and monitoring	i. Interdepartmental coordination
i. Delay in acquiring land	j. Collaboration with developers
j. Lack of foreign exchange	k. Parallel processing of plans/ permits
k. Absence of proclamation and regulatory organ	
l. Lack of completeness of regulatory organ	
m. Lack of completeness of the contract agreement	
n. Lack of skilled manpower	
o. Political instability	
p. Lack of properly planned schedule and inventory	
q. Lack of coordination between project stakeholders	
r. Delayed payment from client	
s. Lack of incentives on land issues	
t. Lack of experienced person on the design review at municipality or sub city and permit issue	
u. Fluctuation on labor price and absence of labor index	
v. Lack of feasibility study before project starts	
w. Inadequate specification and procurement issues	

Table 4 Respondent's profile

Role in the RE	Count	%	Experience Years (General)	Count	%	Qualification	Count	%
Project manager	8	40	>10 years	11	45.8	BSc.	9	39.1
Office engineer	4	20	6-10 years	9	37.5	MSc.	13	56.5
Site engineer	1	5	2-5 years	4	16.7	Adv. Dipl.	1	4.3
			Total	24		**Total**	23	
Support service director	1	5	**Years (In RE)**	**Count**	**%**			
Design supervision and contract admin	2	10	>10 years	1	4.3			
Engineering department head	1	5	6-10 years	13	56.5			
Project coordinator	2	10	2-5 years	8	34.8			
Construction department head	1	5	< 2 years	1	4.3			
Total	23		**Total**	23				

Table 5 Responses on questionnaire survey

Initial category of the Real estates			**Rating the performance of the real estate company**			**Real estate performance monitoring**		
Category	**Count**	**(%)**	**Range**	**Count**	**(%)**	**Duration**	**Count**	**(%)**
Contractor	6	26.1	>90%	7	30.4	Daily	4	16.7
Real estate	9	39.1	90-60%	8	34.8	Weekly	11	45.8
Both	4	17.4	60-30%	5	21.7	Monthly	7	29.2
Share company	3	13.04	<30%	3	13.1	Quarterly	0	0
Other	1	4.36				Annually	2	8.3
Any support/ monitoring by governmental authorities			**How likely the chance of finalizing as per original schedule**			**Is feasibility study conducted before any concept design**		
Response	**Count**	**(%)**	**Response**	**Count**	**(%)**	**Response**	**Count**	**(%)**
Yes	10	43.5	Likely	5	21.7	Yes	19	86.4
No	13	56.5	Average	11	47.8	No	3	13.6
			Less likely	7	30.5			
			Not at all	0	0			

.

Table 6 Responses on Questionnaire survey – Housing delivery

Type of housing constructed			**Apartment housing delivery to date**			**Apartment blocks delivered**		
Villa	**Count**	**(%)**	**Range**	**Count**	**(%)**	**Duration**	**Count**	**(%)**
Yes	4	16	Delivered	10	41.7	<5	4	16.7
No	20	83	Not- delivered	14	58.3	20-50	3	12.5
For yes, Villa count						50-100	3	12.5
>1000	1	4.2				Not yet	14	58.3
50-100	1	4.2						
20-25	2	8.3						

Factors affecting the performance: Within the realm of performance influencers, the effects of these factors and their outcomes were analyzed. Subsequently, the data collected was organized and depicted graphically. Figure 3 demonstrates a deeper understanding of the significance of the factors that shaped the real estate industry according to the participants. It is apparent that the subsequent factors, stand as the primary five influencers of real estate performance in their respective order of importance.

1st- Material price fluctuation
2nd- Exchange rate fluctuation
3rd- Shortage of construction materials
4th- Shortage of foreign currency
5th- Political instability

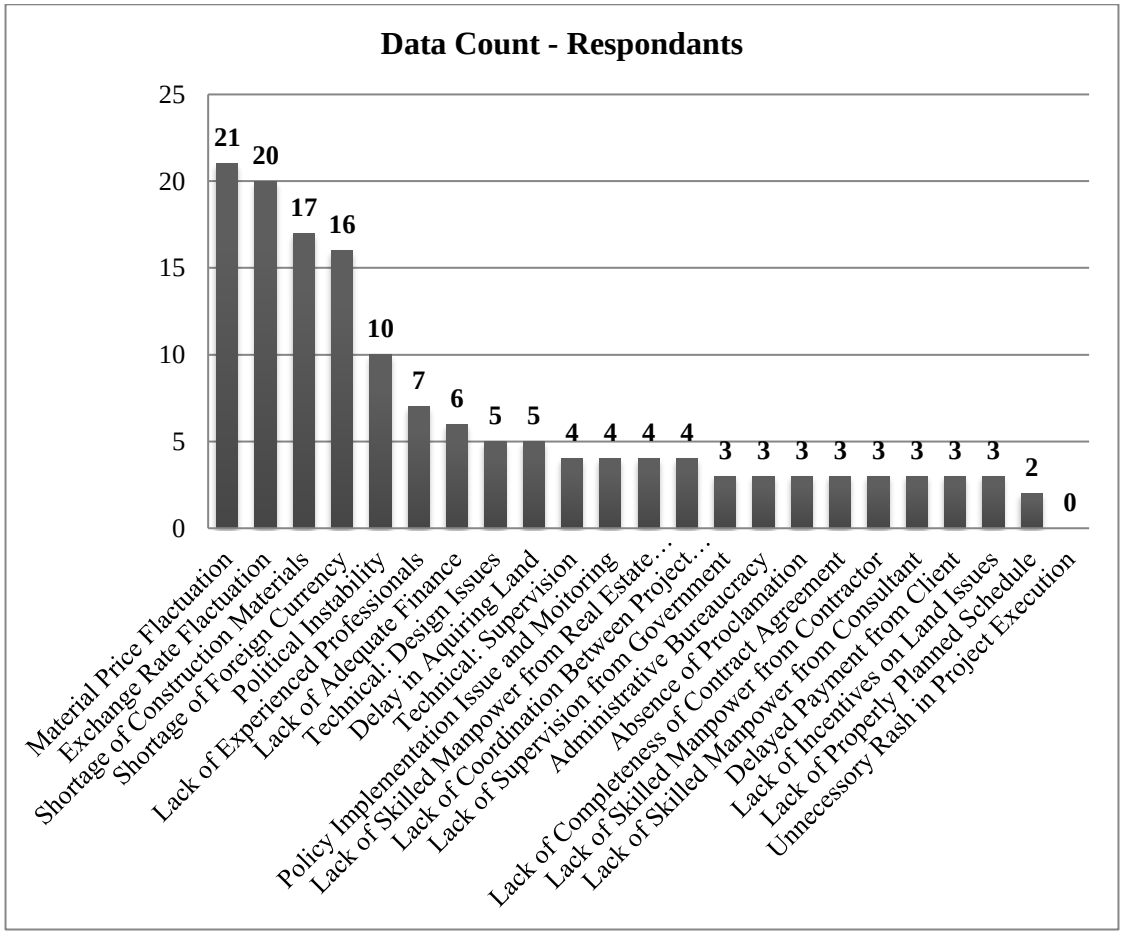

Figure 3 Factors affecting performance of residential real estate developers

Therefore, the factors identified as highly significant should be carefully addressed to prevent any obstacles to the success of the private residential real estate sector.

Performance measuring indices: The description of performance indices, their significance in performance monitoring and their prioritization based on questionnaire response data are detailed. The data is systematically organized utilizing a tally table, as depicted in Figure 4. The figure visually represents the importance of performance measuring indices and their

ranking according to the feedback received. Below are the top five performance index considerations that residential real estate developers should concentrate on based on the data count obtained.

1st - Customer satisfaction
2nd - Cost overruns
3rd - Financial perspectives
4th - Timely completion
5th - Community satisfaction

Generally, the current assessment indicates that the average project performance levels under inspection are substandard. There is a noticeable delay in project completion, with instances where projects scheduled for a 3-year duration extended to 5 years or more before handover. This evaluation specifically concerns residential real estate properties in Addis Ababa and is based on first hand observations and feedback from customers.

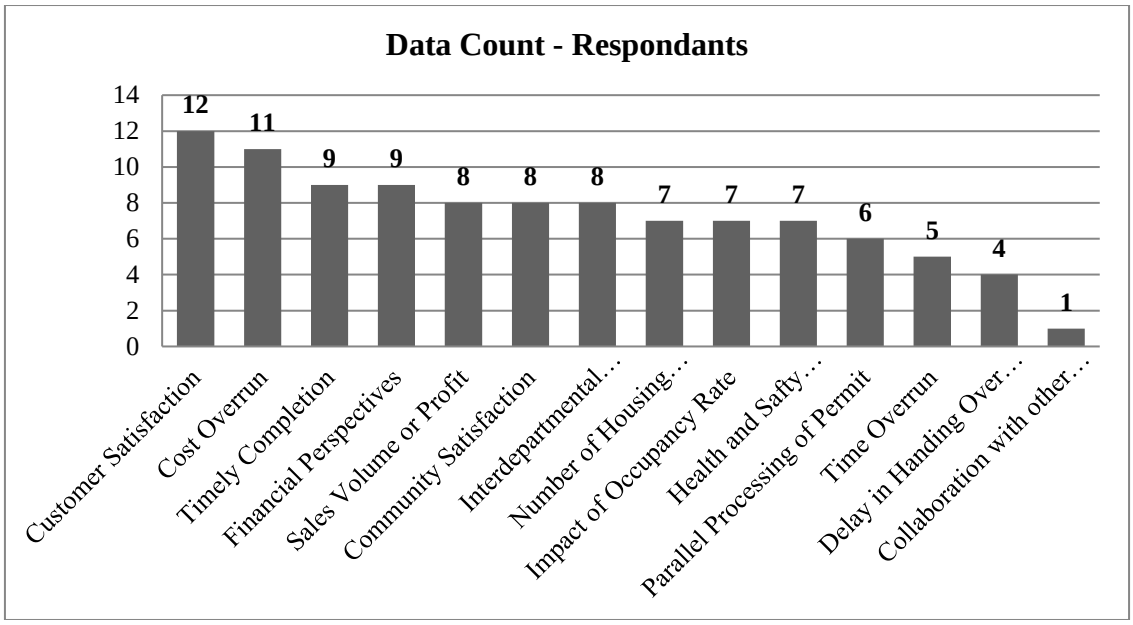

Figure 4 Rating performance index consideration

3.4.Discussion on Improvement Strategy to Boost the Real Estate Industry

Real estate developers have identified various factors that are impeding their performance. To enhance their effectiveness, it is crucial to establish a comprehensive strategy and policy tailored not only from developed nations but also through conducting specific studies pertinent to the country. An argument concerning policies highlights that, on average, the informal sector's relative size in developing countries significantly surpasses that in developed nations [22]. Consequently, this disparity has implications on housing policies that have succeeded in developed countries but may not yield the same success in developing nations.

The research has collated valuable insights from developers, categorizing them as strategic enhancements. These enhancements address multiple areas of improvement required by all stakeholders involved in the construction sector to varying degrees, mainly indicating the necessity of collaboration among the government, real estate developers, consultant firms and financial institutions. Collaboration between the real estate sector and the government, potentially through a joint venture, could foster growth in the real estate industry and alleviate housing

shortages. Implementing Public-Private Partnerships in the housing sector can unlock the government's potential and bolster the private sector's capacity, including developers, financiers and suppliers. Engaging in open dialogues with stakeholders to resolve industry challenges is imperative. Offering special incentives and subsidy processes to real estate developers could help alleviate the acute housing shortage in conjunction with government efforts and financial institutions. These incentives might involve tax breaks on imported materials, for instance. Revising policies and procedures related to the real estate industry to foster a collaborative environment with developers can drive improvements, enhance design outcomes and facilitate professional oversight from governmental bodies. During the feasibility study by the developers, a master plan accessible to all real estate industry stakeholders is essential to prevent major project delays.

Ensuring peace and political stability in the country is paramount since a majority of local construction materials are transported from various parts of the country to Addis Ababa, which includes materials like sand and cement. The government should establish a mechanism to streamline developers' access to cement directly from cement factories. Simultaneously, incentives or subsidies should be provided for raw materials used in local production within the import or supply chain. For instance, in aggregate production, one potential solution could involve importing crusher plants with facilitation from the government. Concerning finishing materials, the majority are imported due to their quality and cost advantages over local options, aggravating the scarcity of local materials. Moreover, imported goods typically arrive through ports in Djibouti and Sudan. Therefore, research is necessary to explore alternative construction materials that address material shortages and cost challenges.

Addressing foreign currency issues and the currency policy set by the national bank demands meticulous attention. By doing so, the economic landscape can stabilize and mechanisms for monitoring and controlling price fluctuations will be clearly defined.

Land stands as a critical resource in housing development, necessitating careful attention from relevant authorities in land allocation and the revision of land policies and regulations. This approach could significantly reduce the purchasing price of housing units and commercial spaces, making them more affordable across all societal segments. Therefore, establishing a functional legal framework is essential to advance sector development. To this end, bureaucratic processes in government offices related to land acquisition, lease matters and permit procedures should be streamlined. Providing reliable utility services such as electricity, water, sewerage systems and permitting services are the major setbacks that require attention.

Contractors should embrace modern technology to enhance work quality and ensure timely project completion. Additionally, implementing a robust equipment management strategy can minimize construction equipment failures and breakdowns.

Consultants should prioritize accountability in their designs, ensuring completion with all necessary details. Emphasis should be placed on quality-focused design improvements that align with clients' needs. Customers and end-users should be closely involved from the initial design stages (from concept to final design package and interior design) to prevent unnecessary design modifications that could delay projects. Finalized designs, including interior design, before commencing construction is critical.

Integrating borehole water distribution design with sanitary and water distribution design is crucial due to limited water supply from municipal sources.

Implementing comprehensive regular project monitoring and evaluation software that integrates project management best practices with agreements for reliable performance analysis in the real estate construction industry is vital. Given the likelihood of design changes, particularly in finishing works, close monitoring of the design process is essential. Increasing the quantity of skilled workforce can effectively address various quality-related issues.

Ideally, design and construction firms should operate independently from real estate companies to ensure impartial progress checks and robust follow-up. Exploring value engineering options and engaging professional advisors for developments can be beneficial in economic and material decision-making. Moreover, ensuring the availability of skilled and efficient laborers is vital by providing incentives to workers and fostering motivation which is key for real estate developers. Monitoring their productivity (labor index) is also crucial. While construction projects generate employment opportunities, benefiting the community, they should also consider environmental and construction safety aspects.

Effective organization and clear communication within the real estate company are also essential. Every real estate firm should factor in the socio-economic landscape of the nation in their business development plans, prioritize customer satisfaction and adopt modern construction management practices over conventional methods. As the development of housing by real estate developers benefits the government, a sustainable strategy should be devised by drawing insights from other countries' experiences to improve the performance.

4. CONCLUSIONS

It is understood that the oversight by governmental bodies is notably limited regarding the real estate registry. New residential real estate developers are entering the market as contractors operating within the city without formal registration as real estate developers.

Among the factors scrutinized, primary obstacles impeding the performance of residential real estate developers include increase in material prices, fluctuations in exchange rates and shortages of construction materials. Over 80% of real estate developers concentrate solely on erecting individual apartment complexes rather than creating a space encapsulating the major infrastructures making up of an ideal real estate. Still, the collective performance in housing provision by residential real estate developers falls below average.

As per the analyzed metrics, principal considerations for gauging performance metrics encompass customer satisfaction and cost overruns. Thus, major supportive and improvement strategies are recommended to create the enabling environment for the real estate industry.

It is imperative to fortify institutional capabilities and governance frameworks to ensure the effective execution of housing strategies and regulations. Sustained endeavors in policy innovation, infrastructure investments and community engagement are indispensable for fostering sustainable urban development and housing security within the city.

The implementation of the PPP model in the housing development strategy and technology transfer is observed to significantly enhance the real estate sector. Academic engagement in researching

various parameters and refining the focus of specific variables to expedite change can be crucial in this regard.

Furthermore, it is advisable that the construction industry and real estate sector be overseen by impartial, independent and responsive professional associations to facilitate consistent evolution and enhancement.

CONFLICT OF INTEREST

The authors declare that there is no conflict of interest.

ACKNOWLEDGEMENTS

The authors acknowledge the Research and Technology Transfer Office of Addis Ababa University for the financial support, the Government Investment Agencies for providing relevant data and the real estate developers for the valuable inputs during the survey.

REFERENCES

[1] World Bank, "*World development report: The consequences of rapid population growth*", 2014, pp. 79-105, doi:10.1596/9780195204605

[2] Desmond, M., "*Evicted: Poverty and Profit in the American City*", Crown Publishers, 2016.

[3] Andy, N., Chris A. and Mike K., "*The Performance Prism: The Scorecard for Measuring and Managing Business Success*", 2002.

[4] Smith, J., *"The project lifecycle of private real estate developers"*, Journal of Real Estate Development, 2020, https://doi.org/10.1234/jred.2020.15.2.123.

[5] Doe, J., "*Review of elements of the real estate housing supply process: Urban Planning Review", 2023*, pp. 75-92. https://doi.org/10.5678/upr.2023.8.2.75.

[6] Thurairajah, N., Wadugodapitiya R. and Sandanayake, Y., *"Building Project Performance Evaluation Model"*, School of Built Environment, 2016.

[7] Ombaba, B. and Daniel I., *"An Empirical Examination of the Effect of Mortgage Financing on Performance of the Real Estate Sector in Kisumu City, Kenya"*, 2019, MSc thesis, Jomo Kenyatta University of Agriculture and Technology.

[8] Pawlos, B., "*Study on private residential real estate development in Addis Ababa*", 2011, MSc thesis, Addis Ababa University, Addis Ababa Institute Technology.

[9] Yao, H. and Pretorius, F., *"Demand Uncertainty, Development Timing and Leasehold Land Valuation: Empirical Testing of Real Options in Residential Real Estate Development"*, Real Estate Economics, vol. 42, no. 4, 2014, pp. 829-868.

[10] Hrelja, R., *"The Tyranny of Small Decisions: Unsustainable Cities and Local Day-To-Day Transport planning"*, Planning Theory & Practice, 2011, pp. 511–524, Malmö University, doi:10.1080/14649357.2011.626312

[11] Frew, M., *"Credibility of institutions in Addis Ababa (Ethiopia), effects of government policies on real estate developers"*, Journal of Ethiopian Civil Service University, 2016.

[12] Addis Ababa City Administration, "*Addis Ababa Housing Strategy 2022-2030*", Center for affordable housing finance in Africa, Addis Ababa, Ethiopia, 2022.

[13] Michail, K., Rachel, C., and Ghassan, A., *"Performance management in construction: a conceptual framework, School of Construction and property Management"*, MSc thesis, University of Salford, UK, 2001.

[14] Kuwait Finance House, *"KFH Report on Local Real Estate Market during Second Half of 2022"*, 2022.

[15] Fed, G., *"The Red-Hot Housing Market: the Role of Policy and Implications for Housing Affordability"*, The Blog: Unassuming Economist, 2022.

[16] Kaviya, B. and Hema, C.,*"Performance Management in Construction,"* Bharath University, International Journal of Innovative Research in Science, vol. 4, no. 4, 2015,

[17] Shashi, A., *"Handbook of research methodology,"* A compendium for scholar and researchers, India: Education ISBN: 978-1-5457-0340-3, 2017.

[18] Ajayi, O. and Olotuah, A., *"Housing challenges in Nigeria: An overview",* Journal of Housing and the Built Environment, 2019, pp. 45-67. https://doi.org/10.1007/s10901-018-09622-1

[19] World Bank, *"Vietnam affordable housing finance report: Affordable housing challenges and solutions",* World Bank Group World Bank., 2018.

[20] Ministry of Works and Urban Development (MOWUD), "*Alternative housing programs strategic package and proposal*", Addis Ababa, 2018

[21] Sekaran, U., *"Research methods for business: A skill building approach"*, 4th edition, Wiley & Sons Inc., 2003.

[22] Richard, A., *"Housing Policy in Developing Countries: The Importance of the Informal Economy"*, Department of Economics University of California, Riverside, 2008.

Performance Enhancement of *Kality* Wastewater Treatment Plant's Up Flow Anaerobic Sludge Blanket Reactor Using Surface Response Methods

Johnny Girma[1,*], Asie Kemal [1], Agizew Nigussie [1], Dionisis Mantzavinos[2], Zecharias Frontistis[3] , Alexandra A. Ioannidi[2], John Vakros[2], Ioannis D. Manariotis[4]

[1]School of Civil and Environmental Engineering , Addis Ababa Institute of Technology, Addis Ababa University, Addis Ababa, Ethiopia
[2]University of Patras, Department of Chemical Engineering, Greece.
[3]Department of Chemical Engineering, University of Western Macedonia, 50100 Kozani, Greece.
[4]University of Patras, Department of Civil Engineering, Patras, Greece.
**Corresponding author's E-mail address: johnny.girma@aait.edu.et*

DOI: https://doi.org/10.20372/zede.v42i.10182

ABSTRACT

The main aim of this study was to examine and optimize the performance of up flow anaerobic sludge blanket reactor (UASB) using the surface response method-central composite design (RSM-CCD). The influences of several operational parameters were considered, including temperature (0 to 30°C), organic loading rate (OLR) (1 to 3 kg COD/m^3·d), pH (6.3 to 7.8), and hydraulic retention time (HRT) (4 to 12h). The pilot-scale reactor had a volume of 48.8 L. The RSM-CCD was used for the determination of the number of runs and the optimization of operational parameters. According to the derived model, the reactor exhibited optimal results under the following conditions: Temperature (23.0°C), OLR (2.3 kg COD/m^3·d), pH (7.5), and HRT (11.4 h). Removals of 84.1 %, 99.9 %, and 100 % for chemical oxygen demand (COD), total suspended solids (TSS), and volatile suspended solids (VSS), respectively, were achieved using the optimized parameters. In comparison with the inlet concentrations, the outlet concentrations of volatile fatty acids (VFAs) and alkalinity decreased. Whereas, the outlet concentrations of sulfate ions increased, since the sulfur-reducing bacteria effect was hindered due to the anaerobic condition of VFA and alkalinity. Even though the removal efficiency of the locally utilized wastewater treatment plant employing a UASB reactor was set at 55 % and 70 % for COD and TSS, respectively, the experimental results showed that it was possible to achieve higher removal efficiency at psychrophilic temperatures for unregulated sewage by optimizing controllable operational parameters.

Keywords: Operational parameters Optimization; Performance enhancement; Surface response method; UASB reactor**.**

1. INTRODUCTION

UASB reactors are considered a common anaerobic treatment method for wastewater. In developing countries, the UASB reactor is viewed as an effective strategy for treating domestic and industrial wastewater [1, 2].

The primary goal of their use is to achieve high efficiency in removing organic and inorganic contaminants from wastewater [3]. For evaluating UASB performance, some common indicators include the removal efficiencies of COD, Biological Oxygen Demand (BOD), and TSS [4-6]. The locally existing wastewater treatment plant employing UASB reactor was designed for the removal efficiency of 55 % for COD, BOD_5 and 70 % for TSS at 20°C but the OLR and HRT were not fixed. Since the set removal efficiencies of the UASB reactor for COD, BOD, and TSS were below global practices, enhancing the removal

efficiencies of the UASB reactor presents a challenge. Several studies have examined the optimization of UASB reactors. Some studies identified temperature as the sole factor affecting the efficiency of the UASB reactor [7-9], while others considered only HRT as the parameter affecting UASB performance [10-12]. Other studies investigated the effects of two operational parameters, such as temperature and OLR, on the efficiency of UASB reactors [13-15]. However, due to the nature of anaerobic biological systems, the performance of UASB reactors is not a simple function of two or three operational parameters; rather, it is influenced by a combination of controllable and uncontrollable parameters.

The seasonal variations also result in the concentration differences and the HRT needed for removal of the pollutants [16]. The research took seasonal differences into account to improve the performance of the UASB reactor. Data were collected for rainy seasons for 30 different operational parameters and surface response method central composite design was used for optimization of operational parameters and data analysis.

The main aim of this research was optimization of operational parameters such as temperature, HRT, OLR, and pH, and their interactions on the efficiency of the UASB reactor in removing COD, VSS, and TSS. The combinational effects were also observed in the removing of alkalinity, VFA, VFA-to-alkalinity ratio, and sulfate ion concentrations.

1.1. Effects of operational parameters

Microorganisms used in wastewater treatment operate at psychrophilic (0 to 30°C), mesophilic (30 to 45°C), and thermophilic (45 to 70°C) temperatures. Anaerobic treatment is possible in these three temperature ranges, and generally, the removal efficiency of anaerobic reactors increases as the temperature shifts from psychrophilic to mesophilic conditions [17, 18].

In a UASB reactor, an appropriate OLR should be maintained to enhance the COD removal efficiency, biogas production, and process stability. A decrease in OLR would result in a gradual rise in pH. Conversely, an increase in OLR increases the probability of contact between biomass and substrate, potentially leading to poor degradation of incoming COD [19]. HRT is the average retention time of wastewater inside the UASB reactor. It is one of the major parameters affecting the performance of anaerobic reactors treating municipal wastewater [20-22]. Prolonging HRT beyond a certain limit can produce granular sludge or might cause re-suspension of granules. However, a large HRT could be beneficial in shortening the start-up time of the reactor. On the other hand, biomass washouts can occur with short HRT [23, 24].

The pH in UASB reactors should be maintained between 6.3 and 7.8 to enhance methanogenesis due to the buffering capacity of the acid-base system [25, 26]. When the OLR is low in the UASB reactor, the pH will increase. To reduce the pH, the temperature should be changed from mesophilic to hemophilic conditions, demonstrating that pH affects the removal of COD, TSS, VFA concentration, and biogas production in UASB systems [27].

The present work examined the effects of temperature, HRT, OLR, and pH, and their interactions on the efficiency of the UASB reactor in removing COD, VSS, and TSS. The combined effects were also observed in the removal of alkalinity, VFA, VFA-to-alkalinity ratio, and sulfate ion concentrations.

2. MATERIALS AND METHODS

2.1. Chemicals and materials

The influent and effluent COD concentrations were determined according to the Standard Methods for the Examination of Water and Wastewater, using medium (0-1500 mg/L) and high range (0-15,000 mg/L) COD kits provided by Hach. NaOH and H_2SO_4 were used to adjust the pH of the raw wastewater during the experiments. A Hach DR890 Colorimetric instrument and relevant medium kits (0-700 mg/L) were used to measure the influent and effluent concentrations of sulfate ions. Alkalinity was measured using Alkaphot tablets and a Palintest 7100 photometer. The pH was measured using a pH meter purchased from Hach.

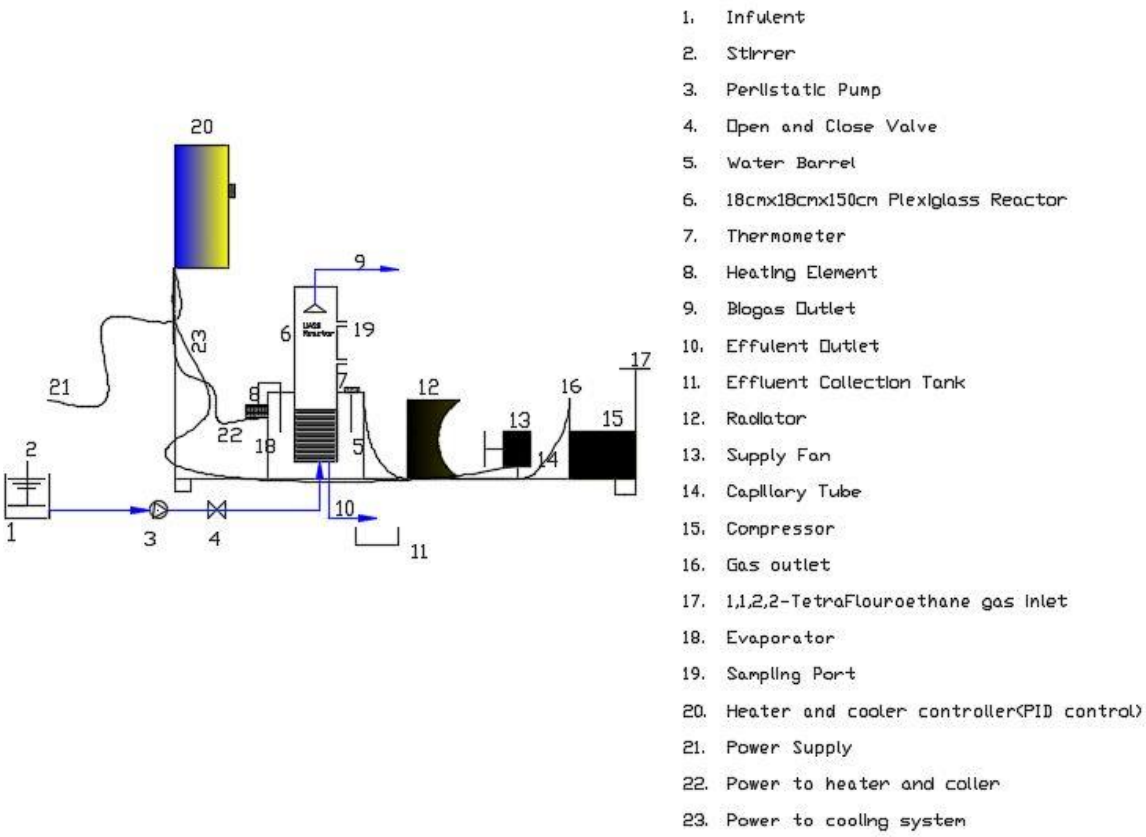

Figure 1 Process integrated derivative control board with pilot scale UASB reactor,fan, radiator ,compressor and barrel filled of water

2.2. Experimental reactor set up

The configuration of the pilot-scale reactor used is shown in Figure 1. The UASB reactor consisted 100 L water-filled barrel and evaporator installed atthe sides of the barrel. The evaporators were attached with compressors, radiators, and a supply fan mounted outside the setup to lower the temperature to the appropriate value.

A 2500 W heater was fitted inside the water-filled barrel and used to elevate the temperature when needed. The control board panel(PID) included thermostat, temperature sensors and timer. The heating,cooling system, sensors, and power sources were all linked to the Process Integrated Derivatives control board. The control board was the central control unit of the pilot-scale UASB reactor, managing temperature, HRT,

heating, and cooling systems. The determination of initial COD concentration of the sample wastewater was used in the HRT determination, which was later became input into the timer. The thermostat was used to set the desired temperature, estimated from the CCD-RSM, and the sensor measured the temperature of the wastewater in the barrel. Inside the barrel, a 0.0486 m³ square reactor was submerged and filled with wastewater. This reactor volume was chosen because it was not possible to obtain a larger capacity compressor for cooling, and heating the wastewater in the barrel. The barrel was wrapped with aluminum foil to maintain a stable wastewater temperature inside the reactor and the water temperature in the barrel. One benefit of the employed system was that it made it possible to integrate the PID board for data collecting through temperature control using HRT and heating and cooling systems. The reactor setupintegrated to the PID board could operate independently, but the influent for the reactor setup was sourced from the WWTP using UASB reactor.

2.3. Inoculation of the pilot-scale UASB reactor

Starting up a UASB reactor typically takes nearly four months [28]. However, in this experimental study, 10 L of sludge from the sludge blanket of an operating UASB reactor was extracted and inoculated into the UASB reactor.

2.4. Sampling Methods

The grab sampling method was used to determine the influent and effluent concentrations. For all runs, influent samples were collected daily in the early morning from the inlet of a WWTP employing a UASB reactor. The effluent concentration for every run was determined from the UASB after the wastewater remained for the specified OLR, temperature, pH, and HRT. For each experimental run, samples were taken twice. The first sample was taken at half of the determined HRT, and the second at the end of the experiment. The influent and effluent concentrations of VFA, sulfate ions, and VFA to alkalinity ratios were measured to control the UASB reactor's functionality.

2.5. HRT Determination

After determining the initial COD, the wastewater should remain in the reactor setup for the predetermined duration before taking the effluent sample. The HRT can be calculated using the following equation [29]:

$$HRT = \frac{So}{OLR} * 24 * 10^{-3} \quad (1)$$

where:

OLR is in kg COD/m^3.d,

S_o is initial COD concentrations in mg/L,

HRT is in hours.

2.6. Operational parameters

The effects of various operating parameters like temperature (0°C to 30°C), HRT (4 hours to 12 hours), OLR (1 kg COD/m^3·d to 3 kg COD/m^3·d), and pH (6.3 to 7.8) were investigated to increase the performance of UASB for psychrophilic temperatures for the treatment of unregulated sewage during the rainy seasons [30, 31]. The range of the parameters examined (see Table 1) was chosen according to the literature and the instrumentation used [32].

Table 1 Five levels of RSM-CCD and coded parameters [41]:

Parameters	Code	Levels of CCD-RSM				
		-α	-1	0	+1	+α
Temperature, °C	A,	-15	0	15	30	45
OLR, kg COD/m^3.d	B	0	1	2	3	4
pH	C	5.55	6.3	7.05	7.8	8.55
HRT, hrs	D	0	4	8	12	16

2.7. Response Surface Methodology and process efficiency

Response Surface Methodology using Central Composite Design (RSM-CCD) was employed to estimate the effects of four operational parameters (temperature, OLR, HRT, and pH) and their interactions on the removal efficiency and to further optimize the system. RSM-CCD was constructed and analyzed using Stat-Ease, Inc. software, version 13.0.1 (Minneapolis, USA). RSM-CCD was used because it allows the estimation of the main effects and their interactions using a minimal number of experiments compared to the one-factor-at-a-time analysis (30 experiments in our case) [33,34] reducing cost of chemicals and time needed for experiments. COD, TSS, pH, VSS, VFA, sulfate ion concentration, and alkalinity were measured as response factors. The following formula was used to determine the efficiency of the pilot-scale UASB reactors: [35].

$$\% \text{ Performance efficiency of UASB Reactor} = \left[\frac{C_{influent} - C_{effluent}}{C_{influent}}\right] * 100 \quad (2)$$

where:

$C_{influent}$ −is the concentration of raw influent (mg/L)

$C_{effluent}$ −Concentration of effluent (mg/L)

2.8. Statistical analysis

According to the RSM-CCD used for the design of the experiments, data analysis, and optimizations [36, 37], there are five levels for each operational parameter. The coding is from -α to +α (-α, -1, 0, +1, +α). Each parameter was coded as follows:

Temperature as (A), OLR as (B), pH as (C), and HRT as (D) [38]. The following formula was used to determine the total number of pilot-scale experimental runs:[39,40].

$$N = K^2 + 2k + C_0 = 4^2 + 2*4 + 6 = 30 \quad (3)$$

where:

N- represents the total runs,

K- is the operational parameters considered;

C_o- is center point.

Table 2 HRT values obtained using Eq. (1), inlet COD and %COD removal for 30 experimental runs

Experimental number	Temperature (℃)	pH	OLR (kg COD/m^3.d)	HRT (hrs.)	Inlet COD (mg/L)	%COD removal
1	-5	7.05	2	9.60	800	10.00
				4.8		5.01
2	0	6.30	3	12.00	980	15.52
				6.00		6.23
3	0	6.30	3	3.22	403	0.00
				1.61		0.00
4	0	6.30	1	12	500	72.40
				6.00		25.52
5	0	6.30	1	16.00	1250	70.85
				8.00		44.85
6	0	7.80	3	4.56	570	34.10
				2.28		24.23
7	0	7.80	3	6.24	780	30.24
				3.12		24.36
8	0	7.80	1	13.20	550	74.11
				6.6		52.32
9	0	7.80	1	16.00	1570	62.20
				8.00		6.96

Experimental number	Temperature (℃)	pH	OLR (kg COD/m^3.d)	HRT (hrs.)	Inlet COD (mg/L)	%COD removal
10	15	7.05	4	8.00	1333	78.20
				4.00		29.65
11	15	7.05	0	0.00	0	0.00
				0.00		0.00
12	15	8.55	2	11.52	960	96.08
				5.76		45.96
13	15	7.05	2	0.00	1000	0.00
				0.00		0.00
14	15	7.05	2	10.20	850	73.64
				5.10		45.21
15	15	7.05	2	14.40	1200	70.52
				7.20		28.32
16	15	7.05	2	11.52	960	11.52
				5.76		9.65
17	15	7.05	2	16.00	1333	62.65
				8.00		35.51
18	15	7.05	2	15.12	1260	70.00
				7.56		42.21
19	15	7.05	2	8.00	667	72.25
				4.00		25.91
20	15	7.05	2	8.00	667	72.45
				4.00		32.10
21	15	5.55	2	13.44	1120	99.25
				6.72		52.54
22	30	6.30	3	12.00	1500	93.86
				6.00		52.96
23	30	7.80	3	6.72	840	87.14
				3.36		45.78
24	30	7.80	3	5.84	730	82.55
				2.92		58.54
25	30	6.30	3	7.68	960	81.00
				3.84		23.52
26	30	7.80	1	15.60	650	100
				7.80		55.23
27	30	7.80	1	10.08	420	95.32
				5.04		45.96
28	30	6.30	1	7.44	310	62.01
				3.72		36.65
29	30	6.30	1	12.00	500	97.41
				6.00		54.78
30	45	7.05	2	14.70	1225	50.00
				7.35		29.52

2.9. Modeling COD, TSS and VSS

In general, RSM-CCD methodology developed the following mathematical model for % COD, %TSS and % VSS removal [42, 43].

$$Y = \beta_0 + \sum_{i=1}^{k}(\beta_i x_i) + \sum_{i=1}^{k}\left(\beta_{ii} {x_i}^2\right) + \sum_{i=1}^{k} \sum_{i=1}^{k} \beta_{ij} x_i x_j + \varepsilon \quad (4)$$

Where Y-is the variable for the experimental response, β_0-is the intercept, β_i, β_{ii} and β_{ij} are the regression coefficients for the linear effect, double interaction, and quadratic effects respectively. xi and xj are the independent variables (experimental variables), and ε represents random error.

The appropriateness of the model equations estimated from CCD-RSM for predicting COD, TSS, and VSS was assessed using analysis of variance (ANOVA) [44]. Specifically, the Coefficient of Variation (CV), Coefficient of Determination (R^2), Adjusted Coefficient of Determination (adj-R^2), and Prediction Coefficient of Determination (pred-R^2) were used to examine the quality of the model developed.

3. RESULTS AND DISCUSSION

3.1. Experimental Validation

To evaluate the validity of the obtained model, triplicate experiments (supplementary material) were conducted at the optimal point according to the RSM-CCD design with the following conditions: temperature of 23.0°C, OLR of 2.23 kg COD/m^3·d, pH of 7.50, and HRT 11.4 hours. The experimental values were 84.1% for COD, 99.9% for TSS and 100 % for VSS, which were very close to those predicted by the RSM-CCD model (83.0 % for COD, 99.2 % for TSS, and 100 % for VSS). One common method for estimating a model's capacity to predict overall removal efficiency involves computing the coefficient of determination R^2. Models exhibiting excellent predictive accuracy, as indicated by minimal differences between experimental and modeled values, typically have R^2values close to one [45].

The quadratic model proposed by the RSM-CCD methodology, as compared to the linear model derived from the linear combination of input variables, demonstrates superior accuracy. This is evident from the values of R^2 (the ratio of explained sum of squares (ESS) to the total sum of squares (TSS), R^2= ESS/TSS), Adjusted R^2= (1-[(1-R^2)*(n-1) (n-k-1)]) where 'n' is the experimental observations and k is the predictor variables and Predicted R^2=(1-(PRESS/TSS)) where PRESS is predicted sum of squares are presented in Table 3. Furthermore, according to the ANOVA, the second-order polynomial model, which includes the coded variables A, B, C, and D was statistically significant.

Table 3 Quadratic and linear models R^2 comparison

Quadratic		Linear	
R^2	0.9977	R^2	0.5259
Adjusted R^2	0.9956	Adjusted R^2	0.4719
Predicted R^2	0.9863	Predicted R^2	0.2704

3.1.1. *COD Model output by RSM –CCD*

The % COD removal model is shown as:

$$\%\ COD = 70.5749 + 18.0757A - 7.9972B + 6.9780C + 15.2942D + 12.5759AB + 6.9919AD - 3.1719BC - 11.1343BD - 7.8575CD - 19.5888A^2 + 6.5013B^2 + 4.8995C^2 - 9.4604D^2 \quad (5)$$

The model, with coded parameters A, B, C, D, AB, AD, BC, BD, CD, A^2, B^2, C^2, and D^2, was statistically significant, with a p-value less than 0.05 at the 95% confidence level. A single parameter or the interplay of operational parameters, which might have a positive or negative impact on the model, affected the % removal of COD. The 'F'-test by Fisher was utilized for the ANOVA analysis. The significance of the model was confirmed as its F-value was found to be 465.21. There was only 0.01 % chance that such a large F-value could occur due to noise. In the model, the probability statistics obtained were less than 0.0001. The lack of fit F-value of 232.69 suggested that it was

not significant relative to the pure error. There was a 5.13% chance that this large could occur due to noise. To evaluate the fit between experimental and modeled data, the adjusted R^2 determination coefficient value was estimated 0.9956. An adjusted R^2 close to one indicates that the developed model could approximate 99.56 % of the total variability in the percentage COD removal data. The signal-to-noise ratio was calculated using the fit statistics with sufficient precision. A ratio greater than four was preferred. The adequate precision ratio of 68.89 in this model indicated an adequate signal, suggesting that the proposed model can adequately describe the COD reduction within the range used.

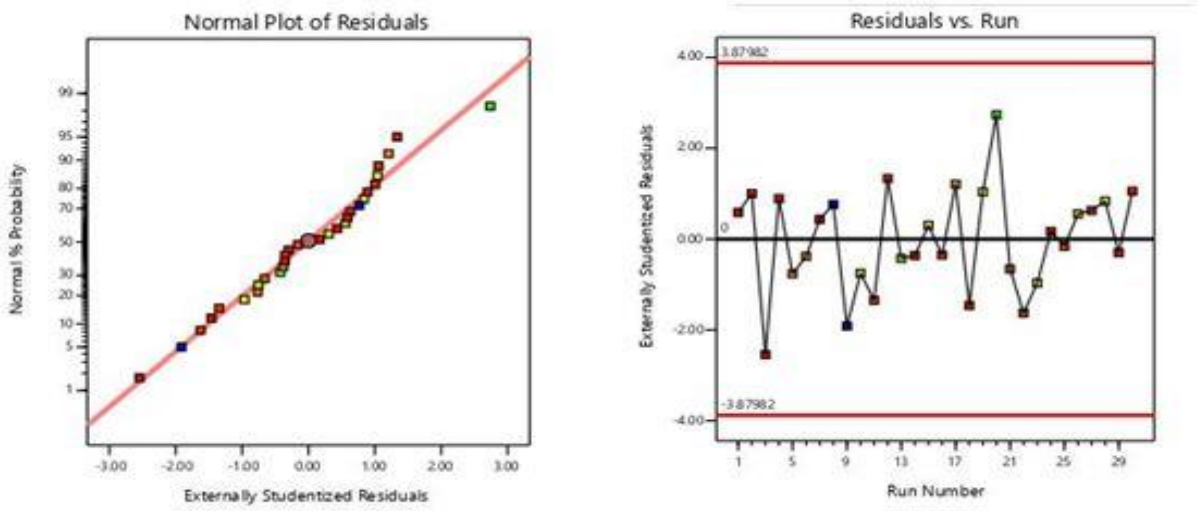

Figure 2 Studentized residuals against collected experimentally collected data

To further illustrate the appropriateness of the model, a plot was created to compare the predicted percentage removals with the studentized residuals. The values ranged between ±3.90, as shown in Figure 2. The plot demonstrates that the model excellently fits the experimental data.

3.1.2. *TSS Model out-put by RSM-CCD*

Similar to COD, Eq. (6) shows the TSS removal model elaborated from the RSM-CCD methodology.

$$\% TSS = 94.9013 - 5.5261A - 8.8758C + 18.3182D + 3.7210AB + 5.6324AC + 7.2205AD - 3.9458BC - 3.3562BD + 6.3232CD - 6.4446A^2 - 12.7649D^2 \quad (6)$$

Equation (6) clearly shows that the TSS percentage removal is influenced either by linear or double interactions of parameters. These parameters can impact the model either negatively or positively, as indicated by their coefficients in the equation.

3.1.3. *VSS Model out puts by RSM-CCD*

Finally, Eq. (7) shows the VSS removal model equation obtained from RSM-CCD methodology.

$$\% VSS = 88.1682 - 7.0277A + 4.4879B + 22.4402D + 7.3832AD - 3.2492A^2 - 9.7178D^2 \quad (7)$$

Single and double interactions of parameters had a negative or positive effect on the percentage removal of VSS, as indicated by the coefficients of the input parameters.

3.2. Model generated Results

A percentage removal for COD ranging from 0 to 98.6%, TSS ranging from 0 to 100%, and VSS ranging from 0 to 99.9% was predicted by the obtained model. The goal of the current research was to improve the performance of the UASB reactor in relation to the surrounding temperature. A temperature of 23.0°C, OLR of 2.23 kg COD/m^3.d, pH of 7.5, and HRT of 11.4hrs were determined as the optimal operational parameters.

3.3. Combined effects of parameters on percentage COD removal

3.3.1. *Combined effect of temperature and OLR*

Figure 3 (a) shows the concurrent effects of OLR and temperature on the removal efficiency of COD which is obtained using Eq. 5. The COD removal efficiency increases from 20 to 80 % as the organic load increases from 1 to 3 kg COD/m^3.d and the temperature rises to 30°C [46]. At a constant OLR of 1 kg COD/m^3·d, increasing the temperature from 0 to 30 decreases the COD removal efficiency from 80 % to 70 %. This reduction is attributed to a decrease in OLR, not temperature. Microorganisms consume substrates more efficiently at higher OLRs, enhancing COD removal efficiency. Maintaining OLR at 3 kg COD/m^3·d and reducing temperature from 30 to 0°C alters the working mechanism of the WWTP necessitating acclimatization and a startup phase [47, 48]**.** At a constant OLR of 3 kg COD/m³·d and a temperature of 0°C, COD removal efficiency decreases from 85 % to 20 %, a drop due to the reduced temperature [49].

Figure 3(b) depicts the interaction effect of HRT and temperature. As HRT increases from 4 to 12 hours and temperature from 0 to 30°C, COD removal efficiency improves from 30 % to 85 %. Maintaining HRT at 4 hours and increasing temperature from 0 to 30°C, COD removal efficiency falls from 85 % to 38 %, a decrease due to shortened HRT [50, 51]. Furthermore, keeping HRT at 12 hours and temperature at 0°C, the efficiency of COD removal drops from 85 % to 30 %, this decline in COD removal attributable to decrease in temperature. The interaction between pH and temperature is presented in Figure 3(c). Increasing pH from 6.3 to 7.8 and temperature from 0 to 30°C boosts COD removal efficiency from 45 % to 80 %. However, with a constant pH of 6.3 and increasing temperature from 0 to 30℃, COD removal efficiency decreases from 80 % to 65 %, a decrease due to lower pH levels [52]. If temperature remains constant at 0℃ and pH increases from 6.3 to 7.8, COD removal efficiency drops from 85 % to 45 %, a decrease resulting from the lower temperature.

Figure 3(d) shows the interactions between OLR and pH. Increasing OLR from 1 to 3 kg COD/m³·d and pH from 6.3 to 7.8 results in a decrease in COD removal efficiency from 100% to 78. Keeping OLR at 3 kg COD/m³·d and lowering pH from 7.8 to 6.3 decreases COD removal efficiency from 78% to 69 %, a reduction due to the lower pH. Figure 3(e) reveals the combined effects of OLR and HRT for COD removal. Increasing OLR from 1 to 3 kg COD/m³·d and HRT from 4 to 12 hours reduces COD removal efficiency from 100 % to 64 %. Maintaining OLR at 3 kg COD/m³·d and HRT at 4 hours decreases COD removal efficiency from 64% to 58 %, a decrease attributed to the reduced HRT [53]. Figure 3(f) presents the combined effect of HRT and pH for COD removal. Increasing pH from 6.3 to 7.8 and HRT from 4 to 12 hours

improves COD removal efficiency from 80% to 82%. However, keeping HRT at 4 hours and increasing pH from 6.3 to 7.8 decreases COD removal efficiency from 82 % to 65 %, a reduction attributed to the shortened HRT [54]. The fit summary response, lack of fit tests, ANOVA for the quadratic model response, fit statistics, and 3D surface percentage removal for TSS and VSS are provided in supplementary materials.

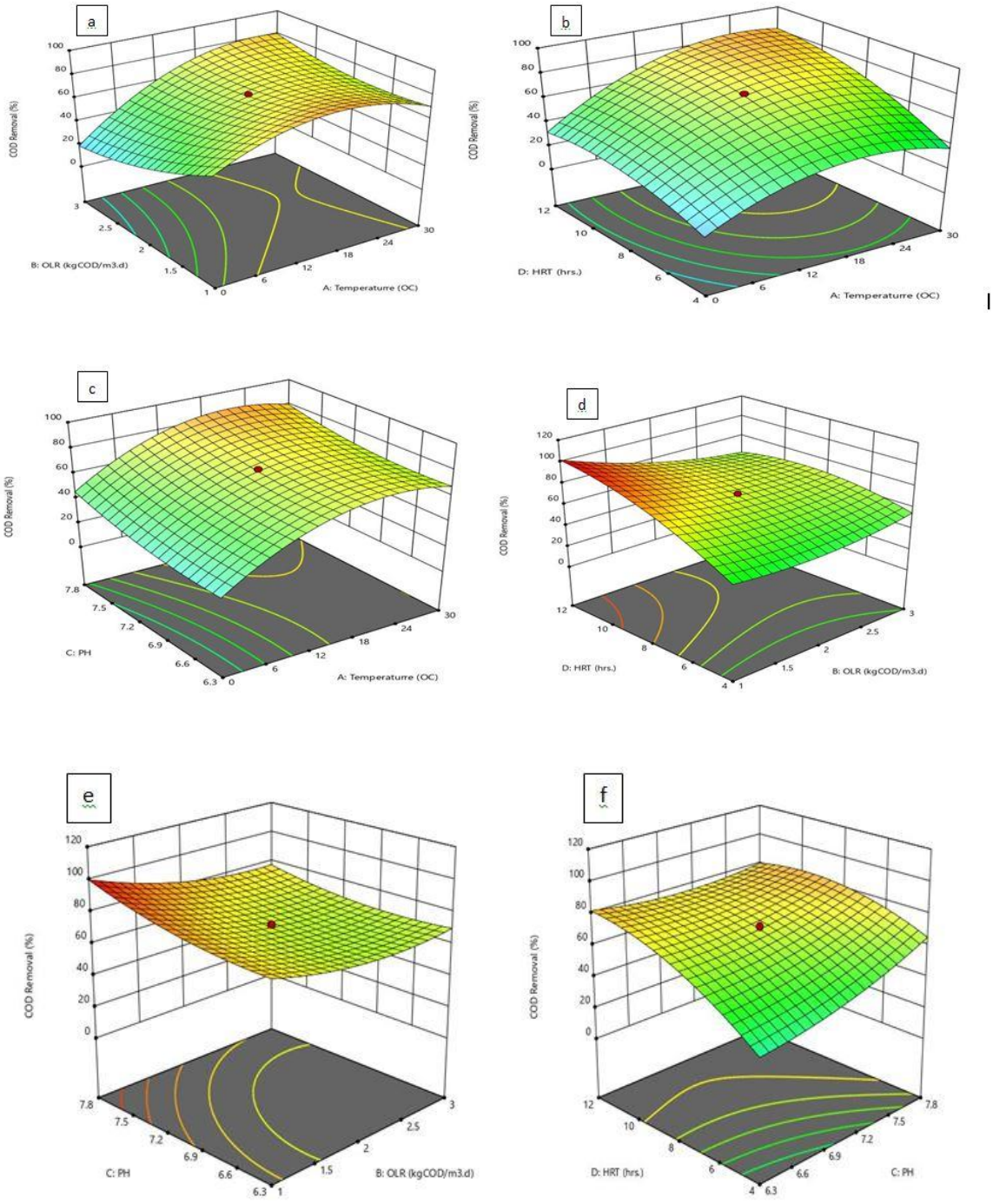

Figure 3 Response 3D surfaces for %COD removal (a) OLR vs. Temperature (b) HRT vs. Temperature (c) PH vs. Temperature (d) HRT vs. OLR (e) pH vs. OLR (f) HRT vs. pH

3.4. Sulfate ion (SO_4^{2-}) Concentration

In this research, the effluent SO_4^{2-} ion concentration was greater than the influent concentration. This phenomenon was attributed to the high rate of methanogenesis, which inhibits the activity of sulfur-reducing bacteria, and showing that the reactor set-up was well functioning [55, 56].

Table 4 Inlet and outlet sulfate ion concentrations

No	Temperature (°C)	OLR (kg COD/m^3.d)	HRT (hrs.)	pH	Inlet SO_4^{2-} (mg/L)	Outlet SO_4^{2-} (mg/L)
1	30	3	12	6.30	6.0	80
2	30	1	10.08	7.80	23	52
3	30	3	7.68	6.30	21	80
4	30	3	6.72	7.80	29	70
5	30	3	5.84	7.80	70	80
6	30	1	7.44	6.30	33	80
7	30	1	15.60	7.80	30	20
8	30	3	12.00	6.30	43	80
9	15	2	11.52	8.55	37	80
10	15	0	0.00	7.05	0.0	0.0
11	15	4	8.00	7.05	19	72
12	15	2	8.00	7.05	22	0.0
13	15	2	8.00	7.05	22	76
14	15	2	16.00	7.05	28	61
15	15	2	10.20	7.05	26	66
16	15	2	11.52	7.05	26	67
17	15	2	15.12	7.05	20	54
18	15	2	14.40	7.05	28	51
19	15	2	0.00	7.05	28	56
20	15	2	13.44	5.55	26	54
21	0	3	3.22	6.30	70	80
22	0	3	4.56	7.80	50	80
23	0	3	12.00	6.30	21	80
24	0	3	6.24	7.80	25	75
25	0	1	12.00	6.30	59	80
26	0	1	13.20	7.80	53	80
27	0	1	16.00	6.30	45	59
28	0	1	16.00	7.80	28	73
29	-5	2	9.60	7.05	45	5.0
30	45	2	14.47	7.05	27	22

At a temperature of -15°C, pH of 7.05, OLR of 2 kg COD/m³·d, and HRT of 9.6 hours, it was observed that the outlet SO_4^{2-} ion concentration significantly decreased. This is attributed to the fact that at extremely low temperatures, the activity of anaerobic microorganisms diminishes [57].

3.4.1. VFA to Alkalinity ratio

The VFA to alkalinity ratio was observed to be in the range of 0.055 to 0.15. This indicates that the UASB reactor was operating under normal conditions. In the system, saprophytes break down complex molecules, producing acids such as acetic,

propionic, and butyric acids. The alkalinity in the solution neutralizes hydrogen ions released by these acids and methanogenesis subsequently takes over to maintain the pH balance.

At a temperature of -15°C, pH of 7.05, OLR of 2 kg COD/m^3.d, and HRT of 9.58 hrs, the outlet volatile fatty acid to alkalinity ratio was out of the set range since acid genesis and methanogenesis were inhibited by decreasing temperature.

Table 5 Volatile fatty acid to alkalinity ratio

Expt. no	Temperature (°C)	OLR (kg COD/m^3.d)	HRT	pH	$\frac{in\ let\ VFA}{Alkalinity}$	$\frac{out\ let\ VFA}{Alkalinity}$
1	30	3	12.00	6.30	0.080	0.075
2	30	1	10.08	7.80	0.090	0.065
3	30	3	7.68	6.30	0.065	0.060
4	30	3	6.72	7.80	0.090	0.065
5	30	3	5.84	7.80	0.060	0.050
6	30	1	7.44	6.30	0.090	0.140
7	30	1	15.60	7.80	0.090	0.060
8	30	3	12.00	6.30	0.098	0.080
9	15	2	11.52	8.55	0.100	0.150
10	15	0	0.00	7.05	0.000	0.000
11	15	4	8.00	7.05	0.088	0.060
12	15	2	8.00	7.05	0.080	0.060
13	15	2	8.00	7.05	0.055	0.080
14	15	2	16.00	7.05	0.090	0.088
15	15	2	10. 20	7.05	0.100	0.080
16	15	2	11.52	7.05	0.099	0.054
17	15	2	15.12	7.05	0.080	0.090
18	15	2	14.40	7.05	0.060	0.090
19	15	2	0.00	7.05	0.000	0.000
20	15	2	13.44	5.55	0.100	0.067
21	0	3	3.22	6.30	0.090	0.060
22	0	3	4.56	7.80	0.089	0.075
23	0	3	12.00	6.30	0.043	0.020
24	0	3	6.24	7.80	0.080	0.053
25	0	1	12.00	6.30	0.086	0.050
26	0	1	13.20	7.80	0.120	0.050
27	0	1	16.00	6.30	0.055	0.053
28	0	1	16.00	7.80	0.060	0.050
29	-5	2	9.60	7.05	0.110	0.095
30	45	2	14.47	7.05	0.106	0.103

4. CONCLUSIONS

According to the results derived from the RSM-CCD the main factors influencing the performance of the pilot UASB reactors were the following operational parameters: Temperature (0 -30°C), OLR of (1- 3 kg COD/m^3.d), pH of (6.3-7.8), and HRT of (4-12hrs). CCD-RSM with five levels was used to optimize these operational parameters. An optimized operational parameter of temperature (23.0°C), OLR of (2.23 kg COD/m^3.d), pH of (7.5), and HRT of (11.4 hrs) were achieved. Using optimized operational parameters, 84.1 % for COD, 99.9 % for TSS and 100 % for VSS were obtained. The CCD-RSM predicted a

removal efficiency of 83.0, 99.2, and 100 %, for COD, TSS, and VSS. Furthermore, the influent and effluent concentration of sulfate ions, total nitrogen, alkalinity, total phosphorous, VFA, pH, and volatile fatty acid to alkalinity ratio, were measured to check the functionality of the pilot scale reactor set up. Relative to the influent concentration, the effluent concentration of volatile fatty acid and alkalinity were decreasing. The reason was as microorganisms break the organic compounds, acids like acetic, propionic and butyric acids were produced and release hydrogen which later accepted by the alkalinity to maintain the pH by methanogenesis. The effluent concentration of sulfate ion (SO_4^{2-}) was seen increasing since the activities of sulfur reducing bacteria were hindered due to anaerobic conditions created by acid, and alkalinity. This creates higher production of methane gas than hydrogen sulfide. In general, there is a possibility to increase the removal efficiency of the WWTP employing UASB reactor by optimizing operational parameters such as temperature, HRT, pH and OLR without incurring energy. This can be achieved practically either through dilution of the wastewater at an inlet by the service water or heating the wastewater using the solar panel. The amount of heat energy needed and the source of energy will be the future potential research.

CONFLICT OF INTEREST

No conflict of interests exists between the authors

ACKNOWLEDGEMENT

The authors are grateful to Addis Ababa University, University of Western Macedonia and University of Patras for the support provided.

REFERENCES

[1]. Kaviyarasan, K. "*Application of UASB Reactor in Industrial Wastewater Treatment–A Review*". Int J Sci Eng Res. 2014, pp. 584-589. http://www.ijser.org/researchpaper/

[2]. Cruz-Salomón, A., Ríos-Valdovinos, E., Pola-Albores F, et al. *"Expanded granular sludge bed bioreactor in wastewater treatment"*, 2019, pp. 119-138. doi:10.22034/gjesm.2019.01.10

[3]. Doong, R. Lee, S., Lee, C., Sun, Y., Wu, Se. "*Characterization and composition of heavy metals and persistent organic pollutants in water and estuarine sediments from Gao-ping River*", Taiwan. Mar Pollut Bull. 2008; pp. 6-12. doi. 10.1016/j.marpolbul.2007.12.015

[4]. Sushma and Pal, J. "*Performance of UASB reactor at different flow rate treating sewage wastewater*", Int J Chem Tech Res. 2013; pp. 676-681.

[5]. Rizvi, H., Ahmad, N., Abbas, F., et al. "*Start-up of UASB reactors treating municipal wastewater and effect of temperature/sludge age and hydraulic retention time (HRT) on its performance*". Arab J Chem. 2015; pp. 8. doi.org/10.1016/j.arabjc.2013.12.016

[6]. Musa, M., Idrus, S., Hasfalina, M., Daud, N.N.N. "*Effect of organic loading rate on anaerobic digestion performance of mesophilic (UASB) reactor using cattle slaughterhouse wastewater as substrate*", Int J Environ Res Public Health. 2018; pp. 15. doi:10.3390/ijerph15102

[7]. Álvarez, A., Armstrong, E., Presas, J/, Gómez, M., Soto, M. "*Performance of a UASB-digester system treating domestic wastewater*". Environ Technol. 2004; pp.1189-1199. doi: 10.80/095933325086183

[8]. Ojoawo, O., Udayakumar, G. Physico-Chemical Characterization of Dry-

"*Weather-Flow Wastewater and Assessment of Treatment Plants in Nitte and Environs*", Civ Environ Res Environ Res. 2015, pp. 56-66.

[9]. Reino, C., Carrera, J,. "*Low-strength wastewater treatment in an anammox UASB reactor*", Effect of the liquid upflow velocity. Chem Eng J. 2017; pp. 313. doi:10.1016/j.cej.2016.1

[10]. Yoochatchaval, W., Kubota, K, Kawai,, T, Yamaguchi, T, Syutsubo K. "*Treatment of Sugar Containing-Low Strength Wastewater at 20°C by Anaerobic Granular Sludge Bed Reactor*", Water Pract Technol. 2010, pp. 5. doi:10.21662010.055

[11]. Ahmad, A., Ghufran, R., Abd,. Wahid, Z. "*Effect of cod loading rate on an upflow anaerobic sludge blanket reactor during anaerobic digestion of palm oil mill effluent with butyrate*", J Environ Eng Landsc Manag. 2012; pp. 20. doi:10.3846/16486897.2012.656647

[12]. Jijai, S., Srisuwan, G., O-Thong, S., Ismail, N., Siripatana C. "*Effect of Granule Sizes on the Performance of Upflow Anaerobic Sludge Blanket (UASB) Reactors for Cassava Wastewater Treatment"*, vol 79. Elsevier B.V.; 2015. doi:10.10162015.11.48

[13]. Matangue, M.T.A., Campos, C.M.M. "*Determination of kinetic parameters of an upflow anaerobic sludge blanket reactor (UASB), treating swine wastewater*", Cienc e Agrotecnologia. 2011; pp. 1204-1210.

[14]. Pandya, P., Sharma AK, Sharma S, Verma, S. "*Effect of operational and design parameters on removal efficiency of a pilot-scale uasb reactor treating dairy wastewater*", J Ind Pollut Control. 2011; pp. 103-111.

[15]. Zhang, S.J., Liu, N.R., Zhang CX. "*Study on the performance of modified UASB process treating sewage*", Adv Mater Res. 2013;610-613, pp. 2174-2178.

[16]. Girma, J., Kemal, A., Nigussie, A. "*Performance enhancement of up-flow anaerobic sludge blanket reactor for psychrophilic temperature during the dry season: Kality wastewater treatmentplant*", Heliyon. 2023; pp. 9: e19781.

[17]. Elmitwalli, T., Zeeman, G., Lettinga , G. "*Anaerobic treatment of domestic sewage at low temperature"*, Water Sci Technol. 2001; pp.44.

[18]. Schultz, J., Jensen, A.L., Pinheiro, A., Da Silva JD. m. *Proc - 2015 9th Int Conf Complex, Intelligent, Softw Intensive Syst CISIS 2015*. pp. 398-401. doi:10.11092015.57

[19]. Parthasarathy, P., Narayanan SK. "*Effectof Hydrothermal Carbonization Reaction Parameters on. Environ ProgSustainEnergy"*, 2014;pp.676-680. doi:10.1002/ep

[20]. Farajzadehha, S., Mirbagher,i S.A., Farajzadehha S, Shayegan J. "*Lab Scale Study of HRT and OLR Optimization in UASB Reactor for Pretreating Fortified Wastewater in Various Operational Temperatures*", *APCBEEProcedia*.2012;pp.9095. doi:10.10162012.03.016

[21]. Manariotis, I.D., Grigoropoulos, S.G. "*Anaerobic Filter Treatment of Municipal Wastewater: Biosolids Behavior*", J Environ Eng. 2006; pp. 1323. doi:10.106107339372132

[22]. Manariotis ID, Grigoropoulos SG. "*Restart of anaerobic filters treating low-strength wastewater"*, Bioresour Technol. 2008; pp.3579.

doi:10.1016/j.biortech.2007.07.048

[23].Ladu, J.L.C., Lü, X.W. "*Effects of hydraulic retention time, temperature, and effluent recycling on efficiency of anaerobic filter in treating rural domestic wastewater*", *Water Sci Eng*. 2014;pp.68. doi:10.388216742370.2014.02.005

[24]. Daud, K, Rizvi, H., Akram, M.F., et al. "*Review of upflow anaerobic sludge blanket reactor technology: Effect of differentparameters and developments for domestic wastewater treatment*", *J Chem*.2018. doi:10.1155/2018/159631

[25]. Ali, M.A.G. "*Problems encountered during the start-up of up flow anaerobic sludge blanket reactors (UASB) at 20 ^0C & 15 ^0C*". Adv Food Sci Sustain Agric Agroindustrial Eng. 2020; pp. 3. doi:10.21776/ub.afssaae.2020.003.01.

[26]. Barceló-Quintal, I, Salazar-Peláez, M., García-Albortante, J., Garza-González, M. "*Performance of an UASB Reactor at Lab-Scale Treating Domestic Wastewater with Low Concentrations of Copper",* Appl Sci Technol. 2015; pp. 7. doi:10.97342015/152

[27]. Loganath, R., Mazumder, D. "*Performance study on organic carbon, total nitrogen, suspended solids removal and biogas production in hybrid UASB reactor treating real slaughterhouse wastewater*", J Environ Chem Eng. 2018; vol. 6, no. 2, pp. 3474-3484. doi:10.10162018.05.031

[28]. Pererva, Y., Miller, C.D., Sims, R.C. "*Approaches in design of laboratory-scale uasb reactors*", Processes. 2020; vol. 8, no.6, pp. 12. doi.org/10.3390/pr8060734

[29]. Resolutions taken at the World "*Conference on Lung Health B 1990. Resolutions taken at the World Conference on Lung Health, Boston 1990*", Bull Int Union Tuberc Lung Dis. 1990; pp. (2-3). doi:10.10162022.09.274

[30]. Azbar, N., Tutuk, F., Keskin, T. "*Effect of organic loading rate on the performance of an up-flow anaerobic sludge blanket reactor treating olive mill effluent*", Biotechnol Bioprocess Eng. 2009; pp.14. doi:10.100712257-008-0065-9

[31]. Arthur, P.M.A., Konaté, Y., Sawadogo, B., et al. "*Performance evaluation of a full-scale upflow anaerobic sludge blanket reactor coupled with trickling filters for municipal wastewater treatment in a developing country",* Heliyon. 2022; pp.8. doi:10.1016202210129

[32]. AKTOR. VOLUME 1 "*OPERATION & MAINTENANCE MANUALS SECTION B AAWSA-Water and Sanitation Development and Rehabilitation Project Office PROJECT*": Kaliti Wastewater Treatment Plant-Civil and Electromechanical Works-Design Supply and Built VOLUME 1 OPERATION & MAINTENAN. Published online 2017.

[33]. Sharma, .P, Sivaramakrishnaiah, M., Deepanraj, B., Saravanan, R., Reddy, M.V. "*A novel optimization approach for biohydrogen production using algal biomass*", Int J Hydrogen Energy. 2022. doi:10.10162022.09.274

[34]. Spruce, L., Lee, J.Y., Greco, T.M., Cohen, S.L., Seeholzer, S.H. Number of Runs. 2009; pp.27

[35]. Kim, Y., Cho, H., Choi, Y., Koo, J., Lee, S. "*Optimization and Evaluation for the Capacitive Deionization Process of Wastewater Reuse in Combined Cycle Power Plants*", Membranes. 2023; pp.13. doi:10.3390/membranes13030316

[36]. Rahman, S.M.A., Sharma, P., Said, Z. "*Application of Response Surface Methodology Based D−optimal Design for Modeling and Optimisation of Osmotic Dehydration of Zucchini"*, Vol 4. Elsevier Ltd; :pp. 100039. doi:10.101620221000

[37]. Alkhatib, M.F., Mamun, A.A., Akbar, I. "*Application of response surface methodology (RSM) for optimization of color removal from POME by granular activated carbon*", Int J Environ Sci Technol. 2015; vol. 12, no. 4, pp. 1295-1302. doi:10.100713762-014

[38]. Zhao, B.H., Yue, Z.B., Zhao, Q.B., et al. "*Optimization of hydrogen production in a granule-based UASB reactor*", Int J Hydrogen Energy. 2008; vol. 33, no. 10, 2454, pp. 2461.

[39]. Chollom, M.N., Rathilal, S., Swalaha, F.M., Bakare, B.F., Tetteh, E.K. "*Comparison of response surface methods for the optimization of an upflow anaerobic sludge blanket for the treatment of slaughterhouse wastewater,*" Environ Eng Res. 2020; pp.114-122. doi:10.44912018.366

[40]. Ansari K, Shrikhande A, Malik MA, et al. "*Optimization and Operational Analysis of Domestic Greywater Treatment by Electrocoagulation Filtration Using Response Surface Methodology*", Sustain. 2022; pp. 14 doi:10.3390142215230

[41]. Bui, H.M. "*Applying response surface methodology to optimize the treatment of swine slaughterhouse wastewater by electrocoagulation*", Polish J Environ Stud. 2018; pp. 1975-1981. doi:10.1524478440

[42]. Bashir, M.J.K., Amr, S.S.A., Aziz, S.Q., et al. "*Wastewater Treatment Processes Optimization Using Response Surface Methodology (RSM) Compared with Conventional Methods*", Middle-East J Sci Res. 2015; pp. 244-252. doi:10.58292015.23.02.5

[43]. Bashir, M.J.K., Aziz, H.A, Aziz, S.Q., Amr SA. "*An overview of wastewater treatment processes optimization using response surface methodology (RSM)*", *4th Int Eng Conf*. 2012; pp. 8. doi:10.100713762

[44]. Tripathi, B.D., Sikandar, M., Shukla, S.C."*Physico-chemical characterization of city sewage discharged into river Ganga at Varanasi, India*", Environ Int. 1991; pp. 469. doi:10.1016/0160412090281

[45]. Nair, A.T., Makwana, A.R, Ahammed, M.M. "*The use of response surface methodology for modelling and analysis of water and wastewater treatment processes: a review*", Water Sci Technol. 2014; pp. 464-478. doi:10.2166/wst.2013.733

[46]. Besharati, F.M., Mirbagheri, S.A., Pendashteh, A., Alavi, J.. "*Biological treatment of slaughterhouse wastewater: Kinetic modeling and prediction of effluent"*, J Environ Heal Sci Eng. 2019; pp. 731-741. doi:10.100740201019-003894.

[47]. Daija, L., Selberg, A., Rikmann, E., Zekker, I., Tenno, T., "*The influence of lower temperature, influent fluctuations and long retention time on the performance of an upflow mode laboratory-scale septic tank*", Desalin Water Treat. 2016; pp. 1867-1868. doi:10.10801944399420151094 4

[48]. Zwain, H.M., Barghash, H., Vakili, M, Majdi, H.S., Dahlan, I. "*Modeling and optimization of process parametric interaction during high-rate anaerobic digestion of recycled paper mill wastewater using the response surfacemethodology*", Water Reuse.

2022; vol. 12, no. 1, pp. 7-9. doi:10.2166.2022.088

[49]. Zhang, L., De Vrieze, J., Hendrickx, T.L.G., et al. "*Anaerobic treatment of raw domestic wastewater in a UASB-digester at 10 °C and microbial community dynamics*", Chem Eng J. 2018; pp.33-42. doi:10.1016201711073

[50]. Bhatti, Z.A., Maqbool, F., Malik, A.H., Mehmood, Q. "*UASB reactor startup for the treatment of municipal wastewater followed by advanced oxidation process"*, Brazilian J Chem Eng. 2014; vol. 31, no. 3, pp. 715. doi:10.1590/0104-6632.20140313s00002786

[51]. Ma, B., Peng, Y., Zhang, S., et al. "*Performance of anammox UASB reactor treating low strength wastewater under moderate and low temperatures*", Bioresour Technol. 2013; 129: pp. 606. doi:10.1016/j.biortech.2012.11.025

[52]. Paltahe, A., Cornelius, T., Sambo, B., et al. "*Physico-Chemical Characterization of Local Tannery Waste Water Before and After Flocculation Treatment"*, Int J Chem. 2019; vol. 11, no. 2, doi:10.5539/ijc.v11n2p77

[53]. Cunha, M.P., Ferraz, R.M., Sancinetti, G.P., Rodriguez, R.P. "*Long-term performance of a UASB reactor treating acid mine drainage: effects of sulfate loading rate, hydraulic retention time, and COD/SO 42− ratio*", Biodegradation. 2019; pp. 4758. doi:10.100710532-018-9863-8

[54]. Leitão, R.C., Silva-Filho, J.A., Sanders, W., van Haandel, A.C., Zeeman, G, Lettinga, G. "*The effect of operational conditions on the performance of UASB reactors for domestic wastewater treatment*", Water Sci Technol. 2005; pp. 52. doi:10.21662005.0531

[55]. Sun. J/, Dai. X/, Wang./ Q, Pan. Y/, Ni B/J. "*Modelling Methane Production and Sulfate Reduction in Anaerobic Granular Sludge Reactor with Ethanol as Electron Donor*," Sci Rep. 2016; pp. 18. doi:10.103835312

[56]. Li, W.W.,and Yu, H.Q. "*Advances in Energy-Producing Anaerobic Biotechnologies for Municipal Wastewater Treatment. Engineering"*, Env. Protection Review. 2016; pp. 4. doi:10.1016/J.ENG.2016.04.017

[57]. O'Flaherty, V., Collins, G., Mahony, T. "*The microbiology and biochemistry of anaerobic bioreactors with relevance to domestic sewage treatment*", Rev Environ Sci Biotechnol. 2006; pp. 5. doi:10.10071115700554788

Comparative Assessment of the Effects of Plant Based Gums on Rheological Characteristics of Maize Dough and its Bread Quality

Tullo T. Ketaso[1, 2], Kumsa D. Kuffi[1,*]

[1]*School of Chemical and Bio Engineering, Addis Ababa Institute of Technology, Addis Ababa University, Addis Ababa, Ethiopia.*
[2]*School of Agricultural and Food Engineering, Department of Food Engineering, Ambo University.*
**Corresponding author's E-mail address: kumsa.delessa@aait.edu.et*

DOI: https://doi.org/10.20372/zede.v42i.10183

ABSTRACT

Bread made from maize is considered as gluten free and thus recommended for people living with celiac disease. However, bread made from maize has inferior quality when compared to bread made from wheat. The aim of this investigation was to explore how plant-based gums affect the rheological attributes of dough made from maize flour and the resulting bread quality. Various types of plant gums were used at a ratio of 3 % to the flour weight basis. Control samples were prepared using maize and wheat flours. To provide a basis for comparison, dough and bread samples made from wheat flour were also used. The study examined the farinographic, pasting, gaseous release and dough development characteristics. Proximate composition, loaf specific volumes, texture character, and sensory qualities of bread were also examined. The inclusion of gums in maize flour reduced the dough's water absorption capacity (WAC) and degree of softening (DS). Treatment with gums also had a considerable impact on most of the pasting profile. Furthermore, treatment with gums improved bread loaf weight and specific volumes. The firmness of the maize bread was higher than the maize bread prepared from the dough samples treated with gums.

Keywords: Bread quality; Celiac disease; Gum; Maize; Rheological property.

1. INTRODUCTION

These days, celiac disease is considered in many nations as one of the main health issues [1]. It affects the mucosa and the lining of the small intestine, which prevents the body from absorbing certain nutrients, most notably wheat gluten [2]. Consumption of gluten protein from commonly available food sources such as wheat, rye and barley may cause celiac disease in people having problems linked to gluten consumption [3]. Approximately1-2 % of the global population is affected by celiac disease, and the most effective solution for managing it is the development of breads that are free from gluten [4].

One of the most significant proteins that build structure is gluten, which gives wheat-based products their desirable structure and quality as well as their dough-like quality [5]. It is responsible for extensibility, elasticity, mixing tolerance, resistance to elongation, and gas holding ability of doughs. Using alternative ingredients that adds the aforementioned qualities to breads made from gluten free cereals is required.

Among the food grains, maize is the most abundant and cheapest crop, particularly in Sub-African nations like Ethiopia. With 17-20 % of the total calories consumed, it gives consumers the largest portion of their calorie intake. However, maize lacks gluten, and thus bread made from maize has low quality

as compared to bread made from cereals rich in gluten such as wheat [6].

Complete replacement of wheat flour with maize flour does not result in viscoelastic dough when kneaded in conventional method for bread-making. Hence, they create batter as a replacement compared to dough. Unlike the popular wheat bread, the batter tend to lose carbon dioxide gas during backing process, which result in decreased loaf's unique volume, moisture content and crumb hardness[7].

To improve the quality of bread made from maize and its mixture, various researchers have developed a range of gluten-free formulations by using starches, hydrocolloids, whey proteins, gums and emulsifiers as flour additives[3].

Bread baked without gluten, from maize and chickpea flours, used to be extensively expanded by addition of 3 % (w/w) hydroxypropyl methylcellulose (HPMC) [2]. According to previous study, hydrocolloid, carboxymethylcellulose (CMC) and xanthan gum mixing with flours increased unique extent and decreased crumb firmness of bread baked without gluten from formula containing maize, rice and soya flour [8]. Similarly, the addition of exceptional gums like guar, locust bean and xanthan gums with emulsifiers (Purawave & Datem) to rice dough increased its rheological characteristics significantly [9].

Furthermore, researcher on similar area reported that the incorporation of wheat and maize starch to rice flour extended the precise volume, style and over all acceptability of gluten free bread made from rice [10].

Although these findings have contributed a lot on how to solve the quality issues related to bread without gluten, the availability and affordability of the ingredients on which these studies were focused is still a big challenge for practical use in low- income countries. Therefore, the objective of this research was to examine the impact of gums derived from tree stems and branches on the overall quality and dough rheological characteristics of gluten-free maize based bread.

2. MAT ERIALS AND METHODS

2.1 Sample Collection and Preparation

2.1.1 Gums

About 2 kg of three gum samples, namely *Gumero* gum (GG), *Humera* gum (HG) and *Harar-Sidamo* gum (HSG), were procured from the Ethiopian Forestry Product and Agriculture Enterprise. These gums were produced from Acacia tree stems and branches grown in various regions of Ethiopia [11]. They were identified as nontoxic, odorless and tasteless natural product consisting of high molecular mass polysaccharides and their inorganic salts which hydrolyze to produce glucuronic acid, galactose, arabinose and rhamnose [12]. Before analysis, the gums were milled and dried to 14 % moisture content.

2.1.2 Flours

Maize was obtained from Holata Agricultural Research Center, and was milled with small scale hammer mill (England Model NO. 212/10 E) to pass through 0.05 mm sieve size. This flour was dried to 14 % moisture content, then enclosed in a polyethylene plastic bag and kept in laboratory shelf with lamination until used. Commercial wheat flour was procured from KOJJ Food Processing Complex (Addis Ababa, Ethiopia). Additional components like live yeast, table salt (edible quality), and sunflower seed oil were bought from the nearby markets in Addis Ababa.

2.2 Dough Preparation

The dough samples were made in accordance with method outlined in

previous study [8]. The recipe was: 97 g flour, 2 g sugar, 2 g salt, 3 g yeast, 170 mL water, and 3 % gum, on flour weight base, for gum treated doughs, and 100 g flour for the control ones, as shown in Table 1.

Table1 Ingredients used for dough samples preparation

Ingredients	Dough samples				
	C_1	C_2	T_1	T_2	T_3
Wheat flour (g)	100	---	---	---	---
Maize flour (g)	----	100	97	97	97
Yeast (g)	3	3	3	3	3
Sugar (g)	2	2	2	2	2
Salt (g)	2	2	2	2	2
Water (mL)	170	170	170	170	170
HG (g)	---	---	3	---	---
HSG (g)	---	---	---	3	---
GG (g)	---	---	---	---	*3*

C_1 & C_2 are control samples (without gum) made from wheat and maize flours, respectively while T_1, T_2 and T_3 are maize flours treated with HG, HSG and GG, respectively.

Dough preparation was done as follows: first, bowl used for mixing was washed and then rinsed with water. Then water, salt, sugar, yeast and gum were physically mixed in mixing bowel mixture after being added. Finally, flour was added and combined properly at 160 rpm for 10 min until the dough became smooth and elastic. The resultant dough was kept to ferment at room temperature for about 2 h. Then the fermented dough was divided into small sizes of 100 g, rounded and rested to proof in the fermentation chamber for 10 min at 30°C and 85 % relative humidity.

Breads were made at a temperature of 200°C in an oven for 40 min at (micro mini oven, Germany). Before undergoing a quality assessment, the breads were allowed to cool for one hour at a room temperature.

2.3 Pasting Property Analysis

The samples pasting characteristics were determined by using a rapid Visco-analyzer (Starch Master R & D pack, Anton par, France). For analysis of pasting property maize flours treated with HG, HSG and *GG* were denoted by P_1, P_2 and P_3, respectively. For this analysis, about 3 g flour sample with gums was used for each treatment. Flour was weighed and placed in an aluminum canister and 25 mL distilled water was added to it. Then, the material was rapidly blended for 30 s at 960 rpm with paddle and afterward, under continuous shear during regulated heating procedure and thereafter at 160 rpm during a controlled heating and cooling process under constant shear in the rapid visco-analyzer (RVA). In two minutes, the temperature rose from 50-95°C, then in another two minutes, it dropped to 50°C. Pasting parameters were read from the pasting profile using thermo cline software that was connected to a computer. Pasting parameters include peak viscosity, hold viscosity, breakdown viscosity, final viscosity (also known as paste viscosity) and setback viscosity [17].

2.4. Farinographic Characteristics Analysis

Farinographic characteristics of each flour were determined following the procedure of previous work [13]. For farinographic characteristics analysis, maize flours treated with HG, HSG and were denoted by F_1, F_2 and F_3, respectively. About 300 g of the flour sample was weighed and put in to the farinographic mixing bowl for this analysis. Known volume of distilled water was added to the flour and mixed to form dough. The farinograph recorded a curve on graph paper as the dough was mixed. The curve was centered on the 500 BU line ±20 BU by adding the appropriate amount of water and was run until the curve left the 500BU line. At the end of the test, the farinographic data

was recorded on a computer. WAC, dough development time (DDT), uniformity, stability, and softness level are among the parameters that are recorded. Each analysis was done in triplicate.

2. 5 Rheofermentor Test: Dough development and Gas release

Using rheofermentometer (Chopin Rheofermentometer F2, Tripette Renaud, France), the rheology of the dough throughout fermentation was assessed [14]. For this analysis, maize flours treated with HG, HSG and GG were denoted by R_1, R_2 and R_3 respectively. For analysis of gas release and dough development property, 250 g of each flour sample was weighed, which was then combined with water 5 g salt and 3 g yeast in 200 mL of distilled water. The doughs were fermented for 3h in a rheoferementor and then the total carbon dioxide released (CO_2), retained volume of carbon dioxide (*R*), maximum height of dough development (Hm), maximum height of gaseous emission ((H'm) and maximum height of dough at test completion were recorded.

2.6 Analysis of Bread Quality

2.6.1 Physical Characteristics of Bread

Specific volumes of bread

The American Association of Cereal Chemist (AACC) approved method 10.05 [13]. was used to measure the loaf volume and specific volume of bread using rapeseed displacement method by using the Eq. (1).

$$\text{Specific volume } \left(\frac{\text{cm3}}{\text{g}}\right) = \frac{Loaf\ volume}{Loaf\ weight} \qquad (1)$$

Crust Firmness of bread:

Using a 500N load cell, the texture analyzer was done (TA Plus, Lloyd Instruments, UK) [8].

2.6.2 Proximate Composition Determination

The ash and moisture content of the bread samples were ascertained using the method 925.09 and 923.03 [15], respectively. Association of Official Chemist AOAC approved Kjeldahl method 979.09, 4.5.01 and 962.09 were used for measuring Protein, fat and crude fiber content of bread respectively.

2.6.3. Sensory Analysis of the Bread

The sensory analysis was carried out using 10 semi trained panelists. They were conversant with a method of sensory evaluation .Using a 9 factor hedonic scale, the freshly baked breads were presented for the acceptance test [16]. Panelists had been requested to determine the breads for acceptance of color, aroma, flavor, taste, texture, and overall-acceptability to rank samples from 1 to 9, with 1 representing the least score (dislike extremely) and 9 the highest score (like extremely).

2.7. Statistical Data Analysis

The data gathered were analyzed through one-approach evaluation of variance (ANOVA). Duncan's multiple tests, which make use of the statistical package for social science (SPSS software) compares differences in means. A P-value of substantially less than 0.05 was formerly considered statistically significant. The mean ± standard deviation was used to express the results.

3. RESULTS AND DISCUSSION

3.1. Pasting Properties

Table 2 provides a summary of pasting characteristics made with the flour samples. The addition of the gums had a substantial impact on the pasting qualities of maize flour, as shown in the table, with the exception of pick time and pasting temperature.

Greater peak viscosity was seen in C_1 and C_2 than in maize flour combined with gums. When compared to its control counterpart, the peak viscosity of maize flour treated with 3 g HG was lowered by around 51%, as indicated in Table 2. Among the samples that were treated, samples treated with GG had a 430.50 RVU peak viscosity, followed by samples treated with HSG, which had a 487.50 RVU peak viscosity. Reduction in peak viscosity of the treated samples could be linked to the capacity of the gums to encapsulate starch granules and limit swelling during gelatinization process. Furthermore, the interactions between mixture's protein, fat and starch components as well as a decrease in starch may be the cause of the reduction in peak viscosity. The outcome agreed with previous findings [18].

According to the claim by previous researchers, interactions between the mixture's protein, fat, and starch components as well as a decrease in starch contribute to the reducing of the trough, break down, setback and, final viscosities [19]. Setback viscosity, which affects the texture of food products containing starch, is a good indicator of starch retro-gradation, or the re crystallization of amylose molecules. When starch paste cools, leached amylose molecules quickly combine to create the amylose connection zones of which then were to blame for the setback [20].

Gum addition significantly decreased the final, setback, trough, and breakdown viscosities of maize flour by 57.3, 15.2, 52.4, and 48.95 %, respectively. The combination of *HG* with maize flour showed reduced values of breakdown (16.85 RVU), setback (415.60 RVU), trough (332.90 RVU), and final (748.5 RVU) viscosities (Table 2).

Table 2 Effect of gums on pasting properties of control and treated flours

Pasting Sample	Parameters						
	Peak viscosity (RVU)	Trough Viscosity (RVU)	Breakdown Viscosity (RVU)	Final Viscosity (RVU)	Setback Viscosity (RVU)	Pasting temperature (°C)	Pick-time (s)
C_1	1489.50±0.71^a	815.50±0.71^a	672.00±2.83^a	1747.0±0.0^a	928.50±0.71^a	67.50±0.70^b	89.51±0.73^b
C_2	689.50±0.71^b	579.00±1.41^b	110.5±0.71^b	1428±0.71^b	849.50±0.71^b	80.75±0.35^a	94.95±0.71^a
P_1	349.75±0.35^e	332.90±0.14^e	16.85±0.21^e	748.5±0.71^e	415.60±0.85^e	80.50±0.00^a	94.43±0.11^a
P_2	487.50±0.71^c	433.50±0.71^c	54.00±1.41^c	996.0±0.00^c	562.50±0.71^c	80.00±0.00^a	94.90±0.14^a
P_3	430.50±0.71^d	408.50±0.71^d	22.00±1.41^d	873.00±1.4^d	464.50±0.71^d	79.90±0.14^a	94.53±0.35^a

All the values are mean ± standard deviation of triplicate analysis.
Means within the same column followed by different letter superscripts are different at 5 % level of significance.

The resistance of disintegration under heating and shearing is exhibited by the low breakdown viscosity displayed by the control and gum-treated maize flours. The creation of a gel network and the final viscosity of the cooled starch granules, especially amylose, indicate re-association during the chilling period after gelatinization [21].

The inclusion of gums had no discernible impact on the temperature of the paste or the pick-up time. However, it was discovered that maize flour, whether it included gum or not, had a substantially lower pasting temperature than wheat flour. The pasting temperature indicates the lowest temperature needed to cook the flour; the higher the pasting temperature, the more firmly connected and organized the starch granule structure will be [22].

In an earlier study, pasting characteristics of maize-starch were reported as 1836 cP, 2760

cP, 1074 cP, 924 cP, 2910 cP, 5.43 min and 75.80°C for trough viscosity, peak viscosity, set back viscosity break down viscosity, final viscosity, pick time and pasting temperature, respectively [23]. Pasting characteristics of the current study were less than the pasting characteristics reported in the previous study. In general, the low pasting property exhibited by dough combined with gums suggest they would be better suited for creating additional gluten-free product such as biscuit, cookies and cakes rather than to make gluten free bread of the same quality as wheat bread.

3.2. Farinographic, Gas release and Dough Development Properties

The results of dough farinography, out gassing character and dough spreading properties measured are shown in Table 3. As shown in this table, gums added at a 3 % concentration had a significant effect on the coloring properties of the dough. The control samples had significantly greater capacity to retain water than the gum treated one. Among the treated samples, GG treated sample had reduced water absorption capacity (52.95 %). Conversely though, HSG treated samples showed the maximum water-absorbing capacity (54.65 %). WAC of gum-treated samples may be due to low water-holding ability of the gum. According to pervious study, the incorporation of hydrocolloids (gums) increased the water-absorbing ability of rice flour from 60.5 % to 67 % [24]. Therefore, the results of this study did not match with prior findings due to the difference in water holding ability of gums used in present study and that used in previous study. The inclusions of gums greatly enhanced the maize flour's dough formation and stability times. The wheat dough produced the quickest development times (3.45 min), while the dough with HG produced noticeably longer development times (10.35 min).There was no noticeable difference found in the remaining dough samples [25]. A study on similar topic indicated that, dough protein level and dough development time are positively correlated, and strong dough has a longer dough development time [25]. Following the dough mixed with HG (16.55 min), the dough treated with GG had the high stability time (11.65 min). The stability value indicates the dough's strength and specifies a duration at which the dough maintains its maximum consistency. Furthermore, previous study showed that the longer the stability, the higher the force needed for mixing and the bigger the fermentation tolerance [26]. The integrations of gums resulted in reduction in softness value. The dough treated with HG softened substantially less (90.50BU) than the others. Dough with a softness values between 80 and 100 BU is frequently considered adequate [27]. This is due to the fact that the earlier the weakening occurs, the shorter the fermentation time and the less abuse the flour can bear [26]. The low WAC and degree of softness of the dough incorporated with gums suggest that they may be better suitable for manufacturing other gluten free products such as biscuit, cookies and cakes rather than to make gluten -free bread of equivalent quality to wheat bread. The results of the gaseous release and dough development properties of the maize flour during fermentation showed that the additions of gums greatly affected the gaseous release and dough development properties. The increased retention coefficient of the maize flour dough could be attributed to the gums' high gas retention ability. The inclusion of the gums greatly enhanced the Hm, H'm and h. The GG had a higher Hm (66.75 mm) than the other two gum types, although HSG had a higher H'm (7.00 mm) and h (3.10 mm). In terms of h values, there was no considerable difference between dough combined with HG (1.85 mm) and GG (1.65 mm). The h values

obtained from present study agree with the findings of previous study [28].

Table 3 Effects of gums on farinographic, gas release and dough development parameters of maize flour dough

Farinographic samples		**Farinographic parameters**			
		WAC (%)	DDT (min)	Stability (min)	DS (BU)
C_1		61.55 ± 0.21^a	3.45 ± 0.07^c	3.45 ± 0.07^c	151.50 ± 0.71^b
C_2		59.20 ± 0.42^b	4.45 ± 0.35^b	4.60 ± 0.42^c	193.00 ± 8.49^a
F_1		53.00 ± 0.14^d	4.75 ± 0.63^b	16.55 ± 1.77^a	90.50 ± 0.71^d
F_2		54.65 ± 0.07^c	4.15 ± 0.07^{bc}	10.25 ± 0.07^b	121.50 ± 0.71^c
F_3		52.95 ± 0.07^d	10.35 ± 0.07^a	11.65 ± 0.07^b	96.50 ± 0.71^d
Gas release and dough development Parameters					
Rheofermentor samples	V_{CO2} (ml)	RC (%)	Hm (mm)	H'm (mm)	h (mm)
C_1	1858.00±0.71^a	74.33±0.01^a	76.00±0.14^a	58.80±0.14^a	41.50±.71^a
C_2	1358.75±0.35^e	62.56±0.20^d	52.35±0.07^e	0.00±0.00^e	0.00±0.00^d
R1	1578.95±0.07^d	65.77±0.01^b	64.00±0.14^d	6.15±0.07^d	1.85±0.07^c
R_2	1662.50±0.71^b	65.61±0.01^b	65.35±0.07^c	7.00±0.14^b	3.10±0.14^b
R_3	1639.50±0.71^c	64.52±0.01^c	66.75±0.07^b	6.65±0.07^c	1.65±0.07^c

F_1-HG treated farinographic dough; F_2-HSG treated farinographic dough; F_3-GG treated farinographic dough; R_1-HG treated rheofermentor dough; R_2-HSG treated rheofermentor dough and R_3- GG treated rheofermentor dough.

3.4. Physical Characteristics of Bread

3.4.1. Specific Volume of Bread

Table 4 demonstrates the influence of the plant-based gums on the loaf weight and loaf volume of the loaves manufactured. The addition of gums had a substantial impact on the loaf volume and specific volume of the bread. The wheat bread had the maximum loaf volume (399.93 cm^3) and specific volume (2.85 cm^3/g), whereas the maize bread had the lowest value for both parameters. A significant ($P<0.05$) difference in loaf and specific volume were observed among the breads. The breads made with GG dough had much larger loaf and specific volume than the maize bread, but it had significantly lower loaf and specific volume than the bread sample made with HG and HSG treated dough. There was also significant difference in the loaf and specific volume of bread made from HG and HSG treated dough. The disparities in loaf and specific volume among the bread samples could be linked to the changes in the gas retention, water holding capacity, and gums fiber concentrations. According to Asghar et al. [29], the addition of gums enhances the loaf volume and specific volume of the bread. many factors influence specific volume and , including water, fiber, starch, and protein content of the flour, as well as processing aid [30].

Table 4 Effects of gum types on the loaf weight and loaf volume of bread

Bread Samples	**Parameters**		
	Loaf weight (g)	Loaf volume (cm^3)	Specific-volume (cm^3/g)
C_1	139.83 ± 0.25^e	399.93 ± 0.11^a	2.85 ± 0.00^a
C_2	149.50 ± 0.71^d	200.10 ± 0.14^e	1.33 ± 0.00^e
T_1	152.90 ± 0.14^b	297.95 ± 1.20^c	1.94 ± 0.00^c
T_2	155.23 ± 0.38^a	314.87 ± 0.18^b	2.03 ± 0.00^b
T_3	151.80 ± 0.23^c	288.77 ± 0.32^d	1.90 ± 0.00^d

3.4.2. Bread Texture

Firmness is a textural property related with bread crumb and is defined as the bread crumb's ability to deform in response to compression force [31]. The results of the crumb firmness of the bread are shown in Figure 1. It can be seen from the figure that incorporation of gums considerably reduced the bread firmness. The maize bread had the highest firmness value (18.09 N), followed by bread made from the GG treated dough (17.393 N).

Significant differences were also observed among breads made from dough treated with gums. Wheat bread produced the softest bread; with firmness value of 8.078 N. The decrease in bread hardiness, when compared to the control maize bread, is due to the high water and gas retention capacity of the gums, which results in a greater porosity of bread. The result on bread hardiness obtained in present study agrees with previous work on similar topic [17].

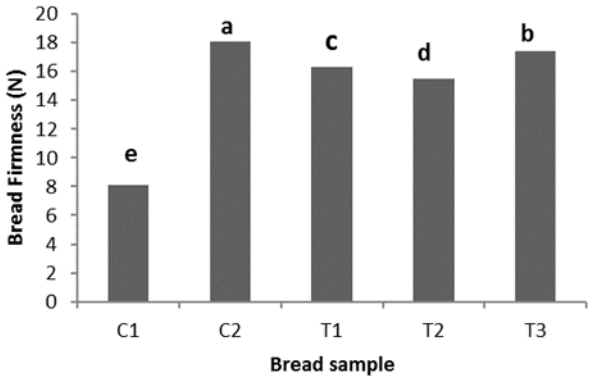

Figure 1 Effect of gums on the firmness values of breads

3.5. Proximate Chemical Composition and Sensory Attribute of Bread

Table 5 indicates the impact of various plant-based gums on the proximate composition, sensory properties, and overall acceptance of bread. It was discovered that the addition of gums had a significant influence on the bread moisture level. The wheat bread had the greatest moisture level (43.20 %), but it did not differ substantially from the HSG-treated dough bread.

The moisture level of bread manufactured from maize flour was much lower (35.95 %) than that of bread added with gums. The moisture content elevation of gum-containing bread could be linked to the gums' high water absorption ability when compared to maize bread. With respect to protein amount, wheat bread had a much greater protein content (13.71 g/100 g) compared to the others. According to the findings of this investigation, the inclusion of gums lowered the protein level of maize bread. However, there were statistically significant differences among the loaves made from gum-treated doughs.

When compared to the control and treated maize bread, the wheat bread had lower fat, ash, fiber, and total carbohydrate content. The inclusion of gums lowered the fat and total carbohydrate content of the maize bread while increasing the ash and fiber content. The maize bread had much higher fat value (2.72 g/100 g) than the GG treated dough bread sample. When compared to HSG (2.47 g/100 g) and HG (2.37 g/100 g), the bread sample made from GG dough had the lowest fat level (2.25 g/100 g) which could be linked to the variations in fat content among the gum types. The ash level of the maize bread (2.15 g/100 g) was similar to that of the breads made from HG (2.26 g/100 g) and GG treated doughs (2.26 g/100g), but it was less than that of the bread prepared from HSG treated dough (2.37 g/100 g) which indicates the mineral content of HSG is most probably greater than the maize flour and the other gums. The bread sample established from HSG treated dough, on the other hand, had much greater fiber level (7.61 g/100 g) than the samples prepared from the other gums.

There was significant difference in fiber content between bread sample prepared with

GG (7.04 g/100 g) and that prepared with HG (7.34 g/100 g). This difference could be linked to the difference in fiber content of the two gums. The maize bread exhibited the highest total carbohydrate content (49.94 g/100 g) compared to the samples of bread prepared from HG (47.89 g/100 g) and HSG (45.16 g/100 g) treated doughs, which shows the gums have lower carbohydrate contents than equal amount of maize flour. The moisture, ash, and fiber values agreed with previous study [19]. The higher fiber and ash contents of the maize bread may be attributed to the gums' high ash and fiber contents, whereas the higher moisture level might be related to the gums' water retention ability.

Wheat bread scored considerably ($p<0.05$) higher in all sensory attribute than the other bread samples. The addition of gums increased the scent, taste, flavor, and texture of the maize bread significantly. However, there were no considerable differences in color score between maize bread and breads made from dough treated with gums. In terms of scent, taste, and flavor, there were no discernible variations between the loaves created from treated doughs. The bread cooked with HSG has got a considerably higher texture level (6.6) than the bread made with HG (5.6) and GG (5.4). General acceptance was much greater for wheat bread, which was followed by breads made from HG and HSG treated doughs, respectively. In general, the control maize bread performed poorly in terms of most sensory qualities. The current findings were similar with previous findings [30], who discovered that gum Arabic improved the flavor and taste of bread. Similar studies have found that gum Arabic lowers the stiffness of bread [17]. The changes in various sensory qualities found among the bread samples, such as texture, could be attributed to variations in the WAC of the gums.

Table 5 Effect of gums on the proximate composition and sensory attribute and over acceptability maize bread

Bread Samples	**Parameter**					
	Moisture (%)	Protein (g/100 g)	Fat (g/100 g)	Ash (g/100 g)	Fiber(g/100 g)	CHO(g/100 g)
C_1	43.20±0.56^{a}	13.71±0.27^{a}	0.57±0.01^{d}	0.94±0.02^{c}	0.84±0.01^{e}	41.18±0.84^{d}
C_2	35.95±0.35^{d}	9.23±0.05^{b}	2.72±0.04^{a}	2.15±0.01^{b}	5.64±0.06^{d}	49.94±0.43^{a}
T_1	40.22±0.01^{b}	7.28±0.02^{c}	2.37±0.08^{bc}	2.26±0.08^{ab}	7.34±0.04^{b}	47.89±0.16^{b}
T_2	42.65±0.30^{a}	7.36±0.01^{c}	2.47±0.08^{b}	2.37±0.08^{a}	7.61±0.01^{a}	45.16±0.45^{c}
T_3	38.87±0.49^{c}	7.26±0.01^{c}	2.25±0.08^{c}	2.26±0.08^{ab}	7.04±0.08^{c}	49.36±0.65^{a}
Sensory attributes						
Bread Samples	Color	Aroma	Taste	Flavor	Texture	Overall acceptability
C_1	8.3±0.16^{a}	7.8±0.19^{a}	7.9±0.22^{a}	7.8±0.17^{a}	8.3±0.17^{a}	7.9±0.16^{a}
C_2	5.5±0.16^{b}	3.5±0.19^{c}	4.0±0.22^{c}	3.6±0.17^{c}	3.2±0.17^{d}	3.4±0.16^{d}
T_1	6.0±0.16^{b}	5.8±0.20^{b}	5.7±0.23^{b}	5.5±0.17^{b}	5.6±0.17^{c}	6.1±0.16^{b}
T_2	5.9±0.16^{b}	6.0±0.19^{b}	5.8±0.22^{b}	5.9±0.17^{b}	6.6±0.17^{b}	6.0±0.16^{b}
T_3	5.7±0.16^{b}	6.0±0.19^{b}	5.6±0.22^{b}	5.5±0.17^{b}	5.4±0.17^{c}	4.5±0.16^{c}

4. CONCLUSIONS

The rheological properties of dough and final quality of bread made from maize were altered by the addition of gums. Maize flours mixed with gums resulted in doughs having low water absorption capacity, peak viscosity, and degree of softening and high dough development time and stability. Even if the addition of gums into maize flour improved the dough development and gaseous release properties, the extent of

improvement was still less than the properties obtained from wheat flour.

In terms of baking properties, breads containing gums had a higher loaf and specific volumes but lower firmness than breads made from maize flour alone. This suggests that the gums improve bread baking characteristics. Moreover, addition of gums improved the fiber and ash contents as well as the sensory properties of the breads. HSG produced the best dough characteristics and quality bread of the three gums tested.

CONFLICT OF INTEREST

The authors declare that there is no conflict of interest regarding the publication of this article.

ACKNOWLEDGEMENTS

The authors gratefully acknowledge Ambo University and Addis Ababa Institute of Technology for the financial and material support.

REFERENCES

[1] Elkhalifa, A.B.D., Elmoneim, O., Mohammed Ashwag, M., Mustafa Mayada, A. and El Tinay Abdullahi, H. *"Use of guar gum and gum Arabic as bread improvers for the production of bakery products from sorghum flour"*, Food Science and Technology Research, vol. 13, 2007, pp. 327-331.

[2] Rostamin, M., Milani, J.M. and Maleki, G. "Physical Properties of Gluten-Free Bread Made of Maize and Chickpea Flour", International Journal of Food Engineering, vol. 10, 2014, pp. 467- 472.

[3] Meybodi, N., Mollakhalili Mohammadifar, M.A. and Feizollahi, E. "Gluten-Free Bread Quality : A Review of the Improving Factors", Journal of Food Quality and Hazards Control, vol. 2, 2015, pp. 81-85.

[4] Bhattacharya, S. and Shanthilal, J. "Rheology of Rice Flour Dough with Gum Arabic: Small and Large-Deformation Studies, Sensory Assessment and Modeling", Journal of Food Science, vol. 80, 2015, pp. 1735-1745.

[5] Tzia, C. and Sabanis, D, "Effect of hydrocolloids on selected properties of gluten-free dough and bread", Food Science and Technology International. vol. 17, 2011, pp.279-2911.

[6] Katjiuongua Hikuepi, B. and Asfaw Muleta, "Cereal Market Performance in Ethiopia: Policy Implications for Improving Investments in Maize and Wheat Value Chains", Agriculture Global Practice GFA13, 2018.

[7] Bourekoua, H., Różyło, R., Benatallah, L., Wójtowicz, Ł., Grzegorz, Z., Mohammed, N. and Sujak, A. "Characteristics of gluten-free bread: quality improvement by the addition of starches/hydrocolloids and their combinations using a definitive screening design", European Food Research and Technology, vol. 244, 2018, pp. 345–354.

[8] Sciarini, L.S., Ribotta, P.D., Leon, A.E. and Perez, G.T., "Incorporation of several additives into gluten free breads:Effect on dough properties and bread quality", Journal of Food Engineering, vol. 111, 2012, pp. 590-597.

[9] Rostamin Mohammad, M., Jafar, M. and Maleki, Gi. "Physical Properties of Gluten-Free Bread Made of Maize and Chickpea Flour", Journal of Food Science and Technology, vol.10, 2014, pp. 467–472.

[10] Camino, M. M., Cristina, M., Mario M. M. and Manuel, G. "Mixture design of rice flour , maize starch and wheat starch for optimization of gluten free bread quality", Journal of Food Science and Technology, vol. 52, 2015, pp. 6323-6333.

[11] Tadesse Wubalem, Getachew Desalegn and Ricardo, A., "Natural gum and resin bearing species of Ethiopia and their potential applications Natural gum and resin bearing species of Ethiopia", Investigación Agraria: Sistemas y Recursos Forestales, vol. 16, , 2007, pp. 211-221.

[12] Rao, M. A. and Mothe, C.G., "Thermal behavior of gum arabic in comparison with cashew gum", Thermochimica Acta, vol. 357, 2000, pp. 9-13

[13] AACC International., "Rheological Behavior of Flour by Farinograph: Constant Flour Weight Procedure", in AACC International Method, 54-21, 2011, pp.1-8,.

[14] Sidhu, Singh Jai Pal and Bawa, Amarinder Singh "Dough Characteristics and Baking Studies of Wheat Flour Fortified with Xanthan Gum", International Journal of Food Properties, vol. 5, 2007, pp.1-11.

[15] A.O.A.C., "Analytical methods for determination of moisture. ash,proteine, fat contene", 2000.

[16] Sharadanant R. and Khan K.,"Effect of Hydrophilic Gums on the Quality of Frozen Dough", Journal of Food technology, vol. 80, 2003, pp. 773-780.

[17] Sagbo, F. S. Y., Aissi, M. V., , Hounkpatin, W. A., Houedo, C., Dans, A. and Soumanou, M. M. "Physicochemical and pasting properties of some local and improved maize varieties cultivated in Benin", International Journal of Biological and Chemical Sciences ,vol. 11, 2017, pp. 1753-1765.

[18] Shahzad, S. A., Hussain, S., Mohamed, A. A., et. al., "Gluten-free cookies from sorghum and Turkish beans; effect of some non-conventional and commercial hydrocolloids on their technological and sensory attributes", Jouranl of Food Science and Technology, vol. 41, 2021, pp.15–24.

[19] Ocheme, Ocheme Boniface, Chinma,C hiemela Enyinnaya, Adedeji, Olajide Emmanuel, Yakubu, Caleb Maina and Ajibo, Ugochukwu Happiness, "Proximate composition, functional, and pasting properties of wheat and groundnut protein concentrate flour blends", Food Science and Nutrition, vol. 6, 2018, pp. 1-6.

[20] Chisenga, S.M., Workneh, T.S., Bultosa, G. and Laing, M., "Characterization of physicochemical properties of starches from improved cassava varieties grown in Zambia", Jouranal of Hydrocolloid, vol. 4, 2019, pp .939–966.

[21] Julianti, E., Rusmarilin, H., Ridwansyah, R. and Yusraini, E. "Functional and rheological properties of composite flour from sweet potato , maize, soybean and xanthan gum", Journal of the Saudi Society of Agricultural Sciences, vol.16, 2017, pp.171-177. doi.org/:10.1016/j.jssas.2015.05.005

[22] Eggleston G., Swennen R., and Akoni S., "Physicochemical studies on starches isolated from plantain cultivars, plantain hybrids and cooking

bananas", Starch-Stärke, vol. 44, 1992, pp. 121-128.

[23] Moses M. O. and Olanrewaju M. J., "Evaluation of functional and pasting properties of different maize starch flours", International Journal of Food Scince and Nutrition, vol. 3, 2018, pp. 95-99.

[24] Lazaridou, A. "Effects of hydrocolloids on dough rheology and bread quality parameters in gluten-free formulations", Journal of Food Engineering, vol. 79, 2007, pp.1033-1047

[25] Yaseen, A.A., Shouk, A.A. and Ramadan, M.T. "Maize-Wheat Pan Bread Quality as Affected by Hydrocolloids", Journal of American Science, vol. 6, 2010, pp. 684- 690.

[26] Chen, R.Y., Seabourn, B.W., Xie, F. and Herald, T.J., "A modified extensigraph method for evaluating dough properties of hard wheat breeding lines", Cereal Chemistry, vol. 86, 2009, pp. 582-589.

[27] Munteanu, M.G., Voicu, G., Ungureanu, N., Zăbavă, B.Ș., Ionescu, M, Constantin, G. and Istrate, I. "Methods for determining the characteristics of flour and dough", In 5th International Conference on Thermal Equipment, Renewable Energy and Rural Development, 2016, pp. 349-355.

[28] Sidhu, J. P. S., and Bawa, A. S. "Dough Characteristics and Baking Studies of Wheat Flour Fortified with Xanthan Gum", Interantional Journal of Food Properties, vol.5, 2007, pp. 1-11.

[29] Asghar, A., Traig, M.W., Anjum, F.M. and Hussain, S., "Effect of Carboxy Methyl Cellulose and Gum Arabic on the Stability of Frozen Dough for Bakery Products", Turkish Journal of Biology, vol. 29, 2005, pp. 237-241.

[30] Trappey, E.F., Khouryieh, H., Aramouni, F. and Herald, T., "Effect of Sorghum Flour Composition and Particle Size on Quality of Gluten-Free Bread", Food Science and Technolology International, vol. 21, 2015, pp.188-202.

Evaluation and Adjustment of Infrastructure Leakage Index for Towns in Developing Countries

Geremew Sahilu Gebrie

School of Civil and Environmental Engineering, Addis Ababa Institute of Technology, Addis Ababa University, Addis Ababa, Ethiopia
E-mail Address: geremew.sahilu@aau.edu.et

DOI: https://doi.org/10.20372/zede.v42i.10184

ABSTRACT

Evaluating water loss and the performance of urban water supply utilities is critical. The objective of this research was to evaluate the applicability of the Infrastructure Leakage Index (ILI) formula for towns of developing countries and suggest adjustment factors. Basic water supply data from nine towns of Ethiopia was used to calculate ILI and develop modification factors. Water supply development level factor was determined based on the actual water production and optimal consumption if there was sufficient supply. Asset management factor was developed considering the categorization of Ethiopian towns which was related to expected water supply level based on development level. The study showed the Unavoidable Annual Real Loss (UARL) formula gave similar values for any type of water supply system whether developed or not. Except for Addis Ababa, the calculated ILIs utilizing the standard formula were less than four indicating unrealistic very good performance. Applying the adjustment factors, realistic ILI values were obtained reflecting the realistic performance of water utilities in developing countries, requiring timely appropriate water loss reduction measures.

Keywords: Adjustment factors; Developing Countries; Ethiopia; ILI; Mode of water supply; Water loss.

1. INTRODUCTION

One of the major challenges of water supply service provision is the water loss between the production and end use points of a water supply system. A number of efforts were made to quantify the amount of water loss and develop key parameters that can be used to compare the performance of water utilities irrespective of their size with regards to population served and production capacity. The International Water Association (IWA) established a Task Force on Performance Indicators which published the standard international "best practice" water balance [1]. The water balance table which introduced the term Non-Revenue Water (NRW) has been used to assess the overall performance of the system with respect to percentage of water loss from a total production and also components of water loss such as apparent and real losses [2]. However, it was not suitable for assessing the efficiency of the distribution system as it was strongly influenced by consumption and its change and pressure; difficult to interpret for intermittent supply and couldn't distinguish between apparent loss and real loss [3].

The IWA's task force on water loss carried out a review of performance indicators for real losses [4] and developed a method that could represent most of the above factors by introducing the concept of UARL and Current Annual Real Loss (CARL) to calculate a dimensionless key performance

parameter – ILI. IL I was calculated as ratio: CARL/UARL, Restegari [5] stated that the UARL/ILI approach was better than previous traditional performance indicators for the management of real losses. The basic concept of UARL was that there is no as such zero real loss. Figure 1 shows that if the real loss is to the left of point *'A',* which is UARL, the cost of active leakage control will not be economically affordable [6]. Thus, the CARL should always be to the right of point *'A' in perfect condition at 'A'* implying ILI greater than or equal to unity implying values closer to one mean good performance.

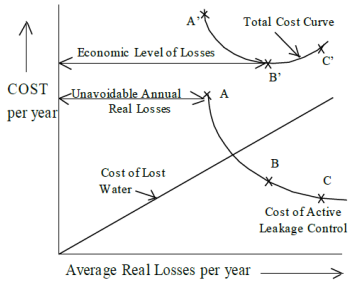

Figure 1 Unavoidable Annual Real Losses and Economic Level of Real Losses [6]

Equation (1) was developed by the task force to determine UARL (liters/day) taking into account most of the factors that were not addressed in the traditional performance indicators.

$$UARL=(18Lm+ 0.80Nc+25Lp)P \quad (1)$$

where:

Lm= Mains length in km
Nc = Number of service connections
Lp = Total length in km of underground pipe between the edge of the street and customer meters
P = Average operating pressure in meter

In the development of ILI as a performance indicator to measure the efficiency of water utilities, the basic assumption in determining UARL was utilities will carry out four necessary measures of asset management practice setting standard level of services (LOS) – pipeline and asset; and pressure management, active leakage control and speed and quality of repairs [7]. As mentioned by Alegre et al [8], the ILI was the result of an empirical expression considering properly constructed and maintained system having the service connection density, average length and the same average operating pressures. It was also mentioned that the indicator doesn't fulfill some of the requirements set for performance indicators. The ILI didn't have a means to consider developmental level of a water supply system. Modifying UARL equation for developing countries to calculate realistic ILI was also discussed by water leakage researchers [9].

Therefore, considering that the ILI was developed based on well-developed water supply systems and utilities the question here was, would such indicator give reasonable values for developing countries? Hence, the first objective of this paper was to check whether the ILI method could give reasonable performance assessment of water utilities in developing countries. The second objective was to recommend adjustment factor to the formula so that the result could reflect the situation of utilities in developing countries.

2. METHODS

The study focused on nine towns shown on Figure 2 including Addis Ababa, which is the only metropolitan city with a population of more than a million.

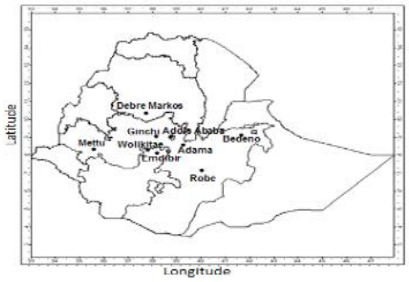

Figure 2 Location map of study towns in Ethiopia

The key formula and data used to determine the ILI and modification factors to make it applicable to the assessment of the performance of water utilities in developing countries is presented in the following sub-sections. The data were extracted with proper quality checking from project documents and graduate thesis works supervised by the author.

ILI Calculation

The towns and key basic data utilized for the calculation of the relevant parameters in the determination of ILI are presented in Table 1.

Table 1 Basic water supply system data of nine towns in Ethiopia

Town	Year	Population	Production (m^3/day)	Billed Consumption (m^3/day)	Length of Main (Lm) (km)	System Average Pressure (P) (m)	Number of Connections (Nc)
Addis Ababa	2012	3,000,000	307,328.08	184,472.88	2,840.00	25.00	298,900.00
Adama	2014	308934	18,496.88	12,194.47	410.00	35.00	36,226.00
Mettu	2015	46,306	1,211.67	791.98	20.92	38.43	3,109.00
Emdibir	2017	20,773	512.75	404.96	21.73	32.00	1,100.00
Wolkitae	2016	78,189	2,219.60	1,779.15	109.00	55.80	6,909.00
Debre Markos	2014	9,2470	3,809.62	2,292.93	55.72	43.00	11,014.00
Robe	2016	80,504	2,255.07	1,686.47	60.06	52.00	8,236.00
Bedeno	2016	13,418	388.80	311.04	10.31	25.00	366.00
Ginchi	2018	53,600	829.00	488.18	24.72	52.00	2,472.00

Sources: [10 -17]

When utilizing the basic data, some assumptions were made to determine CARL and UARL employing the formulas developed by the IWA taskforce and get the ILI for each town. The various parameters developed in the process of determining ILI with the ones utilized during the development of the ILI formula were compared with coefficient of determination (R^2) and a separate data from Addis Ababa Water and Sewerage Authority (AAWSA) branch offices was used to validate some of the relationships developed between UARL's and density of customer connections. The key parameters determined and used to determine the applicability of ILI in the study towns were:

i. UARL=(18Lm + 0.80Nc + 25Lp)P; (liter/day) (1)
ii. UARL: liter/connection/day(i/Nc)
iii. UARL: liter/connection/day/meter of pressure (ii/P)
iv. UARL: liter/km of Main/day/meter of pressure (i/Lm/P)
v. CARL: Current Actual Real Loss (75 % of NRW) based on estimation of apparent losses and known values of measured and not measured consumptions which ranges from 20 % to 30% (average 25 %) gives a real loss of 75 % of NRW
vi. Density of connection = Nc/Lm
vii. ILI: CARL/UARL

The UARL value of each town was calculated utilizing equation 1 and data in Table 1.

Technical Performance

A physical loss assessment matrix, presented in Table 2, that sets technical performance category considering ranges of ILI values based on physical loss in liter/connection/day when a system is pressurized from 10 m to 50 m that was developed by Liemberger et al. [18] for

developing countries was used to determine performance levels based on calculated ILI values. This was done before and after adjustment of ILI values to check the change in technical performance category.

Water quantity

Another set of data focusing on water production, billed water consumption and NRW in liter per capita per day (l/c/d) and percentage of mode of water supply connections is presented in Table 3 based on the data on Table 1 and additional regarding connections. This was used to determine modification factor based on water supply development level that depends on the quantity of water used to adjust the ILI in order to make it applicable for developing countries.

Table 2 Physical loss assessment matrix for developing countries [18]

Technical Performance Category	ILI	Liters/connection/day when the system is pressurized				
		10m	20m	30m	40m	50m
A	1-4	<50	<100	<150	<200	<250
B	4-8	50-100	100-200	150-300	200-400	250-500
C	8-16	100-200	200-400	300-600	400-800	500-1000
D	>16	>200	>400	>600	>800	>1000

Table 3 Water production, billed consumption and NRW and percentage of modes of water supply in study towns

Town	Water production (l/c/d)	Billed water consumption (l/c/d)	NRW (l/c/d)	House Connection (%)	Yard Connection (%)	Public Tap (%)
Addis Ababa	102.44	61.49	40.95	34.00	60.00	6.00
Adama	59.87	39.47	20.40	5.00	60.00	35.00
Mettu	26.17	17.10	9.06	2.20	43.80	25.00
Emdibir	24.68	19.49	5.19	0.38	64.89	20.99
Wolkitae	28.39	22.75	5.63	7.00	93.00	0.00
Debre Markos	41.20	24.80	16.40	3.00	25.00	39.00
Robe	28.01	20.95	7.06	3.12	59.28	37.60
Bedeno	28.98	23.18	5.80	0.00	15.00	85.00
Ginchi	15.47	9.11	6.36	2.96	51.57	34.66
Average	**39.47**	**26.48**	**12.98**	**6.41**	**52.50**	**31.47**

Asset management

In Ethiopia, the category of the town in addition to population size reflected the stage of water supply development with respect to service delivery which is highly affected by availability of a systematic asset management. The asset management was reflected by activities which are being carried out by water utilities to provide safe water satisfying standard LOS which includes in general decreasing NRW and particularly water loss. In the Ethiopian context, as per the second growth and transformation plan (GTPII), towns are categorized based on population into the following five categories [19]:

- Category I: > 1,000,000
- Category II: 100,000 to 1,000,000
- Category III: 50,000 to 100,000
- Category IV: 20,000 to 50,000
- Category V: < 20,000

This categorization which indicates the expected l/c/d of water supply of each category as 100, 80, 60, 40, 20 for categories I, II, III, IV and V, respectively was used to estimate asset management factor.

The water quantity and asset management factors were multiplied to determine modified ILI value which better reflects the performance level of the utilities in the study towns.

3. RESULTS AND DISCUSSION

3.1 Results

3.1.1 Pressure and Density of Connection

The first comparison was made between the UARL estimated (liter/connection/day) utilizing the field data and the table produced by the developers of the formula based on data from 27 countries [6], as shown in Table 4. The field values of average pressure and density of connection per km of main were taken and the UARL was interpolated from the table. For density values greater than 100 Nc/km, UARL values corresponding to 100 Nc/km were taken as values become almost constant as observed from the table developed to estimate UARL during the ILI formula development [4].

Table 4 UARL values calculated based on field data and interpolated initial ILI document (liter/connection/day))

Town	Addis Ababa	Adama	Mettu	Emdibir	Wolkitae	Debre Markos	Robe	Bedeno	Ginchi
UARL Field	33.65	48.26	49.81	48.98	81.41	54.44	67.93	42.05	70.46
UARL Interpolated	31.00	44.05	47.11	45.45	84.71	45.15	66.30	40.04	66.30

The coefficient of determination (R^2) value of 0.968 for estimated values of UARL based on field data and interpolated based on initial ILI document presented in Figure 3 shows that the table can directly be used to calculate UARL as long as the basic data in ILI equations are available. The estimation has reasonable accuracy and this indicates that the developed table can be used irrespective of the level of the water supply system of the data source.

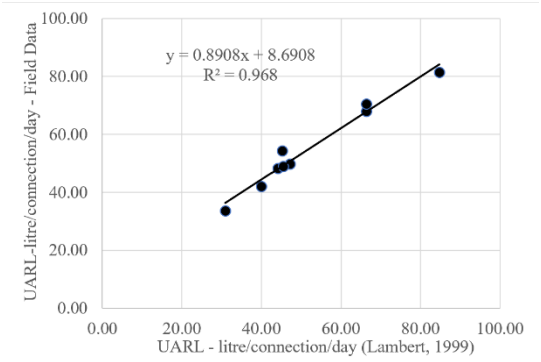

Figure 3 UARL - Field value as a function of tabular values [6]

3.1.2. UARL per Unit Pressure

During the development of the ILI method, graphs were developed which showed the relationship between density of service connections per km and UARL: in liter/km-main/day/meter of pressure and liter/connection/day/ meter pressure when fully pressurized [6]. The developed graphs show as density increases UARL (liter/connection/day/meter pressure) decreases and becomes almost constant if the density of connection exceeds 100 Nc/km. Moreover, the UARL (liter/km of main/day/meter pressure) increases linearly with density of connection except when considering only the main which is constant. Figures 4 and 5 were developed for the nine towns based on field data.

Comparison of the graphical representation of the source document for ILI method and the one plotted for the nine showed that the trends were similar in that UARL – liter/connection/day decreased with increase in density of service connection and vice

versa in the case of UARL-liter/km/day/meter pressure.

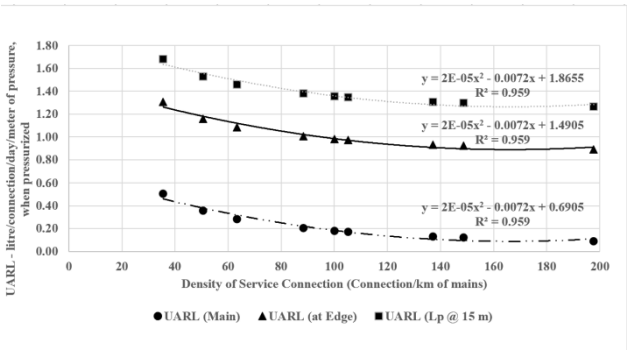

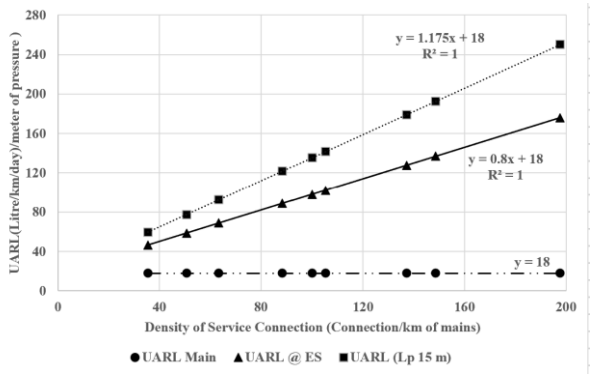

The equations developed to calculate UARLs per unit pressure based on the density of service connection in Figures 4 and 5 needed to be validated. The data for seven branch offices of AAWSA and calculated density and UARLs based on the data and developed equations as shown in Figures 4 and 5 are presented in Table 5. An average pressure of 25 meter is used as suggested in the Water Audit and Bench Marking Report [20].

Table 5 Water distribution system data, calculated density and UARLs of AAWSA Branch offices and estimated values based on developed equations

AAWSA Branch Office	Nc	Lmain (km)	Lp[1] (km)	Density (Nc/km (main)	UARL Calculated based on data[2]		UARL Calculated based on equation[3]	
					(liter/connection/day/ meter pressure)	(liter/km (main)/day/ meter pressure)	(liter/connection /day)/meter of pressure) (y = 2E-05x² - 0.0072x + 1.8655)	(liter/km (main)/day) /meter of pressure (y = 1.175x + 18)
Addis Ketema	40693	233.04	542	174.62	1.24	215.84	1.22	223.18
Arada	22317	219.91	307	101.48	1.32	134.09	1.34	137.24
Gulele	41841	274.23	665	152.58	1.32	200.69	1.23	197.28
Gurd Shola	32955	333.41	391	98.84	1.28	126.39	1.35	134.14
Megenagna	28580	235.12	337	121.55	1.24	151.08	1.29	160.83
Mekanisa	38066	270.97	534	140.48	1.28	179.65	1.25	183.06
Nifas Silk	39864	316.72	569	125.87	1.30	163.61	1.28	165.89

Calculated based on:

[1]Lpranging from 12 m to 16 m is used source being bench marking report
[2]Equation 1
[3]Equations of Figures 4 and 5

The RMSE of UARL (liter/connection /day)/meter of pressure) determined based on field data and developed equation is 0.0476 which is insignificant. Moreover, the coefficient of determination (R^2) between UARL (liter/km(main)/day/meter pressure) determined through field data and developed

equation was 0.9834. Both validate the equations developed in Figures 4 and 5.

3.1.3 Infrastructure Leakage Index

The key parameter used to determine ILI was CARL which was calculated considering 75 % of the NRW based on the estimation of the apparent losses and unmetered and metered unbilled water consumption to be 25% of NRW. Table 6 shows the ILI calculated according to a formula: ILI = CARL/UARL.

Table 6 Calculated ILI for Ethiopian towns based on field data indicated in table 1.

Town	CARL (liters/connection/day)	UARL (liters/connection/day)	ILI
Wolkitae	47.81	81.41	0.59
Robe	51.78	67.93	0.76
Emdibir	73.49	48.98	1.50
Mettu	101.24	49.81	2.03
Debre Markos	103.28	54.44	1.90
Ginchi	103.40	70.46	1.47
Adama	130.48	48.26	2.70
Bedeno	159.34	42.05	3.79
Addis Ababa	311.06	33.65	9.24
Average	**120.21**	**55.22**	**2.66**

In general, it is clear that increased CARL coupled with decreased UARL results in increased ILI. Comparing average values of CARL of Ethiopian towns with that reported by Lambert et al. [6], it was less than half – 120 against 270 liter/connection/day and corresponding ILI was 2.66. If Addis Ababa is taken out, the average value of the CARL of eight towns is about 96 liter/connection/day while ILI is 1.84. Except for Addis Ababa, all calculated ILI values were less than 4 including less than one values for *Wolkitae* and *Robe* towns.

The ILI for the towns of *Emdibir*, Metu, *Ginchi* and *Bedeno* were considered though, Nc, is less than 5,000 as most of the towns in developing countries have such nature and checking the applicability of ILI is necessary

Technical performance category

The technical performance category of a utility was determined assuming pressurized system by considering the ILI range, average pressure in the system and the extent of the current actual real loss [21]. The physical loss matrix developed for developing countries was used to categorize the 9 towns as presented in Table 7. Based on the parameters presented in the table, all but Addis Ababa were in the technical performance category of A. This category represents the ultimate good performance where further loss reduction may be uneconomical unless there was shortage of water, which needs careful analysis to identify cost-effective improvement measures. In the case of Addis Ababa, the technical performance category is C which is poor and requires immediate asset management and leakage control actions.

3.1.4 Modification factor

The technical performance category of A in Table 8, except for Addis Ababa, required attention. The question here was what was the situation on the ground in the various utilities that have registered performance category of A. Do they deserve such high-level technical performance? Does it mean these utilities do not need further leakage control activities? Though developed for developing countries, can one really utilize this table to categorize technical performance in developing countries like Ethiopia? What modification is required to get realistic technical performance measurement? Considering the situation on the ground, there was a need to develop factors to modify calculated ILI.

Table 7 Technical performance category of water supply utilities in study towns of Ethiopia

Town	System Average Pressure (P) (m)	Infrastructure Leakage Index (ILI)	CARL (liter/connection/ day)	ILI-Range	CARL-Range	Technical Performance Category
Addis Ababa	25.00	9.24	311.06	8 - 16	200 - 400	C
Adama	35.00	2.70	130.48	1 - 4	< 150	A
Mettu	38.43	2.03	101.24	1 - 4	< 150	A
Emdibir	32.00	1.50	73.49	1 - 4	< 100	A
Wolkitae	55.80	0.59	47.81	<1	<50	A
Debre Markos	43.00	1.90	103.28	1 - 4	<150	A
Robe	52.00	0.76	51.78	<1	<100	A
Bedeno	25.00	3.79	159.34	1 - 4	<200	A
Ginchi	52.00	1.47	103.40	1 - 4	< 150	A

Water quantity perspective

The per capita water production, billed consumption, NRW and mode of water supply of the various utilities can be referred from Table 3. The average per capita production per day was about 40 liters while the billed consumption was just over 26 liters. If Addis Ababa is treated separately the average per capita production and consumption in liters will be about 32 and 22 liters, respectively which is very minimal.

The minimal consumption of water is reflected in the percentages of mode of water supplies in the towns with very low water consumption levels. A very low percentage of house connection of about 6.5% indicates that the maximum per capita water consumption is governed mainly by yard connection, 52.5 %, which could not be greater than 50 l/c/day. The fact that on the average about 32 % fetch water from public tap with a maximum possible daily per capita consumption of 20 liter justifies the low daily per capita consumption rates.

If Addis Ababa is not considered, the house connection, yard connection and public tap users will be about 3 %, 52 % and 35 %, respectively. Considering similar average pressure and NRW, if the production amount is increased, CARL will increase. However, UARL will remain the same since it is not a function of water production or consumption as the key parameters in the equation are pipe length, number of connection and pressure. The UARL could not differentiate whether the water supply system is highly developed with most population house connected or yard connected or get water from the public taps.

The key implication of the lesser production and insignificant percentage of house connection and hence less CARL coupled with unchanged UARL is that the ILI will be lower. The issue here is to determine a correction factor which is greater than one for the calculated ILI to cater for the development level of water supply system. Considering the factor to be determined the adjusted ILI can be calculated as follows:

$$ILI_{adj1} = WSDLF*ILI \quad (2)$$

where:

ILI_{adj1}= Adjusted ILI considering the development level of water supply

ILI= ILI determined with available water assuming system is fully pressurized

WSDLF= Water Supply Development Level factor used to adjust ILI

Asset Management Perspective

Initially the ILI was developed considering utilities have proper asset management to achieve a certain level of service (LOS) which includes active leakage management practice. A recent study carried out in 10 small and medium towns of East Shoa Zone of Oromia region of Ethiopia [22] showed the following key technical factors which can be considered common problems in almost all towns of Ethiopia.

- the consumption was low due to underdevelopment of the system coupled with NRW which is a big concern and poor management,
- Infrastructure stability was also one attribute with low achievements of the evaluation in which many of the physical assets were found aged and needs replacement and repair; regular inspection periods were missed
- Product quality was very low expressed as service reliability, continuity, interruptions, working hours, and quality of water

Considering the nine towns with regards to asset management, the situation is not different. For example, in Debre Markos town 11.5 burst/km/year of main per year was encountered which clearly shows very poor asset management of the water supply system. Except Addis Ababa which started limited efforts on NRW management, other towns do not have proper asset management that leads to leakage control.

$$ILIadj2 = AMF*ILI \quad (3)$$

where,

ILIadj2 = Adjusted ILI considering lack of proper asset management

ILI= ILI determined with available water assuming system is fully pressurized

$$ILIadj = AMF*WSDLF*ILI \quad (4)$$

where:

ILIadj=Adjusted ILI considering lack of proper asset management and low water supply development level

ILI=ILI determined with available water assuming system is fully pressurized and proper asset management practiced

WSDLF=Water Supply Development Level Factor used to adjust ILI

Determining Adjustment Factors

Water Supply Development Level Factor (WSDLF)

Water supply development factor can be determined on assumed per capita daily water demand if a substantial population of the urban population is getting water through house connection. The WSDLF is basically determined considering the per capita production should be between 100 l/c/d to 150 l/c/d where more than 80 % of the population is utilizing water from house connection including NRW was considered as optimal. In this study a per capita production of 125 l/c/d which is an average of the two was considered to calculate WSDLF. The factors developed and the resulting adjusted ILI is presented in Table 8.

Asset Management Factor (AMF)

The category of the town in the asset management perspective section in addition to population size reflects the stage of water supply development with respect to service delivery which is highly affected by availability of a systematic asset management. Hence, depending on the

status of asset management, correction factors that vary from 1.25 to 2.0 have been assigned. The maximum factor is given this range since the level of development with respect to asset management within Ethiopia or other developing country could not be more than double from the best scenario which is one. Otherwise, it can exaggerate the ILI value unnecessarily downgrading technical performance. The minimum AMF was assigned for Addis Ababa as it has a system in place but not that much effective since significant reduction in leakage is not yet observed. *Adama* is just beginning the introduction of the system with a service delivery improvement support through NRW reduction project and hence an AMF of 1.75 was assigned. For the other towns which have no system or not started proper asset management except some reactive responses when problems are encountered, AMF value of 2.0 was assigned.

Based on these adjustment values the WSDLF adjusted ILI values are multiplied by AMF to get the final adjusted ILI value that takes into account both water supply development level and conditions of asset management as indicated in Table 8.

3.1.5 Change in technical performance category

The adjustment of the ILI through the introduction of WSDLF and AMF increased the value of ILI and hence could initiate utilities to improve their water supply system from both perspectives. The last row of Table 8 shows the change in technical performance category.

Table 8 Determination of ILI adjusted for shortage of water and lack of efficient asset management

Town	Addis Ababa	Adama	Mettu	Emdibir	Wolkitae	Debre Markos	Robe	Bedeno	Ginchi
Production (l/c/d)	102.44	59.87	26.17	24.68	28.39	41.20	28.01	28.98	15.47
WSDLF (125/Production)	1.22	2.09	4.78	5.06	4.40	3.03	4.46	4.31	8.08
ILI(before adjustment)	9.51	2.97	2.25	1.63	0.64	2.10	0.84	4.09	1.62
$ILI_{adj\ (WSDLF)}$	*11.60*	*6.21*	*10.75*	*8.27*	*2.83*	*6.39*	*3.76*	*17.66*	*13.07*
AMF	1.25	1.75	2.00	2.00	2.00	2.00	2.00	2.00	2.00
$ILI_{adj(WSDLF\_AMF)}$ (after adjustment)	14.50	10.86	21.49	16.55	5.66	12.77	7.52	35.32	26.13
Performance Category (before adjustment)	C	A	A	A	A	A	A	A	A
Performance Category (after adjustment)	C	C	D	D	B	C	B	D	D

All utilities that had performance category of A before adjustment are changed to B, C or D category. Those which moved to category D are the ones with connection of less than 5,000 and where the applicability of the ILI method is in question and are in the urban category IV and V except *Ginchi*. The two towns - *Wolkitae* and Robe - that had a performance category of B were the ones that had ILI of less than 1 which is unrealistic. This is due to higher average pressure and length of main and connection pipe which increased the UARL without a change in CARL. If the initial ILI is changed to one which is theoretically the least and best value of ILI, the adjusted ILI will be 8.80 and 8.92 for *Wolkitae* and *Robe*, respectively which gives a performance category of C for both. Therefore, all the towns had a performance category of poor

or very poor that require urgent action to improve the water supply system with respect to real loss which reflects the situation on the ground.

Sensitivity Analysis of Adjustment Factors

The WSDL adjustment factor was varied without changing the AMF to check its sensitivity by decreasing and increasing the per capita water consumption by 25 liters to the minimum and maximum values of 100 and 150 l/c/d. No change in technical performance category was observed in the seven towns. Downgrading to the next technical performance level is observed in Addis Ababa and Robe when the per capita consumption level is above 140 l/c/d. A sensitivity analysis was also carried out by varying the AMF factor from 1.25 to 3.00. No change was observed for *Bedeno* and *Ginchi* towns as their initial technical performance was the last one D. With the others change was observed when the AMF is doubled from the minimum to 2.5 and more. In general, the sensitivity analysis showed that both the adjustment factors are robust.

3.2 Discussion

Globally the utilization of the ILI as an index showing utilities performance with regards to real loss management in the last 20 years has shown its effectiveness in a number of cases. However, there were also questions about its applicability in various circumstances. Most of the issues raised were with regards to the reliability of UARL estimate under various circumstances. The main concern was overestimation of UARL due to high pressure in a system leading to lower and misleading ILI values.

In his evaluation of the ILI Wnarni [3], attempted to show that there is no relationship between ILI and NRW expressed as percentage of system input and hence less percentage of NRW does not mean lower ILI. However, it didn't cover the issue of very low water consumption due to different modes of water supply and per capita consumption rates as well as the degree of asset management efforts of utilities. Moreover, the issue of lower ILI values even below 1, UARL being greater than CARL was discussed and attempts were made to develop system correction factor. The expected possible causes that justified the development of correction factors were [23]:

- errors in low CARL volumes derived from Water Balances, or Minimum Night Flows and Night-Day Factors
- errors in infrastructure and/or pressure data inputs to the UARL equation
- lower pressure systems where pressure: leak flow rate relationships are more sensitive than the simplified linear assumption used in the UARL equation
- systems where all bursts surface quickly or are easily and rapidly identified from night flow measurements, including small District Metered Areas.

The adjustments made to address these issues did not consider the effect of the low level of water supply development with respect to prevailing mode of water supply and the lack of proper asset management to decrease leakage in the water utilities of developing countries which are the focus of this paper.

4. CONCLUSIONS

Previous efforts to develop factors could give improved ILIs addressing the issues raised. The author explored other dimensions that contribute for low ILI and recommended adjustment factors to the calculated ILI. This research shows UARL formula is dependent on distribution system parameters and gives similar values whether

the system is highly developed with a substantial mode of domestic water supply of house connection or not. The low water consumption levels in developing countries which are mostly based on yard connection implies the quantity of CARL is low. On the other hand, ILI assumes the presence of a systematic asset management with leakage management efforts which is not mostly the case in towns of developing countries. Thus, this paper strongly recommends application of adjustment factors while utilizing the ILI formula in towns of developing countries. The two adjustment factors that consider water supply development level and asset management efforts are developed based on Ethiopian experience and tested. The application of the adjustment factors resulted in higher ILI value that is in line with the extent of the problem. Hence, the author highly recommends the utilization of the formula while investigating urban water supply system of developing countries with similar problems of very low house connections and lack of leakage management system so that the results lead to necessary actions to improve the water supply system and achieve reduction of real water losses.

CONFLICT OF INTEREST

No conflict of interest exists with the author

ACKNOWLEDGMENT

The author would like to thank the water utilities of *Adama, Metu, Emdibir, Wolkitae, Debre Markos, and Ginchi* for providing the basic water distribution system data.

REFERENCES

[1] Alegre, H., Hirner, W., Melo Baptista, J., Perena, R., "*Performance Indicators for Water Supply Services"*, IWA Manual of Best Practice, 1st Edition. ISBN 90022227, 2000

[2] Hamilton, S., Mckenzie, R., and Seago, C. "*A Review of Performance Indicators for Real Losses from Water Supply Systems"*, 2005, miya-water.com

[3] Winarni, W. "*Infrastructure Leakage Index (ILI) as Water Losses Indicator"*, Civil Engineering Dimension, Vol. 11, No. 2, 2009, pp. 126-134.

[4] Lambert, A.O., "*International Report on Water Losses Management and Techniques"*, Report to IWA Berlin Congress, October 2001. Water Science and Technology: Water Supply vol. 2 no. 4, August 2002.

[5] Rastegari, E., "*How Average Operating Pressure Impacts on Infrastructure Leakage Index"*, Advances in Ecological and Environmental Research, 2018, 94-103 |Science Signpost Publishing.

[6] Lambert, A.O., Brown. T. G., Takizawa M., and Weimer, D., "*A review of performance indicators for real losses from water supply systems",* Journal of Water Supply: Research and Technology-Aqua, vol. 48, no. 6, 1999, pp. 227–237.

[7] Lambert, A.O. and McKenzie, R.D., "*Practical Experience in using the Infrastructure Leakage Index, 'Leakage Management: A Practical Approach"*, International Water Association Conference in Lemesos, Cyprus in November 2002. Water Board of Lemesos, www.wbl.com.cy

[8] Alegre, H., Melo Baptista, J., Cabrera, Jr. E., Cubillo, F., Duarte, P., Hirner, W., Merkel, W., Renato Parena, R., "*Performance Indicators for Water Supply Services"*, 3rd Edition, IWA Publishing, 2017.

[9] Kadu, S. and Dighade, R., *"Infrastructure Leakage Index and Challenges in Water Loss Management in Developing Countries"*, World Environmental and Water Resources Congress: Flood, Droughts and Ecosystems, ASCE, 2015.

[10] Melaku Abebaw, "*Assessment of Water Loss in Water Supply Network, A Case of Debre Markos Town, Regional State of Amhara, Ethiopia"*, 2015, MSc thesis, School of Civil and Environmental Engineering, Addis Ababa University, Ethiopia.

[11] Zerihun Abiyu, "*Hydraulic Performance Modeling and Improvements of Water Supply Distribution Systems, the Case of Ginchi Town, Regional State of Oromiya, Ethiopia"*, 2018, M. Sc. thesis, School of Civil and Environmental Engineering, Addis Ababa University, Ethiopia.

[12] Tegenu Alemayehu and Jemal Mohammed, "*Detail Design Report of Bedeno Town Water Supply and Sanitation Project"*, 2017, Regional State of Oromiya, Ethiopia.

[13] Addis Ababa Water and Sewerage Authority, "*Non-Revenue Water Reduction, Hydraulic Modeling and GIS Development for Addis Ababa City Water Supply System"*, Water Audit and Benchmarking Report, 2012, Ethiopia

[14] Majer Behute, "*Assessment of Wolkite Water Supply System in Gurage Zone, SNNPR, Ethiopia, School of Civil and Environmental Engineering"*, 2016, M. Sc. thesis, Addis Ababa University, Ethiopia.

[15] Biniyam Bogale, "*Assessment of the Water Distribution Network of Metu Town Water Supply System, Regional State of Oromiya, Ethiopia*",2016, MSc thesis, School of Civil and Environmental Engineering, Addis Ababa University, Ethiopia.

[16] Dereje Wakjira, "*Performance Evaluation of Distribution System, Case Study of Adama Town, Regional State of Oromiya, Ethiopia",* 2014, M. Sc. thesis, School of Civil and Environmental Engineering, Addis Ababa University, Ethiopia.

[17] Antoniyos Wodajo, "*Assessment of Emdibir Town Water Supply System, Cheha Woreda, Gurage Zone, SNNPR, Ethiopia",* 2017, M. Sc. thesis, School of Civil and Environmental Engineering, Addis Ababa University, Ethiopia.

[18] Liemberger, R. and Brothers, K., Lambert, A., McKenzie, R., Rizzo A., and Waldron, T. "*Water Loss Performance Indicators"*, Water Loss Conference, 1, 2007, pp. 148-160, Bucharest, Romania.

[19] Federal Democratic Republic of Ethiopia, National Planning Commission. *"Growth and Transformation Plan II (GTP II) (2015/16 – 2019/20) Volume I: Main Text"*, National Planning Commission, 2016, Ethiopia.

[20] Addis Ababa Water and Sewerage Authority, "*Addis Ababa Water Distribution and Operation Management and Hydraulic Modelling Report"*, 2019, Ethiopia.

[21] Liemberger R. and Mc Kenzie., "*Accuracy Limitations of the ILI - Is it an Appropriate Indicator for Developing Countries?",* 2005, Leakage 2005 - Conference Proceedings, D Pearson, SW Trow - rash.apanela.com .

[22] Yoseph Kebede, Geremew Sahilu, Kefyalew Muleta and Tesfaye Adnew., "*Technical and Social Factors affecting service quality of water utilities in small and medium towns, the case of East Shewa zone of Oromia"*, 2019, Ethiopia, Ethiopian Water Technology Institute, Ministry of Water and Energy, Ethiopia.

[23] Lambert, A. O., "*System Correction Factor SCF can customize the standard UARL equation for pipe materials, small systems and pressure: bursts relationships"*, 2020, Leakssuite Library Ltd.

Deformational Behavior of Fiber Reinforced Cement Based Materials Under Repeated Loading

Abrham Gebre Tarekegn

School of Civil and Environmental Engineering, Addis Ababa Institute of Technology, Addis Ababa University
**Corresponding author's E-mail address: abrham_gebre@yahoo.com*

DOI: https://doi.org/10.20372/zede.v42i.10180

ABSTRACT

Bond degradation of the constitute materials of the structure causes an increase in residual deflection and total surface crack width which reduces overall performance of structures. Advanced construction materials such as ultra-high strength fiber-reinforced concrete, commonly known as engineered cementitious composite (ECC) and fiber-reinforced strain-hardening cement-based composites (SHCC)are designed to offer superior mechanical properties with multiple fine cracks and deformability than conventional concrete materials because of the bridging effect of embedded fibers. In general, both ECC and SHCC can be suitable for applications involving repeated loadings. However, the performance depends on magnitude, type of loads, etc. In this study, deformational behavior of fiber reinforced cement-based materials, ECC and SHCC, under repeated loading (low cycle fatigue) were investigated. Test results showed that, ECC is bendable, the deformation can be easily detected and has high impact resistance. On the other hand, SHCC has the potential for multiple cracking and strain-hardening behavior. ECC and SHCC can thus be used for strengthening and retrofitting of structural elements in addition to their benefits for new construction works.

Keywords: Crack width; Deformational behavior; ECC; Impact resistance; Repeated loading; SHCC.

1. INTRODUCTION

ECC is an ultra-ductile mortar based composite reinforced with short random fibers. ECC, unlike common fiber reinforced concrete, is a micromechanically designed material [1]. ECC has high bond strength of embedded fibers as well as compressive strength and bending toughness. It uses steel and the curing process takes place in a high temperature chamber. Since the hydration process of ECC is completed by high temperature curing, the creep recovery of ECC specimen is insignificant and can be neglected. Under distributed loads ECC gives multiple finite micro cracks due to the bridging effect of fibers [2]. This behavior exists even under the action of concentrated loads. Some of the advantages of bendable concretes include; ability to bend like a metal, higher durability and lower emission of harmful gases as compared to that of conventional concrete [3], resistance to cracking and fire resistance at elevated temperatures [4], etc.

The specific benefits stated vary depending on the volume and type of fibers used in the mix. So far, they have been mainly used for pavement overlay, link-slab for bridge expansion joints, repair of existing concrete structures, footbridge construction and so on [5, 6]. Fischer and Li [7] examined the behavior of ECC elements reinforced with fiber-reinforced polymer (FRP), focusing on the failure mode and residual deflection under reversed cyclic loading. However, the

research did not address the performance of ECC members for repeated number of impact loading with and without FRP.

On the other hand, SHCC use plastic fibers and cure under controlled conditions. SHCC exhibit superior crack width and spacing control in the pseudo strain hardening phase. SHCC, distinguished by its ability to develop multiple, finely spaced cracks of tight crack widths, generally below 100 μm. This crack control may be exploited for its potential inherent durability and the durability it may afford structures [8, 9]. Studies showed that polyvinyl alcohol-engineering cementitious composites (PVA-ECCs) reduce the brittle nature of concrete and have been widely used for repairing bridge deck, widening, asphalt overlay, etc. However, use of PVA-ECCs as a major structural material does not have economic benefits [10].

Addition of polypropylene (PP) fibers up to a volume ratio of 1.5 % to PVA-ECC mixes significantly increases its impact strength of PP-PVA-ECC [11]. Research conducted on reinforced concrete (RC) slabs showed that use of SHCC layers on the tension side enabled the slab to resist high impact resistance as compared to the un-strengthened RC slab [12]. The residual deformation of structures due to repeated loadings increases as a result of bond degradation of the constitute materials. Structural deterioration is increased by loading condition and the type of loads as well as environmental factors [13].

Many studies on the deformation behavior of fiber reinforced cement-based materials have been conducted, with a particular emphasis on static, impact, torsional, and reverse cyclic loading. However, researches on the performance of ECC and SHCC under repeated static and impact loading with different level of loading is limited. In this study, deformational behavior of ECC and SHCC under different level of repeated loadings (low cycle fatigue) and damping properties is investigated. The objectives of this study aim to enhance the understanding and performance of ECC and SHCC materials, ensuring their capacity to withstand the demands of real structural applications to resist sudden impacts.

2. MATERIALS AND METHODS

2.1 Materials

Mix proportions for ECC and SHCC were made as per the JSCE recommendations for design and construction of ultra-high strength fiber reinforced concrete structures [14]. In all cases, Type II fly ash was used.

2.1.1 ECC mix proportion

Table 1 shows the total quantities of component materials of ECC used in this study. Steel fiber used for ECC was as per JSCE with tensile strength not less than $2x10^3$ N/mm^2 [14]. Steel fibers had a diameter of 0.2 mm. Figure 1 shows the sample of steel fibers used in the study.

Table 1 Component materials of ECC

Materials	Quantity (kg)	(%)
Water	19.18	6.30
Binder (cement and fly ash)	154.44	50.74
Fine aggregate	107.30	35.25
Super plasticizer	5.41	1.78
Shrinkage reducing agent	1.54	0.51
Steel fiber, 15mm and 22mm in length (1.75% by vol.)	16.49	5.42

Figure 1 Steel fiber

2.1.2 SHCC mix proportion

The mix proportion for SHCC is shown in Table 2. For SHCC specimens, a water to binder ratio of 43.2 %, sand to binder ratio

of 72 %, fiber volume of2 %, air content of 9.6 % and 12 mm PVA fibers with 0.04 mm in diameter were used. The tensile strength of the fiber is 1500 MPa and the Young's modulus is 40 GPa [14]. PVA fibers used in this study are shown in Figure 2.

Table 2 Mix proportion of SHCC

Materials	Quantity (kg/m^3)	(%)
Water	353	19.51
Cement	571	31.56
Fly ash (Type II)	245	13.54
Expansion admixture	20	1.11
Silica sand	585	32.34
PVA fiber (1.2% by vol.)	25	1.38
Super plasticizer	8.36	0.46
Viscous additive	1.67	0.09

Figure 2 PVA fibers

2.1.3. Mixing procedure and curing

In preparing ECC and SHCC mixes, the following mix procedures were used [14]:

- The dry ingredients were thoroughly mixed for 2 to 5 minutes
- 2/3 of the amount of water was added to the dry mix and mixing was continued for 1 minute
- Super plasticizer was added and mixed for 1.5 minutes
- The remaining water (1/3) was added and mixed for 1.5 minutes
- Finally, the fibers were added and mixed for 3 minutes

Casting of specimens with different depths was made by putting the mixes in a mold and tamping with a metal rod. Plastic sheets were used to cover the ECC specimens during the curing process. For SHCC specimens, the specimens were placed in a curing pond for 28 days. The specimen size, particularly the depth, was selected based on the experimental test results of trial ECC specimens with various depths loaded at mid-span. Because the overall effects (deflection and surface crack widths) were found small, a 2 cm deep specimen was chosen for repeated static and impact load tests. The ECC specimens (2cm thick) are shown in Figure 3.

Figure 3 ECC specimens (2cm thick)

2.2 Test Equipment and Setup

Hydraulic jack machine, data logger, impact loading apparatus, dynamic data logger, laser displacement sensor, crack width scale and Linear Variable Displacement Transducers (LVDT) were used. The specimen was simply supported with a span length of 120 mm and for repeated static load test case, it was loaded with two-point loads spaced at 40mm apart. Hence, the specimen size considered in this study was 16 cm×4 cm×2 cm.

2.2.1. Static loading apparatus

Hydraulic jack was used for static load testing and measurements of deflection and crack widths were made using LVDT and crack width scale, respectively. Clamping of specimen at the ends was made using steel plates and bolts as shown in Figure 4.

The residual deflection and crack widths were measured indirectly by taking out the specimens at every 50 cycles as shown in Figure 4, in which the LVDT was fixed to the loading frame. Loading rates were set as per the specification stipulated in JIS R 5201. For compressive strength test, load

rates of 2400±200 (N/s) and for flexural strength tests 50±10 (N/s) have been used [15].

Figure 4 Measuring deflection using LVDT

2.2.2. Impact loading apparatus

The drop weight impact loading method used in this study was based on the method proposed by ACI Committee 544 [16]. A schematic diagram of a drop-weight impact testing apparatus is shown in Figure 5.

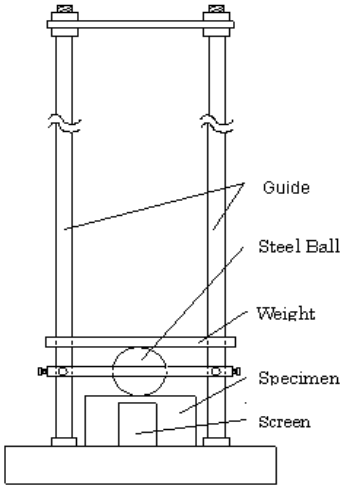

Figure 5 Schematic diagram of a drop-weight impact testing apparatus

A 5 kg square steel plate with dimensions of 250 mm by 10 mm thick and a 2 kg square steel tube of 40 mm in side length, 4mm in thickness, and 45 cm in length were applied through a steel ball to the top surface of ECC and SHCC specimens, respectively. As the drop-weight impact testing apparatus has a guide post spacing of 200 mm, in this study, the specimen's length was considered to be 160 mm.

2.2.3. Vibration loading test

ECC and SHCC specimens were subjected to drop-weight at different heights, and the vibration responses were recorded using a dynamic data logger. A picture showing the experimental set-up for direct measurement of impact/ dynamic test using laser displacement sensor is shown in Figure 6.

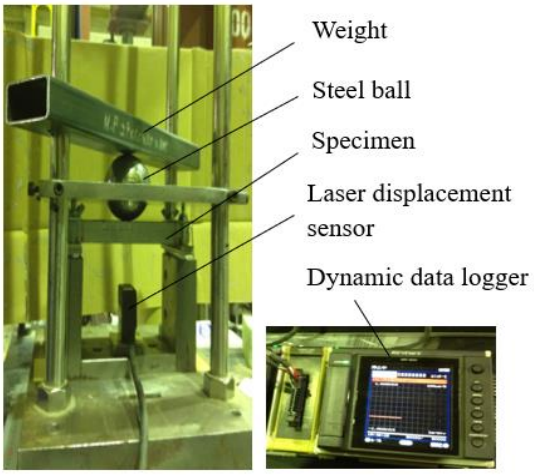

Figure 6 Direct measurement setup of impact test

2.3 Loading Conditions

Initially, a reference load of 75 % of the maximum load was applied statically to all ECC and SHCC specimens (maximum load carrying capacity of ECC specimens was 4kN and for that of SHCC specimens was 1.6 kN). This initial loading was used to generate finite multiple cracks.

2.3.1. ECC specimens

The loading condition of specimens due to static load (SL) and impact load (IL) for ECC is shown in Table 3.

Table 3 Loading conditions for ECC

Specimen	Loading condition
SL-1	3kN (high load level)
SL -2	3kN and 1.5 kN with an interval of 50 times (medium load level)
SL -3	1.5 kN (low load level)
IL -1	Drop height of 30 mm
IL-2	Drop heights of 20 and 30 mm with an interval of 50 times
IL -3	Drop height of 20 mm

2.3.2. SHCC specimens

The loading condition of specimens due to impact load (IL) for SHCC is shown in Table5. The impact loading test was repeated for 1000 times. The loading condition for SHCC is shown in Table 4.

Table 4 Loading conditions for SHCC

Specimen	Loading condition
IL -1A	Drop height of 30 mm
IL -2A	Drop heights of 20 and 30 mm with an interval of 50 times
IL -3A	Drop height of 20 mm

3. RESULTS AND DISCUSSION

3.1 Mechanical Properties

3.1.1. ECC specimens

The compressive and flexural strengths of ECC specimens are shown in Table 5 below.

Table 5 Mechanical properties of ECC

Properties	Strength (MPa)
compressive strength	186.9
Flexural strength	30.9

3.1.2. SHCC specimens

Mechanical properties of SHCC specimens are shown in Table 6.

Table 6 Mechanical properties of SHCC

Properties	Strength (MPa)
compressive strength	41.29
Flexural strength	16.39

3.2 Static Load Test Results

A hydraulic jack was used to apply load to ECC and SHCC specimens, with the load rates being manually controlled. In some cases, the load-deflection curves might not appear smooth due to fluctuations in the applied load and minor disturbances in the test set-up. In this study, for the first load cycle, the data points are adjusted to fit a smooth curve.

3.2.1 ECC Specimens

From test results, it was observed that ECC's ability to resist loads at higher number of loadings was found to be good. The load-displacement diagrams of ECC specimens under repeated static loadings (with 75% of the maximum load) are shown in Figure 7. Due to slight differences in the specimens' depth, the defections of the specimens for the first load cycle were found to be different.

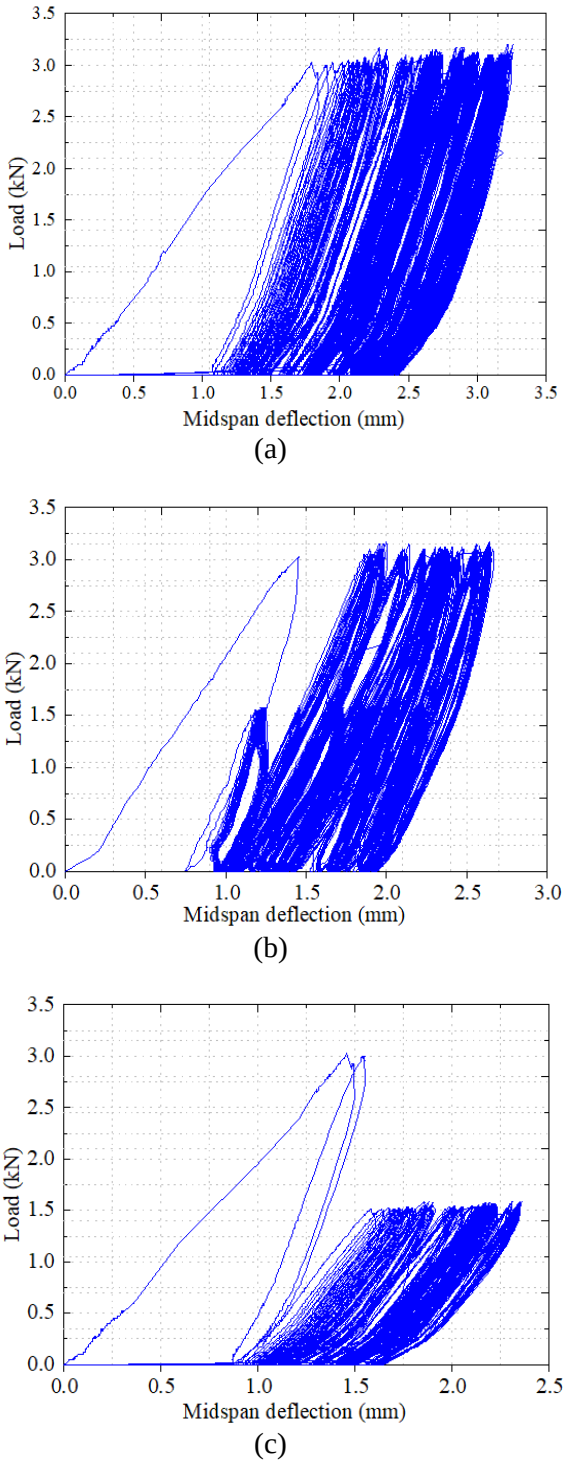

Figure 7 Load deflection diagram of ECC (a) SL-1 (b) SL-2 and (c) SL-3

The maximum deflection of the ECC specimen after the end of the 1000th static load was 3.25 mm with a residual deflection of 2.40 mm (for SL-1 loading condition). For the first load cycle, the total crack width for high level of static loadings remained below 0.35 mm and for that of low load level was found below 0.10 mm. The crack width result is in line with related researches conducted on fiber reinforced polypropylene ECC beams under reverse cyclic loadings [17]. Test results shown in Figure 7 revealed that the deformations of ECC specimens due to repeated static loading was increased gradually and it was small. This is due to the bridging effect of randomly distributed small diameter micro-fibers with high tensile strength and their ability to resist cracks as studied by Yang et al. [18].

Deformed and cracked ECC specimen under repeated static loading (SL-1) is shown in Figure 8.

(a)

(b)

Figure 8 Deformed ECC specimen under (a) high load level (SL-1) and medium load level (SL-2)

3.2.2 SHCC Specimens

SHCC beam specimens could not be loaded repeatedly as the member failed after a few numbers of static loadings. This is due to the fact that performance of SHCC under repeated static loading is relatively poor as studied by Zhu et al. [19]. The load-displacement diagram of SHCC specimen during the initial load cycle is shown in Figure 9.

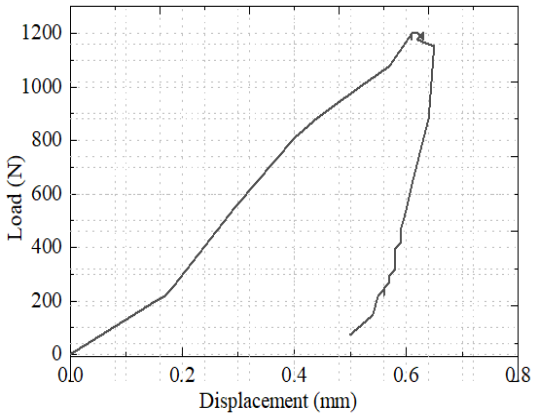

Figure 9 Load-displacement diagram of SHCC

3.3 Impact Load Test Results

3.3.1 ECC Specimens

The drop weight impact loading test results of ECC specimens for residual deflection and total crack widths are summarized in Figures 10 and 11, respectively. The residual deflectionswere computed with reference to the residual deflection of the first load cycle.

As shown in Figures 10 and 11, three different deformation zones of ECC, for IL-1 load case were observed. These zones are initial, steady and saturated zones. Initially, finite cracks are generated in this zone which is referred to as a pre-processing zone. This zone allows for a more accurate assessment of material behavior under practical loading conditions. This result is consistent with related research published by Yoo and Banthia [20], which shows that the fibers that are evenly distributed can sustain initial impacts without suffering substantial internal damage, leading to a linear deformation behavior.

Secondly, especially for medium level of impact loading, uniform and gradual increase in residual deflection was recorded. Finally, after the steady zone

was completed, remarkable and substantial pull-out of steel fibers has occurred and there was a rapid increase in residual deflection and crack width than expected. This condition leads to ductile failure of specimens, undesirable and the ECC specimen is no more useful. It is also observed that crack width varies as the cycle increases and it is an indication for the number of overloading. Deformed and cracked (1.2 mm) ECC specimen under the bottom side (IL-1) are shown in Figure 12.

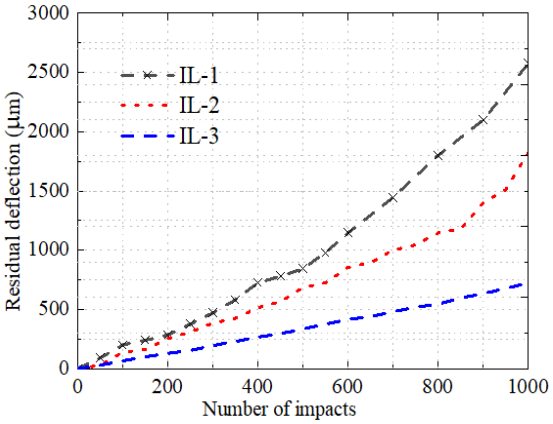

Figure 10 Residual deflection curves

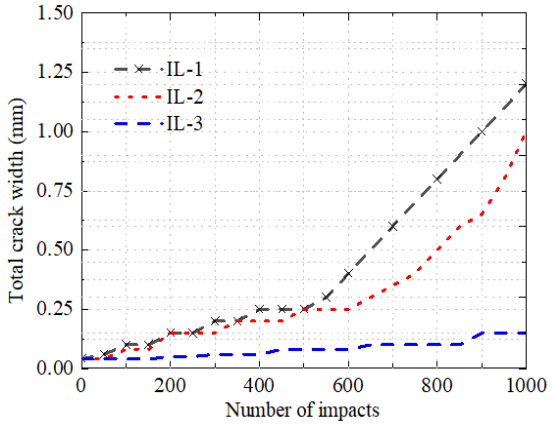

Figure 11 Total crack width curves

(a)

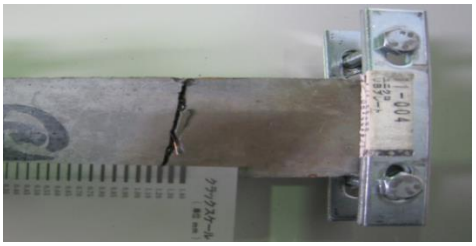

(b)

Figure 12 (a) deformed and (b) cracked pattern of ECC specimen (IL-1)

However, all the three zones were not observed for IL-2 and IL-3 loading conditions because the damages to these specimens due to 1000 number of low-level impact loading were found relatively small. Similar results have been found by Yoo and Banthia [20], showing that ECC tends to form small micro cracks rather than large, discrete cracks under low impact loading. The fibers within ECC bridge these micro cracks, controlling their growth and allowing the material to deform uniformly.

The test results from this study are comparable to those reported by Zhang et al. [21], wherein a uniform and gradual deformation was obtained by ECC's ability to deform under repeated impact loads without experiencing sudden failure. Further cracks eventually developed and as a result of this, increasing the residual deflection. ECC provides better impact resistance and load carrying capacity than conventional RC elements [22].

3.3.2 SHCC Specimens

The curves of residual deflection of SHCC specimens due to repeated impact loadings are shown in Figure 13. Unlike ECC, SHCC exhibited unusual deformation zones for load cases IL-1A and IL-2A due to their weak impact resistance, especially for the first 150 number of impacts.

In Figure 13, it is shown that at high level of impact loading, the deflection curve of IL-3A is non-linear and SHCC's resistance to impact is not good. Furthermore, with 1000 number of impacts, particularly specimen IL-1A (low load level) exhibited remarkable cracks at the center, unable to

resist the load and finally the specimen failed as shown in Figure 14. This could be due to an inconsistency mix of PVA fibers in the matrix [23]. As a result, crack width curves for SHCC specimens could not be measured. Recent research has demonstrated that ductility enhanced high strength SHCC (dHS-SHCC) can improve the drop-weight impact behavior of SHCC specimens [24].

As demonstrated in Figures 10 and 13, ECC exhibited large impact resistance as compared to SHCC specimens. The result is consistent with related experimental results where an ECC panel has a significant impact resistance with reduced damage [21, 22]. The residual deflection of ECC was found to be 28 % to 54 % smaller than that of SHCC.

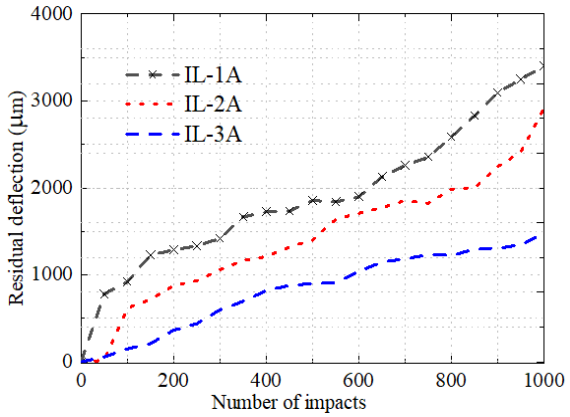

Figure 13 Residual deflection curves of SHCC

Figure 14 Deformed and cracked SHCC specimen under impact loading

3.4 Vibration Test Results

3.4.1 Dynamic responses

A direct measurement of deflection of ECC and SHCC specimens under impact loading with drop heights of 30mm and 40mm was carried out by the use of laser displacement sensor and a dynamic data logger. The impact load in the case of ECC was 5 kg and for that of SHCC was 2 kg. The displacement histories are shown in Figure 15.

In Figure 15, it is shown that, even under the action of smaller impact loads, the impact resistance of SHCC is lower than ECC specimens, i.e., the deflection of SHCC is significantly greater than that of ECC. Moreover, due to number of impacts, closely spaced micro cracks have been developed in ECC specimens. These micro-cracks with low crack width show that the ability of ECC materials to resist cracks is excellent. This makes ECC a better choice of material than SHCC for impact loads. The result on crack width formation is comparable with the research conducted by Qin et al. [25].

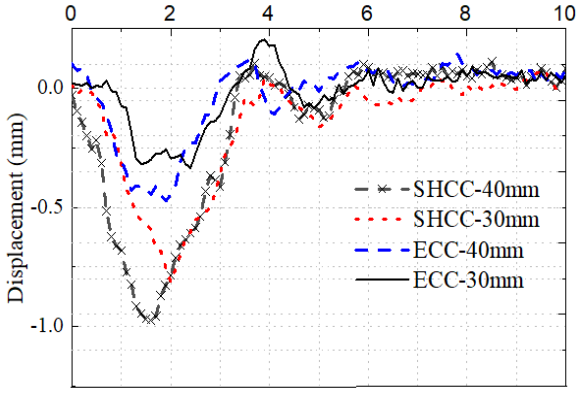

Figure 15 Displacement histories/ dynamic response of ECC and SHCC specimens

3.4.2 Damping Property

The free vibration decay method calculates a logarithmic decrement which helps to find the damping ratio [26]. From the amplitude records of the impact load tests (Figure 15), the values of the damping ratio were calculated using Eq. (1) [27, 28] and the results are summarized in Table 7.

$$\xi = \frac{1}{2n\pi} \ln\left(\frac{A_o}{A_n}\right) \quad (1)$$

where:

ξ is the damping ratio (%)
A_o is an initial amplitude
A_n is the amplitude after *n* cycles

Table 7 Damping ratios of ECC and SHCC

Specimens	Amplitudes		ξ (%)
	A_1	A_3	
ECC-40	0.44	0.03	14.25
ECC-30	0.33	0.02	14.89
SHCC-40	0.94	0.14	10.11
SHCC-30	0.81	0.09	11.65

From Table 7, it is observed that damping ratios of ECC and SHCC range from 10% to 15% and ECC shows a higher damping capacity (on average, ECC had a 34 % higher damping property than SHCC). The average damping ratio of ECC specimens is 26.56 % higher than recent research conducted by Tian, Y., et al. [29], in which the maximum damping ratio of fiber containing cement-based mortar specimens reached to 10.7 %.

3.5 Comparison of ECC and SHCC

Summary of comparison of ECC and SHCC specimens is shown in Table 8.

Table 8 Comparison of test results

Properties		ECC	SHCC
Strength (MPa)	Compression	186.9	41.29
	Flexural	30.90	16.39
Load carrying capacity of specimens for two-point loads (N)		3,500	1,200
Residual deflection(mm) for impact loading		2.60 (IL-1)	3.45 (IL-1A)
Maximum crack width (mm) for impact loading		1.2 (h=30mm & w=5kg)	6 (h=30mm & w=2kg)
Vibration response (mm)		0.44	0.94
Damping ratio (%)		14.57	10.88

From Table 8, for the specific mixes, ECC exhibited less damage during deformation and maintained high impact resistance as specified in other researches [30, 31] than equal-sized SHCC specimens even with a reduced drop weight and height. This behavior is also reflected on the residual deflection and crack width patterns, where SHCC specimens loaded with a 2 kg impact load, cracked five times wider than ECC specimens subjected to a 5 kg drop weight.

Therefore, based on the benefits of ECC material and experimental results of this study, it was observed that ECC can last longer without remarkable deterioration and withstand impact loading safely as compared to SHCC.

4. CONCLUSIONS

According to the experimental test results of this study, ECC specimens exhibited uniform behavior under low loading levels and showed a better resistance to repeated static and impact loads with insignificant damage. It was observed that, on average, the residual deflection of ECC specimens caused by repeated impact loads was less than those of SHCC by 40 %.

For the same drop heights, the vibration response of SHCC specimens was two times larger than that of ECC specimens. The vibration test result also showed ECC had a 34% higher damping ratio than SHCC. Because of this, ECC can be used appropriately for the construction of bridges, pavement overlays, retrofitting and strengthening of structural elements subjected to high impact and repeated loads.

SHCC's resistance to repeated impact loads is much lower than ECC specimens even under low-level of impact loads (60 % of the weight applied to ECC specimen was applied to SHCC specimen) with a reduced height (33.33 % lower than the level where the load was dropped to ECC specimens).

For future work, it is recommended to evaluate the sustainability of ECC and SHCC using a comprehensive life cycle analysis.

CONFLICT OF INTEREST

The author declares that there is no conflict of interest.

ACKNOWLEDGEMENTS

The author acknowledges the Engineering Research Management Learning Program at YNU in Japan and Kajima Corporation for their financial support, Professor Tatsuya Tsubaki and Mr. Dai Oba for their technical assistance.

REFERENCES

[1] Li, V. C., "*Engineered Cementitious Composites* (*ECC*)*-Material, Structural, and Durability Performance*", University of Michigan, Ann Arbor, 2007.

[2] Li, V.C., "*On Engineered Cementitious Composites* (*ECC*) *a Review of the Material and its Applications*", Journal of advanced Concrete Technology, 1(3), 2003, pp.215-230.

[3] Ajin Prasad, "*New Bendable Concrete that is Stronger and More Durable*", 2018. https://www.linkedin.com/ pulse/ new-bendable-concrete-stronger-more -durable-ajin-prasad.

[4] Kaur, M., & Gupta, R. C., "*Performance Evaluation of Hybrid Fiber Reinforced Concrete at Elevated Temperature*", Construction and Building Materials, 68, 2014, pp. 421-428.

[5] Park, P., Jones, R., Castillo, L., Vallangca, M. and Cantu, F., "*Engineered Cementitious Composites* (*ECC*) *for Applications in Texas* (No. FHWA/TX-20/0-7030-1)", Texas. Dept. of Transportation. Research and Technology Implementation Office, 2020.

[6] Matsubara, N., "*Application of a New Type of Ultra-High Strength Fiber Reinforced Concrete to a Prestressed Concrete Bridge*", In the 2nd International Symposium on Ultra-High-Performance Concrete, 2008, pp.787-794.

[7] Fischer, G. and Li, V.C., "*Deformation Behavior of Fiber-Reinforced Polymer Reinforced Engineered Cementitious Composite (ECC) Flexural Members under Reversed Cyclic Loading Conditions*", Structural Journal, 100(1), 2003, pp.25-35.

[8] van Zijl, G.P., Wittmann, F.H., Oh, B.H., Kabele, P., Toledo Filho, R.D., Fairbairn, E.M., Slowik, V., Ogawa, A., Hoshiro, H., Mechtcherine, V. and Altmann, F., "*Durability of Strain-Hardening Cement-Based Composites* (*SHCC*)", Materials and Structures 45, 2012, pp. 1447–1463.

[9] Figueiredo, T.C.S., Curosu, I., Gonzáles, G.L., Hering, M., de Andrade Silva, F., Curbach, M. and Mechtcherine, V., "*Mechanical Behavior of Strain-Hardening Cement-Based Composites* (*SHCC*) *Subjected to Torsional Loading and to Combined Torsional and Axial Loading*", Materials & Design, 198, 2021.

[10] Zhang, X., Liu, S., Yan, C., Wang, X. and Wang, H., "*Effects of Vehicle-Induced Vibrations on the Tensile Performance of Early-Age PVA-ECC*", Materials, vol. 12, no. 17, 2019, pp. 1-17.

[11] Lin, J.X., Song, Y., Xie, Z.H., Guo, Y.C., Yuan, B., Zeng, J.J. and Wei, X., "*Static and Dynamic Mechanical Behavior of Engineered Cementitious Composites with PP and PVA Fibers*", Journal of Building Engineering, 29, 2020.

[12] Elnagar, A.B., Afefy, H.M., Baraghith, A.T. and Mahmoud, M.H., "*Experimental and Numerical Investigations on the Impact Resistance of SHCC-Strengthened RC Slabs Subjected to Drop Weight Loading*", Construction and Building Materials, 229, 2019, pp. 1-19.

[13] Sun, Y., Gu, Z.X., Li, A. and Shao, G.J., "*Effect of Structural Features and Loading Parameters on Bond in Reinforced Concrete Under Repeated Load*", Structural Concrete, vol. 18, no. 6, 2017, pp. 862-871.

[14] JSCE, "*Recommendations for Design and Construction of Ultra-High Strength Fiber Reinforced Concrete Structures- Draft"*, Concrete Library 113, 2004.

[15] JIS, R., 5201, "*Physical Testing Methods for Cement. Japanese Industrial Standard Committee"*, 2015.

[16] ACI Committee 544, "*Measurement of Properties of Fiber Reinforced Concrete*", ACI Material Journal, vol. 85, no. 6, 1988, pp 583-593.

[17] Chia Hwan, Y. and Jian Bo, H., "*The Mechanical Behavior of Fiber Reinforced PP ECC Beams under Reverse Cyclic Loading*", Advances in Materials Science and Engineering, 2014, pp.1-9.

[18] Yang, E.H., Wang, S., Yang, Y. and Li, V.C., "*Fiber-Bridging Constitutive Law of Engineered Cementitious Composites*", Journal of Advanced Concrete Technology, vol. 6, no. 1, 2008, pp.181-193.

[19] Zhu, J.X., Xu, L.Y., Huang, B.T., Weng, K.F. and Dai, J.G., "*Recent Developments in Engineered/Strain-Hardening Cementitious Composites* (*ECC/SHCC*) with *High and Ultra-High Strength*", Construction and Building Materials, 342, 2022.

[20] Yoo, D.Y. and Banthia, N., "*Mechanical and Structural Behaviors of Ultra-High-Performance Fiber-Reinforced Concrete Subjected to Impact and Blast*", Construction and Building Materials, 149, 2017, pp. 416-431.

[21] Zhang, J., Maalej, M. and Quek, S.T., "*Performance of Hybrid-Fiber ECC Blast/Shelter Panels Subjected to Drop Weight Impact*", Journal of Materials in Civil Engineering, vol. 19, no. 10, 2007, pp. 855-863. doi.org/10.1061/(ASCE)0899-1561(2007)19:10(855)

[22] Yang, E.H. and Li, V.C., "*Tailoring Engineered Cementitious Composites for Impact Resistance*". Cement and Concrete Research. vol. 42, no. 8, 2012, pp. 1066-1071.

[23] Lu, C., Pan, J., Luo, B., Li, Z. and Leung, C.K., "*Correlation of Flaw Structure and Cracking Behavior in SHCC with X-Ray CT Scanning Technique*", Construction and Building Materials, 331, 2022.

[24] Kim, M.J., Choi, H.J., Shin, W., Oh, T. and Yoo, D.Y., "*Development of Impact Resistant High-Strength Strain-Hardening Cementitious Composites (HS-SHCC) Superior to Reactive Powder Concrete (RPC) under Flexure*", Journal of Building Engineering, 44, 2021.

[25] Qin, F., Zhang, Z., Xie, B. and Sun, R., "*Experimental Study on Damage Detection in ECC-Concrete Composite Beams Using Piezoelectric Transducers*", Sensors, vol. 19, no 12, 2019.

[26] Gabryś, K., Soból, E., Sas, W. and Szymański, A, "*Material Damping Ratio from Free-Vibration Method*". Ann. Wars. Univ. Life Sci. SGGW Land Reclam, 50, 2018, pp. 83-97.

[27] Yan, L., Jenkins, C. and Pendleton, R., "*Polyolefin Fiber-Reinforced Concrete Composites: Part I. Damping and Frequency Characteristics*", Cement and Concrete Research, vol. 30, no. 3, 2000, pp. 391-401.

[28] Zheng, L., Huo, X.S. and Yuan, Y., "*Experimental Investigation on Dynamic Properties of Rubberized Concrete*", Construction and Building Materials, vol. 22, no. 5, 2008, pp. 939-947.

[29] Tian, Y., Lu, D., Zhou, J., Yang, Y. and Wang, Z., "*Damping Property of Cement Mortar Incorporating Damping Aggregate*", Materials, vol. 13, no. 3, 2020.

[30] Yang, E.H. and Li, V.C., "*Tailoring Engineered Cementitious Composites for Impact Resistance*", Cement and Concrete Research, vol. 42, no. 8, 2012, pp. 1066-1071.

[31] Li, V. C., and Leung, C. K., "*Steel-Fiber-High-Strength-Concrete Composites*", Materials Journal, vol. 89, no. 5, 1992, pp. 441-450.

Machine Learning Based Contamination Detection in Water Distribution System

Akalewold Fikre[1,*], Getachew Alemu[1]

[1]*School of Electrical and Computer Engineering, Addis Ababa Institute of Technology, Addis Ababa University, Addis Ababa, Ethiopia*
*****Corresponding author's Email address: akale98@gmail.com

DOI: https://doi.org/10.20372/zede.v42i.10185

ABSTRACT

Water is a necessary component of all human activities. According to the United Nations World Water Assessment Program, every day, 2 million tons of sewage, manufacturing, and agricultural waste are discharged into the world's water. Due to population demands and dwindling clean water supplies as well as available water pollution management mechanisms; there is an urgent need to use computational methods to intelligently manage available water. This paper proposes artificial neural networks, specifically, Convolutional Neural Networks (CNNs), for automated water impurity detection. To refine the model, the picture of turbid water in the pipe was used to detect events. The algorithm of deep learning achieved 96.3 %t accuracy after extensive training with a dataset of 4220 images reflecting various levels of contamination. This shows that, the model can be used in water system pollution detection.

Keywords: - CNN, NTU, Water quality, Water impurity detection

1. INTRODUCTION

Drinking pure water is an issue for water supply companies around the world, and it is currently a well-known problem due to numerous vulnerable threats. An example is the 1993 contamination event in Milwaukee, which affected 403,000 people, resulting in thousands of hospitalizations and a hundred of fatalities, with $96.2 million in medical and productivity costs [1]. Because of all the threats to public health, water system pollution detection is critical. In recent years, water quality sensors that are connected to the internet can be used to improve real-time monitoring of water quality. In the past, various approaches were proposed to address pollution detection issues, including single or multiple-type measurements that are analyzed separately or in combination from one or more locations in the network, using model-based or model-free approaches. The motivation of this work is the fact that, currently, machine learning techniques become promising for detecting contaminants in water quality. In this work we propose deep learning NN technique to determine the level of contamination of water based on an image.

Turbidity is a calculation of a liquid's relative visibility. Turbidity measures the concentration of light reflected by materials in the water; it increases when the materials found in the sample water rise. Clay, silt, organic and very tiny inorganic matter, algae, plankton, ingested colored organic compounds, and other microscopic species all contribute to the turbidity of water. Previous studies have found a relationship between turbidity levels and gastrointestinal disease [2]. More than 29 water quality parameter tests are monitored using a conventional method, including physical, chemical, and biological properties. From these 29 water quality parameters, in the operation that are most commonly and frequently sampled or

monitored for water quality, include. temperature, disinfectant residual (chlorine concentration), pH, conductivity, ORP, and turbidity. Even among these selected parameters, the most frequently used water quality parameter to detect water contamination is chlorine concentration and turbidity. So, from these two parameters, turbidity was chosen because the other water quality parameters directly or indirectly affect it.

The goal of this work was to develop a model-based approach for pollution detection throughout the water distribution system using turbid water images as they are closely correlated with the physicochemical properties of other water quality parameters. Researches done prior to our work have used different methods and obtained different results. Some studies [3, 4 and 5] planned three water quality detection methods based on a comparison of calculated and observed values and receiver operating characteristic (ROC) curves to test each technique. The US Environmental Protection Agency (EPA) has tested over 30 pollutants (including pesticides, insecticides, metals, and bacteria) that may be used in deliberate acts of water pollution [6, 7].

Yang et. al. [8] used a pilot-scale pipe system to monitor 11 pollutants at various concentrations using adaptive transformation of sensory measurements. As a result, pollutant classification and detection based on chlorine kinetics were made possible. The system developed by Guepie et al., [9] was based on residual chlorine decay. Their hypothesis was that a contaminant in the WDS would absorb a large portion of the measured chlorine, and that this single parameter would provide enough information. The methods used in the previous studies were supervised classification methods. However, when there are no real-time measurements of contamination events, the models must be trained and tested using simulated contamination events. In these models some random disturbances are added to the measured data to reflect the contaminant effect to preserve generality in the absence of sufficient information, In this regard, Eliades et.al, [10] looked into the issue of water quality by using a model-based method for detecting pollution events in water treatment systems. It takes into account well-known chlorine input signals and produces bounds of the predicted chlorine concentration at different sensing locations at each time stage by running several Monte-Carlo simulations in parallel with the real system. The result demonstrates that the system will adjust the detection bounds as the chlorine concentration input varies. Chlorination is the method of adding chlorine to drinkable water to disinfect it and destroy germs. It fixes one of many issues here. Contamination, on the other hand, occurs for a variety of causes and has varying effects on various parameters. As a result, detecting pollution based on chlorine concentration does not provide a complete control mechanism.

Mohammed et.al [11] introduced Adaptive neuro- fuzzy inference system (ANFIS) models. This work prompted us to redesign the algorithm for certain water quality parameters that are highly correlated with one another and have an impact on the algorithm's efficiency.

It is intriguing to find out which parameters are closely correlated and then remodel the algorithm. In the work of Mohammad pour et al. [12] used three separate algorithms, to investigate the issue of water quality. R2, RMSE, and MAE are used to compare results and they found SVM is competitive with neural networks in terms of results.

The system developed by Revathi et al. [13] suggests using a wireless sensor network to develop and implement an actual system of water quality control for drinking water. The

proposed system is low in cost, lightweight, and consumes little power.

An automated Aqua Sight water pollution detection method [14] uses a picture to assess the level of contamination in water. Here, they have used a CNN which involves an image of water to decide whether or not pollutants are present. In a report [18], it was suggested an intelligent real-time water quality monitoring strategy and concentrated on classifying water quality using machine learning techniques. The dataset includes dissolved oxygen, pH, conductivity, nitrate, biochemical oxygen demand, fecal coliform, and total coliform. In this study, among the different machine learning classifiers used, CAT Boost was determined to be the top classifier and stacking model. Shams et.al, [19] the grid search approach is applied in this research to adjust the parameters of four classification models and four regression models. It is reported that, for predicting WQI values, the MLP regressor model using the grid search strategy produced the best results, with an R2 equal to 99.8 %.

Many aspects of the water quality at a specific place and time are covered by the Water Quality Index (WQI). The WQI computation is time-consuming and often influenced by errors when doing subindex computations. Therefore, developing an effective WQI forecasting method is essential.

2. MATERIALS AND METHODS

2.1. Collection of water samples

The first step in data processing is to obtain water samples from various locations. From various locations, a total of 216 water samples were collected. The samples were collected throughout different phases of a treatment plant, including raw water (Figure 1) during sedimentation, and finally from the reservoir (Figure 2) city reservoir, and household. Parts of the city where water pipes were exposed to domestic waste were chosen as sampling sites. Another criteri0n used in the selection process was proximity to contamination sources like industrial wastewater and hospital effluent outlets. Since the water pipe could not be accessed anywhere, locations had to be selected where it would be convenient to take samples if it broke down due to construction or some other reason. The majority of the samples were taken in the morning. The collection protocol followed the Addis Ababa Water and Sewage Authority's procedures (AAWSA).

Figure 1 The raw water at the time of sampling

Figure 2 Water Reservoir at the time of sampling.

The samples were analyzed for turbidity, pH, EC, TDS, Total Alkalinity, Calcium Hardness, Total Hardness, Magnesium Hardness, Ammonia, Nitrate, Nitrite, Phosphate, Fluoride, Iron, Manganese, Silica, Chloride, and Bicarbonate Alkalinity. All measurements were carried out in line with WHO requirements. Designer’s should consider changes throughout the physicochemical properties of water, concentrating on the turbidity of the water that is influenced by the chemical and biological particles of the contaminant (Figure 3 and 4), based on the findings of the previous parts.

Figure 3 Clean water with normal light

Figure 4 Contaminated water with 100mg/liter of sodium nitrate

A single or multiple parameters may affect the quality of water. In the conventional method, if multiple parameters contribute to water pollution, the parameters and their contribution levels are identified in order to apply the treatment mechanism accordingly. For example, the most commonly known water quality parameters that appear together are iron and manganese. Sometimes, they both contribute to water pollution in different levels, to determine the behavior of water quality. This means the highly contributing parameters dominate in determining whether water is potable or not. But the treatment mechanisms consider both of the parameters, based on the WHO standard. In this research, machine learning determines the behavior of the water based on the turbidity of the water, whether a single or multiple parameters contribute to water pollution. We studied the effects of different parameters on the characteristics of turbidity. So, if the turbidity values are higher than the normal values (5 NTU) due to a single or multiple parameters, the model will identify the water as potable. The dataset for the proposed method is generated based on the properties of the turbidity of the water. As the turbidity of the water rises, it decreases the purity of the water and the transmitted light by scattering and adsorbing the light.

When we look at clean water, it transmits light (see Figure 3). Clean water has normal light, and if it is contaminated, it decreases the transmission. (See Figure 4 contaminated water with 100 mg/liter of sodium nitrate in normal light). For example, in the sample taken on January 8, 2020, total dissolved solids (TDS) for clean water were 74 mg/L, and in the sample taken the same day, total dissolved solids (TDS) for polluted water were 524 mg/L. So, for the contaminated one, the water cloudiness increases greatly. The RGB of the images changes as the cloudiness of the images increases. This characteristic of the image plays a great role in determining if the water is potable or not.

2.2. Pre-processing

Noise can seriously affect the quality of digital images. Different factors may be responsible for introduction of noise in the image. In this phase of the system, we apply three different filters used for smoothing, sharpening and denoising to pre-process image in order to obtain a picture with more stable region. Eliminating the noise without blurring the details too much and enhancing edges without amplifying noise is very difficult. So, when using more than one filter, special care should be taken in order to make sure their effect is important. In this regard, the following filters were used sequentially.

i. Bilateral filter: To smooth the image
ii. High-pass filter: To sharpen images
iii. Median filter: To filter out noise from images

2.3. Model Design

Machine Learning (ML) algorithms are well-known for learning the underlying

relationship in data and making decisions without the need for explicit instructions. CNNs are a form of neural network that are used in deep learning. CNNs are large networks of nodes called neurons that create connections as they learn from data. Since CNNs require a person to identify specific features for a model to examine, they perform supervised learning. CNNs are one of the most powerful learning algorithms for comprehending image information, with excellent results in image segmentation, classification, identification, and retrieval tasks [15, 16]. CNN is divided into several learning levels, each of which consists of a mixture of convolutional layers, nonlinear processing units, and subsampling layers [17].

As a result, we constructed the model's structure, spawning numerous layers that perform various functions and contribute to the model's output in various ways. The convolution operation aids in the extraction of useful features (Figure 6) from data points that are globally correlated.

The non- linear processing unit (activation function) receives the output of the convolutional kernels, which not only aids in learning abstractions but also embeds non-linearity in the feature space. This non-linearity results in various activation patterns of different reactions, allowing it easier to understand semantic differences in images.

The proposed architecture consists of pooling and convolution layers alternated with one or more completely connected layers at the end. The convolutional layer executes a process called "convolution." Every neuron performs as a kernel throughout the convolution layers, which would be made up of a collection of convolution kernels.

Create the model: The model is made up of four convolution blocks, each with a max pool layer (Table 1). A relu activation feature is used to enable a completely connected layer with 512 units on top. This model hasn't been fine-tuned for high precision.

Table 1 The designed model.

```
Model: "sequential"
_________________________________________________________________
Layer (type)                 Output Shape              Param #
=================================================================
conv2d (Conv2D)              (None, 73, 73, 64)        1792
_________________________________________________________________
max_pooling2d (MaxPooling2D) (None, 36, 36, 64)        0
_________________________________________________________________
conv2d_1 (Conv2D)            (None, 34, 34, 64)        36928
_________________________________________________________________
max_pooling2d_1 (MaxPooling2 (None, 17, 17, 64)        0
_________________________________________________________________
conv2d_2 (Conv2D)            (None, 15, 15, 64)        36928
_________________________________________________________________
max_pooling2d_2 (MaxPooling2 (None, 7, 7, 64)          0
_________________________________________________________________
conv2d_3 (Conv2D)            (None, 5, 5, 64)          36928
_________________________________________________________________
max_pooling2d_3 (MaxPooling2 (None, 2, 2, 64)          0
_________________________________________________________________
flatten (Flatten)            (None, 256)               0
_________________________________________________________________
dense (Dense)                (None, 512)               131584
_________________________________________________________________
dense_1 (Dense)              (None, 5)                 2565
=================================================================
Total params: 246,725
Trainable params: 246,725
Non-trainable params: 0
_________________________________________________________________
```

The convolutional kernel divides the image into small slices, known as receptive fields, as shown in Figure 6. Extracting feature motifs is easier when an image is divided into small blocks.

Once features have also been retrieved, their actual position is less important as long as their relative position to others is preserved. Down-sampling, also known as pooling (Figure 7) is an intriguing local process. It compiles similar data in the general neighborhood of the receptive field and outputs the dominant response for that area.

Max pooling takes the largest element from the rectified feature map (Figure 6). Taking the largest element could also take the average pool.

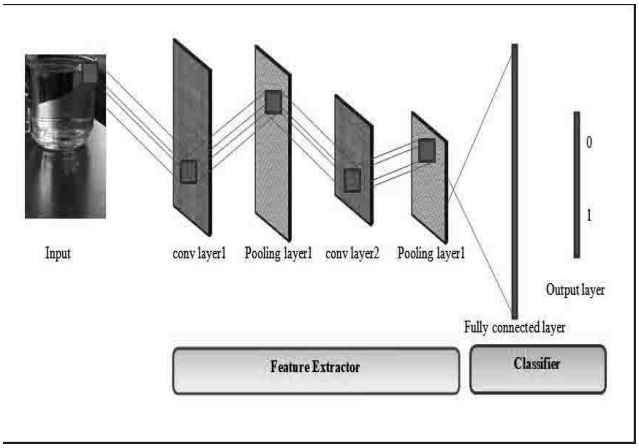

Figure 5 Architecture of the Convolutional Neural Network.

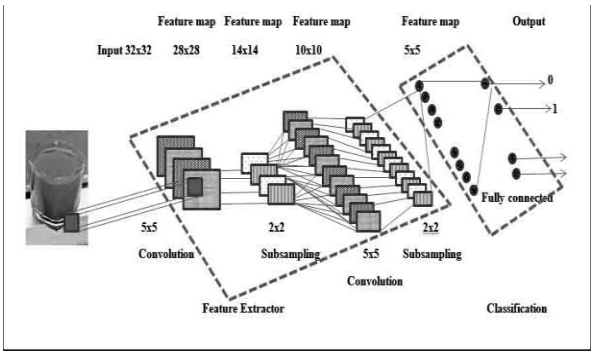

Figure 6 Segmentation Process.

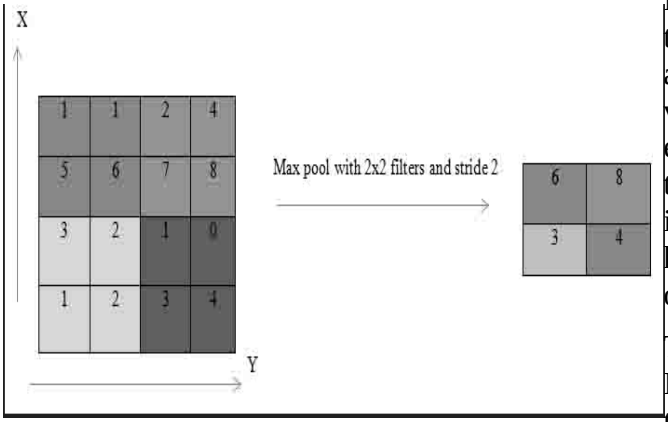

Figure 7 Max Pooling.

3. RESULTS AND DISCUSSIONS

The system model error rates are significant indicators in assessing the model's success in the proposed architecture. The accuracy indicates the likelihood that the picture will fit the target mark correctly. The accuracy level of the model varies throughout the training cycle due to the dataset used for training and validating the model. The model which was created in the previous section is made up of 4 convolutional layers, 4 max pooling layers, and 1 dense layer. The accuracy of validation was 80.49%. This means we can correctly classify 80.49% of the images in the validation collection that the model missed.

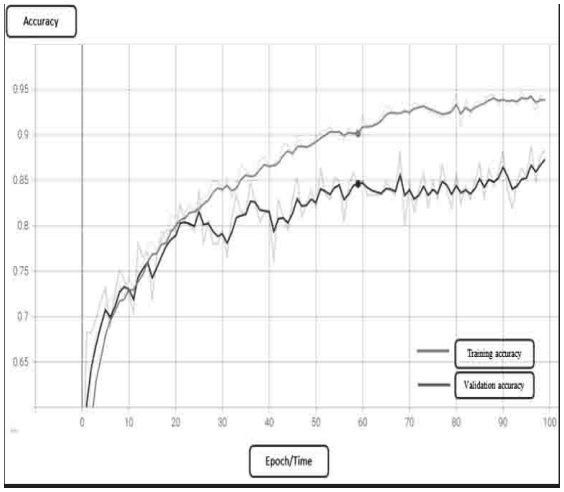

Figure 8 Training and validation accuracy for the proposed model

From Figures 8 and 9, we can see that the training accuracy is above the validation accuracy and training loss is way below the validation loss, especially after the 20th epoch. When there are few training datasets, the model can learn from sounds or unwanted information in the training dataset, which can have a negative effect on the model's output on the new dataset.

This phenomenon is known as over-fitting. It means that the model will have a difficult time generalizing on the new dataset. There are many methods for combating over-fitting during the training period. Using data augmentation and adding Dropout to the model are the two main methods.

Data augmentation is a technique to produce further training data from an existing dataset

by augmenting it with random transformations that result in believable-looking photos. This allows the model to be exposed to more facets of the data and generalize more effectively. The updated model was trained with 4220 images and its testing dataset contained 1055 images, based on the principle of data augmentation.

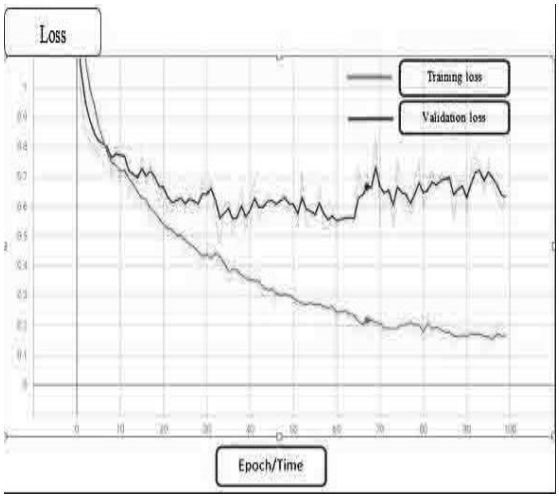

Figure 9 Training and validation loss for the proposed model

Dropout, the kind of regularization, is another technique for reducing over-fitting in the network. When Dropout is applied to a layer, it randomly removes a number of output units from the layer during the training phase (by setting the activation to zero). Dropout accepts fractional numbers as in the manner of 0.1, 0.2, 0.4, and so on as data.

This means that 10 %, 20 %, or 40 % of its output nodes from the applied layer would be randomly removed. In addition to that, it helps to optimize the model until it achieves the best accuracy on training and validation, as well as to get relatively low loss model architecture.

Layers and nodes per layer, as well as 0, 1, or 2 dense layers, are the simplest things to change in the model. Finally, the model achieved an almost match with well-balanced training and validation metrics (Figures 10 and 11), with validation accuracy of 94.82 percent and the highest (lowest) validation loss of 0.1719. The result was achieved using two convolutional layers, each with 64 nodes, 2 max pooling layers, and one dense layer followed by a single dropout.

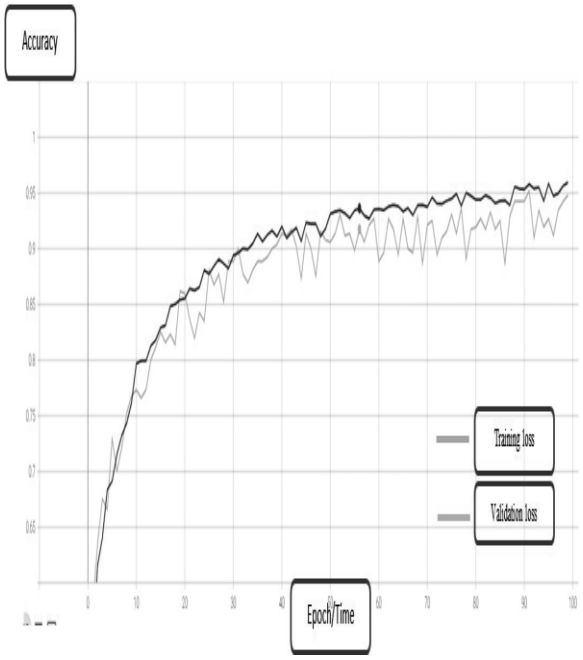

Figure 10 Training and validation accuracy for the best models

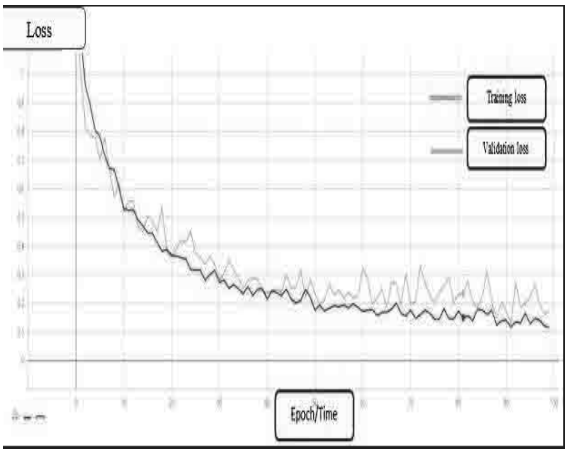

Figure 11 Training and validation loss for the best models

In addition to metrics directly from the model and its prediction values, F1-score, Precision, Sensitivity, and Accuracy can all be calculated. In general, classification accuracy can mask the information essential to diagnose the model's performance. As a

result, generating a confusion matrix can help to figure out what the classification model is getting right and where it is going wrong. Table 2 is a multiclass confusion matrix of the classes.

Table 2 A Multi-classes Confusion Matrix of the classes

		Predicted				
	Class	Chemical	Clay	Clean	Sand	Silt
Actual	Chemical	208	0	0	0	2
	Clay	0	206	0	5	1
	Clean	0	3	203	3	1
	Sand	1	1	5	201	4
	Silt	2	7	0	4	198

4. CONCLUSIONS

The system model error rates are significant indicators in assessing the model's success in the proposed architecture. The accuracy indicates the likelihood that the picture will fit the target mark correctly. The accuracy level of the model varies throughout the training cycle due to the dataset used for training and validating the model. The model was made up of 4 convolutional layers, 4 max pooling layers, and 1 dense layer is used. The accuracy of validation was 80.49 %. This means we can correctly classify 80.49 % of the images in the validation collection that the model missed.

CONFLCT OF INTEREST

The authors declare that there is no conflict of interest in this work.

ACKNOWLEDGEMENTS

We would like to express our gratitude to Addis Ababa University, Addis Ababa Institute of Technology, School of Electrical and Computer Engineering. The accomplishment of the paper would not have been possible without its support.

REFERENCES

[1] Corso, P., Kramer, M., Blair, K., Addiss, D., Davis, J., Haddix, A., *"Cost of illness in the 1993 waterborne cryptosporidium outbreak, Milwaukee, Wisconsin"*, Emerging Infectious Diseases vol. 9. 2003, pp. 426–431.

[2] Schwartz, J., Levin, R., *"Drinking water turbidity and health"*, Epidemiology, vol. 10, no. 1, 1999, pp. 86-90.

[3] Klise, K.A., McKenna, S.A., *"Multivariate application for detecting anomalous water quality"*, In: Proceedings of the 8th Annual Water Distribution Systems Analysis Symposium. WDSA, Cincinnati, Ohio, USA, 2006, pp. 1-11.

[4] Klise, K.A., McKenna, S.A., *"Water quality change detection: multivariate algorithms"*, In: Saito, T.T., Lehrfeld, D. (Eds.), Proc. SPIE, vol. 6203, 2006, pp. 1–9.

[5] McKenna, S.A., Wilson, M., Klise, K.A.,*"Detecting changes in water quality data,"*, Journal of the American Water Works Association, vol. 100, no. 1, 2008, pp. 74-85.

[6].https://nepis.epa.gov/Exe/ZyPDF.cgi/P1004B3M.PDF?Dockey=P1004B3M.PDF. (Accessed on: Jan 13, 2021).

[7]https://nepis.epa.gov/Exe/ZyPDF.cgi/P1004B4D.PDF?Dockey=P1004B4D.PDF. (Accessed on: Jan 13, 2021).

[8] Yang, J.Y., Haught, C.R., Goodrich, A.J., *"Real-time contaminant detection and classification in a drinking water pipe using conventional water quality sensors"*, techniques and experimental results. Journal of Environmental Management, vol. 90, no. 8, 2009, pp. 2494- 2506.

[9] Guepie, B.K., Fillatre, L., Nikiforov, I.,

"*Sequential monitoring of water distribution network",* In: Paper Presented at the IFAC Proceedings Volumes (IFAC-papers Online), vol. 45, no. 16, 2012, pp. 392-397.

[10] Eliades, D. G., Lambrou, T. P., Panayiotou, C. G., & Polycarpou, M. M. *"Contamination event detection in water distribution systems using a model-based approach",* Procedia Engineering, vol. 89, 2014, pp. 1089–1096.

[11] Mohammed, H., Hameed, I. A., & Seidu, R. "*Machine Learning – Based Detection of Water Contamination in Water Distribution Systems*", GECCO18. 2018. pp.1664–1671.

[12] Mohammadpour, R., Shaharuddin, S., Chang, C. K., Zakaria, N. A., Ab Ghani, A., & Chan, N. W., *"Prediction of water quality index in constructed wetlands using support vector machine",* Environmental Science and Pollution Research, vol. 22, no. 8, 2015, pp. 6208–6219.

[13] Kavi Priya, S., Shenbagalakshmi, G., & Revathi, T., *"Design of smart sensors for real time drinking water quality monitoring and contamination detection in water distributed mains",* International Journal of Engineering and Technology, vol. 7(1.1) 2017, pp. 47-51.

[14]https://arxiv.org/pdf/1907.07573.pdf (Accessed on: May 30, 2020).

[15] Ciresan, D., Giusti, A., Gambardella, L.M., Schmidhuber, J., *"Deep neural networks segment neuronal membranes in electron microscopy images",* In: Advances in neural information processing systems. 2012. pp 2843–2851

16] Liu, X., Deng, Z., Yang, Y., *"Recent Progress in semantic image segmentation",* vol. 52, 2019, pp. 1089-1106.

[17] Xiang, Y., & Jiang, L. (2009). *"Water quality prediction using ls-svm and particle swarm optimization",* Knowledge Discovery and Data Mining, 2009. WKDD 2009. Second International Workshop on (pp. 900–904), IEEE.

[18] Nasir, N., Kansal, A., Alshaltone, O., Barneih, F., Sameer, M., Shanableh, A., Al-Shamma'a, A. *"Water quality classification using machine learning algorithms"*, Journal of Water Process Engineering, vol. 48, 2022, 102920, ISSN 2214-7144,

[19] Shams, M.Y., Elshewey, A.M., El-kenawy, ES.M. et al. *"Water quality prediction using machine learning models based on grid search method",* Multimedia Tools Appl (2023).

Calibrating Raspberry Pi v2.1 Camera as an Absolute Luminance Meter for Smart Luminaire System Sensing Applications

Nebyu Yonas[1*] and Enyew Adugna[1]

School of Electrical and Computer Engineering, Addis Ababa institute of Technology, Addis Ababa University, Addis Ababa, Ethiopia
**Corresponding author's E-mail address: nebyu.yonas@aait.edu.et; nebayoni@gmail.com*

DOI: https://doi.org/10.20372/zede.v42i.10186

ABSTRACT

This article presents the conception and realization of a self-contained, absolute luminance level measurement device using a Raspberry Pi v2.1 camera system and single-board pocket size Raspberry Pi computer for a smart luminaire system sensing applications. The work presents Raspberry Pi v2.1 camera module footage in raw Bayer data formats, radiometric characterizations, raw Red, Green, Blue (RGB) to absolute luminance meter calibration and validation results. The developed absolute luminance meter is very simple, efficient, compact and suitable for absolute luminance level sensing measurement. Results obtained from the luminance meter calibration validation experiments showed that the proposed absolute luminance meter has the capability of measuring wide range of absolute luminance levels quickly with an average deviation of less than 2 cd/m^2 from actual measurements or with 97.48 % accuracy.

Keywords: Absolute Luminance, Raspberry Pi v2.1 Camera, Smart Luminaire System.

1. INTRODUCTION

Light, which is a necessity for humans and vision, is a form of electromagnetic radiation that travels through space within the visible electromagnetic spectrum as a wave that can be perceived by human eye [1]. Light from a light source reflects off a surface reaching human eye passing and proceeding in cornea and pupil forming images in retina. Human eye is therefore sensitive to wide range of light intensities for its proper function.

As human brain perceives light and geometry at the same time and interprets it as vision, many scientific and engineering applications in image processing are supposed to be capable of detecting both photometry and geometry at the same time [2]. This is useful in many applications including, smart luminaire systems, glare computation, light quality assessment, natural light harvesting, light control and so forth. Especially in smart luminaire systems, where absolute luminance level measurement is focal, its use is indisputable.

Generally, there are two types of light measurements, illuminance and luminance [3]. Measurement of light from a source that falls on a surface is known as illuminance. It is measured in Lux and devices used to measure it are cheap and easily available. Luminance is measure of light reflecting back from a surface and corresponds to human eye sensation of brightness of a source and is measured in units of cd/m^2. When humans look at the world, their eyes actually detect brightness (the arbitrary sensation of luminance), not illuminance.

The word camera comes from the Latin word 'Obscura', meaning a dark chamber or dark room [4]. Since its invention, camera has been in a continuous evolution and currently it has reached the age of digitalization. Digital cameras compared to their analog counterparts offer better

resolution, minimized noise, better dynamic range, speed, price, size, portability, convenience and etc. [5]. However, the main advantage of digital camera lies in its output digital signals which can easily be attained, analyzed, processed, interpreted, manipulated and stored [6].

Digital cameras evolved quickly, offering tremendous opportunities and enjoying a great market penetration and success in the last few decades. Especially the rapid evolution of Complementary Metal Oxide Semiconductor (CMOS) technologies in the last few decades yielded a very powerful, miniaturized, easy-to-manipulate digital cameras for commercial purposes in a much cheaper price than ever before [5]. These days, digital cameras operate and function as optical instruments in the similar way the human eyes do.

Digital cameras operate based on the principle of sampling light reflected from objects and directly mapping that into sequence of pixel values [7]. They possess a series of lenses which are used to focus light into a semiconductor device to record light intensity electronically. Digital cameras also possess array of sensors, also called photosites, which are used to convert light falling on them to equivalent electrical charges. Photosites are light sensitive tiny sensors which convert light (photon) in to electrons (electric charge). Photosites are sensitive to lights and hence will result in creation of large electrical charge when exposed with brighter lights.

Today, as artificial lightings are solely responsible for a significant portion of global power consumption and environmental pollutions, cutting energy consumption and boosting users' comfort in artificial lighting systems are some of the major research targets. To accomplish visual comfort and reduction in energy consumption in these luminaires systems, absolute luminance measurement is an absolute necessity. Hence, since the last few decades, there are several ongoing efforts underway to calibrate digital cameras as a compact, simple, affordable luminance meter for wide-range of applications. However, the progress made so far is either limited or failed to avail and make the final transformation matrix public. This article deliberates an absolute luminance sensing using Raspberry Pi v2.1 camera for smart luminaire system applications.

2. MATERIALS AND METHODS

2.1. Raspberry Pi v2.1 Camera Overview

Raspberry Pi v2.1 camera module is a mini sized, high-performance, 8 Megapixels' digital camera which is based on Sony IMX219 back-lit CMOS sensors [8-9]. It offers the possibility of multiple character alterations through a software control. It is widely applicable in applications of high dynamic range imaging, remote sensing, computer vision, bio photonics, security and surveillance, light measurement, medical imaging, remote sensing and many more. The main reason for this is the fact that its ability to deliver raw Bayer data formats, which can easily be accessed and used for many different motives.

The Raspberry Pi v2.1 camera used in this study was 3 grams in weight and 25 mm×25 mm×9 mm in size [10]. It could be directly attached to the Raspberry Pi 3 module B single board computer through the Camera Sensor Interface (CSI) port. Its characteristics could easily be controlled and monitored via the Raspberry Pi firmware. The firmware has gone through several development stages in time and currently it has an extended functionality and robust controls. The camera is capable of delivering 3280 × 2464 Bayer data of 8 megapixels. The Bayer data pattern of the camera was Blue Green Green Red (BGGR) and operated only in the visible light

spectrum, i.e. from 380 nm up to 700 nm [8].

Many scientific and engineering applications require raw sensor data to be extracted so further analysis can be carried [9]. Raspberry Pi v2.1 camera is not only fit for this purpose but also one of the best in the market with a reasonable price. The camera requires only 250 mA to run and operate. It is also compact in size and low in weight [8]. This makes it ideal for low-cost application consumptions compared to the highly expensive and bulky digital commercial cameras available in the market.

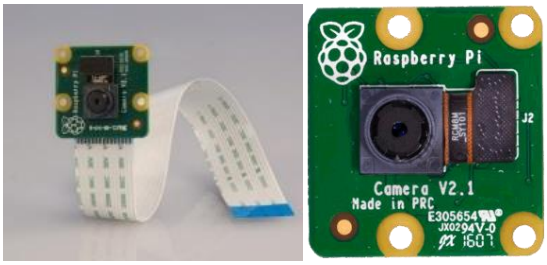

Figure 1 Raspberry Pi v2.1 camera

2.2. Smart Luminaire Systems

Smart luminaire systems are lighting systems that tailor and deliver artificial illuminations automatically, according to user tasks, responses, comfort, and wellbeing with appropriate luminaire color temperature, brightness level and energy consumption reductions [11]. They use different sensors, electronics, circuitries, actuators, gadgets, and communication protocols in a closed-loop control manner to realize that [12]. These lighting systems are created to considerably cut lighting energy consumptions while simultaneously improving user comfort and experience. Additionally, Solid-State Lighting (SSL) devices like Light Emitting Diodes (LEDs) have become more common, and they can now provide the right illumination levels, with suitable luminaire color temperatures in line with users' visual comfort and activities [13]. At present with the rapid evolution of wireless sensor networks and LED luminaire technologies and state of the art LED driver circuitries, delivering different illumination level and color temperature are easier than ever before [14-16].

Smart luminaire systems typically contain three main parts; measurement module: which is the front-end part of a smart luminaire system which is responsible for monitoring real-time situations according to design specification including illumination level and activity to deliver vital information in for decision making. Here is where real time light measurement devices play a crucial role. They are used to measure the actual light levels at the scene. The information processing and decision-making part is the middle part of any smart luminaire system and is responsible for information processing and decision making on the luminance level of luminaires. The last part of any smart luminaire system is the luminaire lighting system, which consists of luminaire drivers and luminaires that are responsible for the artificial illumination. A typical smart luminaire system based on LED luminaires and with its main components is shown in Figure 2.

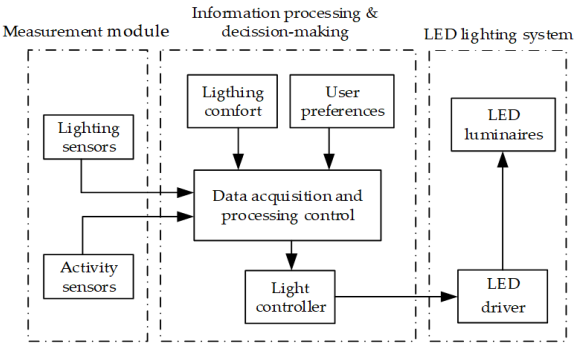

Figure 2 Typical smart luminaire system [14]

2.3. Digital Camera to Absolute Luminance Sensing Calibration

There are several digital cameras that are made specifically for luminance level measurements with very high standards. However, due to their high precision,

accuracy and complex analytic solutions, these cameras are extremely expensive and not commercially practical for many luminance measurement applications. Despite having a history of high reliability and precision, meter-based measurement is a time-consuming, point-by-point process with poor measurement resolutions. Furthermore, given their poor measurement speed and the time intervals between readings, these luminance meters are ineffective for measuring dynamic light scenes and integration with smart luminaire systems.

Today, easily affordable and accessible digital still cameras are opening up the possibility for an absolute luminance level measurement in a wide range of applications. Consequently, several past related works [17-21] showed that relatively cheaper digital cameras can be used to measure actual luminance levels with tolerable precision. However, before utilizing these digital cameras for absolute luminance level measurement, they must be characterized and calibrated. This calibration process will directly affect the reliability, accuracy and precision of such systems.

Hence, the current readily available digital cameras, which use either Charge Coupled Device (CCD) or CMOS light collection technology, can be practical and affordable luminance measurement instruments with proper calibration. Via acquiring the real luminance level of a space, a range of architectural smart lighting applications, such as automated daylight harvesting systems, dynamic lighting control, lighting simulations, and glare assessments, can be made more easily and effectively.

The luminous atmosphere of an architectural space for different tasks cannot be deciphered using illuminance-based metrics and measurements from the perspective of human eyesight. Instead, measurements that are based on luminance level would be more appropriate. Some examples of luminance-based metrics in smart luminaire systems include ambient luminance, target luminance, luminance uniformity, background luminance, luminance contrast, and task/background luminance ratios. Such luminance-based indices have been extensively utilized in lighting applications that are important for vision, including different tasks (reading, surgery, office, recreation, gaming etc.) and road lighting system, which have a significant impact on, vision, visibility, safety, comfort, psychology and efficiency.

However, due to the fact that still digital cameras employ various image-processing techniques which change the digital cameras' default responses, has led to difficulties in direct luminance measurements. These various image processing techniques cannot be completely changed or manipulated by the end user. However, Raspberry Pi v2.1 camera allows that, making it one of the best potential devices in the market for the purpose of absolute luminance level measurement consumptions in different applications.

2.4. Raspberry Pi v2.1 Camera Characterization

2.4.1. Raw Bayer Data Acquisition

One of the main advantages of a Raspberry Pi v2.1 camera is its ability to deliver raw Bayer data values which are significant for scientific and engineering applications [9]. Raw Bayer data are simple data captured via the camera CMOS sensor and prior to processing by the camera Graphical Processing Unit (GPU). The main GPU processes include white balancing, defected pixels' correction, smoothing, metamerism, vignetting compensation, dark frames correction, compression, color adjustments, etc.

By turning off the auto white balance and activating the Bayer data mode on, a 3280 × 2464 raw Bayer data can be acquired from a Raspberry Pi v2.1 camera. Usually, the raw data RGB and YUV data formats of Raspberry Pi camera are GPU post processed data and hence not the real sensor outputs suitable for luminance measurement calibration purposes [8].

2.4.2. Linearity

The linearity test of the Raspberry Pi v2.1 camera was conducted to investigate the Raspberry Pi camera response as a function of shutter speed (exposure time). To excite the camera for this test, a 10 × 10 cm Lambertian flat surface Organic Light Emitting Diode (OLED) light source was positioned perpendicularly 1 m below. Different Shutter Speeds (SS) were used and the corresponding central 80 × 80 data Bayer array outputs were recorded and analyzed. This was done to prevent the data being affected by the vignetting effect of the camera, which is a common phenomenon in digital cameras [22-24]. The OLED luminance level was adjusted from 1 cd/m^2 up to 850 cd/m^2 at different intervals for each shutter speed and raw data readings were recorded.

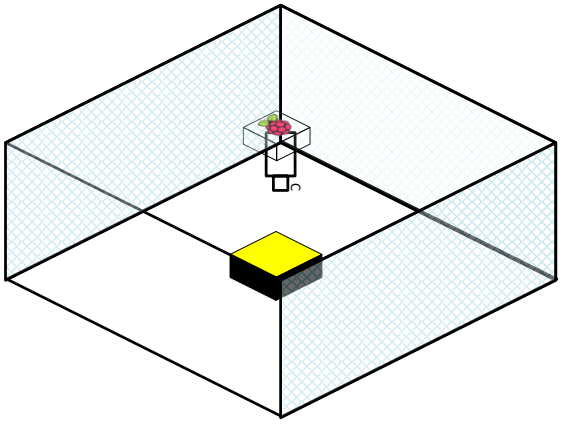

Figure 3 Linearity experiment set up

2.4.3. Uniformity/Vignetting Test

Vignetting effect is a phenomenon noticed in many digital cameras and optical activities where the output data values fade out towards the edge [22-25]. It is the consequence of light intensity fall-off of the camera lens towards the periphery of image. It is clear that both resolving and transmission of a lens are higher at the center and fall off towards the edge. Vignetting correction is manipulation of the raw Bayer data array values in a fixed fashion in order to regenerate the original intensities at the center of an image. To investigate the vignetting effect of the Raspberry Pi v2.1 camera lens, uniformity test with an excitation of a constant luminance level with the OLED light source was used across the entire camera Field of View (FoV). The experimental setup used is given in Figure 4.

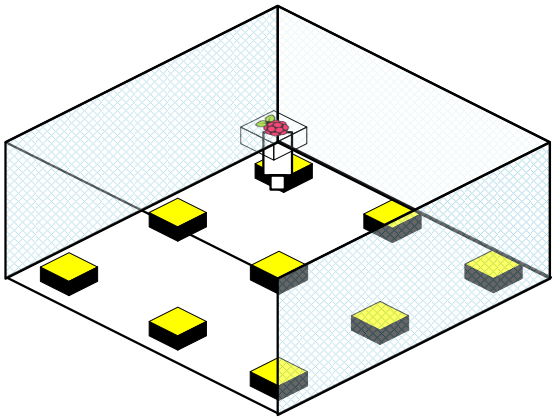

Figure 4 Uniformity test experiment setup

The camera was fixed 1 m above the table and its field of view was initially divided into 9 different zones and each zone's Bayer data responses to a constant luminance level were recorded. Further, to have a better response information on the area close to the center of the camera, additional four extra sub-regions were taken into consideration. This experiment was also done with different shutter speeds to check its uniformity and results showed the camera has similar vignetting responses. Therefore, by fixing the excitation at a constant level, any difference in the Bayer data was accounted for the vignetting effect of the

lens. Again, here also 80 × 80 center data Bayer array outputs were used for the analysis.

2.4.4. Spectral Response

A spectrum response test experiment was carried out to investigate the absolute and relative spectral response of the Raspberry Pi v2.1 camera to various different wavelengths. In this experiment the Raspberry Pi camera was placed in front of an integrating sphere illuminated by an illumination wavelength of a laser light source from 360 nm to 720 nm. The camera was made to target the aperture of the integrating sphere at its center. The laser light source was made to pass through a monochromator (Bentham TMc300) so that only the wavelength of interest makes it to the integrating sphere.

The spectral radiance values, in $W/m^2.sr.nm$ units, were recorded using spectrometer and results were integrated over wavelength in order to get radiance values in units of $W/m^2.sr$ in Matlab. Then the Raspberry Pi camera red, green and blue Bayer data values were recorded to get its absolute spectral response. Then for the relative spectral response, these data values were normalized and plotted against the wavelength. For this task two different experimental setups were used with two different shutter speeds (400 ms and 30 ms) and results recorded were found to be identical.

Therefore, absolute and relative radiance calibrations, raw data value to radiance conversion, were accomplished successfully.

2.4.5. Dark Frame Rate Analysis

For the dark frame rate analysis test, the Raspberry Pi v2.1 camera aperture was covered by a dark material in a dark room around room temperature. Since raw data values depend on temperature, the room temperature was kept constant thorough out the experiment and the camera were warmed up before acquiring the images so that it will not affect the dark frame values recorded. This experiment was conducted to get the Raspberry Pi's constant dark frame (noise) added to the raw data so that it will be considered before further processing. Different shutter speeds were used for this analysis.

3. RESULTS AND DISCUSSION

3.1. Raspberry Pi v2.1 Camera Characterization

The Raspberry Pi v2.1 camera linearity test experimental findings demonstrated that the shutter speed of the Raspberry Pi camera is linear with each of the three channels' raw data Bayer values. However, opposed to the work in [9], the Raspberry Pi cameras red Bayer data responses were found to be higher than that of the green channel. The blue raw Bayer data showed the smallest data values compared to the other two. Hence, based on the results obtained and shown in Figure 5, it was found that the camera response is linear with shutter speed (exposure time).

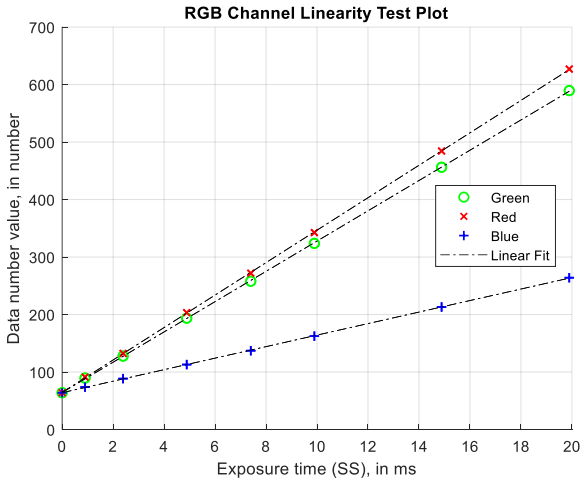

Figure 5 R, G, B typical linearity response

Further, the experimental findings for the Raspberry Pi camera uniformity/vignetting test, based on the recorded data for 3 different shutter speeds (1, 5, and 10

milliseconds), a flat fading surface response towards the periphery in the camera was observed. There was a significant drop in the intensity of the Bayer data values, up to 75 % around the edges. Moreover, the results obtained showed that the camera shows optical symmetry in both diagonals (top left to right bottom and top right to left bottom). The blue and green Bayer data show almost identical responses whereas the red channel showed a little different response with an increased vignetting effect. This result was identical to a previous work [9]. Uniformity test results obtained are shown in Figure 6.

Supplementary, based on the results obtained above, two-term Fourier series expansion lens correction or compensation coefficients were computed in Matlab. The following were vignetting correction equations used for the red, green and blue Bayer data, respectively.

$$F(r) = -1.234 + 1.962\cos(w.x) - 1.751\sin(w.x) + 0.2604\cos(2w.x) + 0.079\sin(2w.x) \quad (1)$$

$$F(g) = 0.49 + 0.4123\cos(w.x) + 0.185\sin(w.x) + 0.0908\cos(2w.x) - 0.057\sin(2w.x) \quad (2)$$

$$F(b) = 0.493 + 0.4216\cos(w.x) + 0.173\sin(w.x) + 0.081\cos(2w.x) - 0.0615\sin(2w.x) \quad (3)$$

where:

w equals; - 0.0007905 for r, 0.001312 for g and 0.001284 for b.

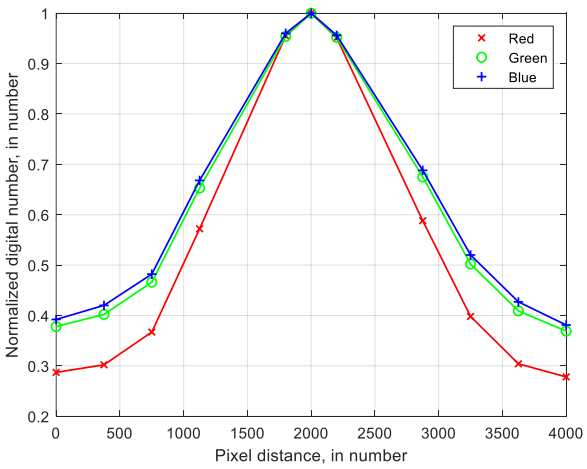

Figure 6 Uniformity test response

After applying the vignetting effect correction, the following results, displayed in Figure 7 to 9, were obtained for each channel. As it can be seen from the plots, the reconstruction exhibits RMSE of 0.0109, 0.0068 and 0.0038 for the red, green and blue channels, respectively.

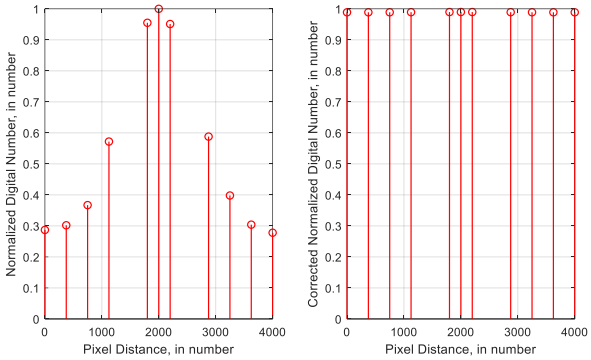

Figure 7 Red channel vignetting correction

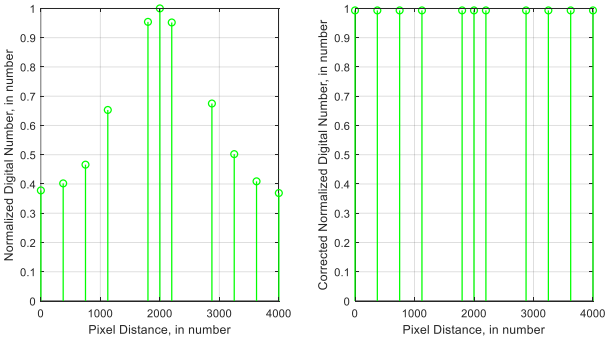

Figure 8 Green channel vignetting correction

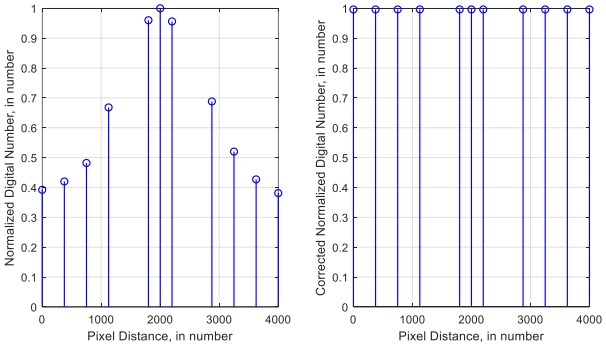

Figure 9 Blue channel vignetting correction

The Raspberry Pi v2.1 camera spectral response characterization experimental setup results for absolute and relative spectral responses are shown in Figures 10 and 11,

respectively. Note that the shutter speed used for this experiment was 400 ms.

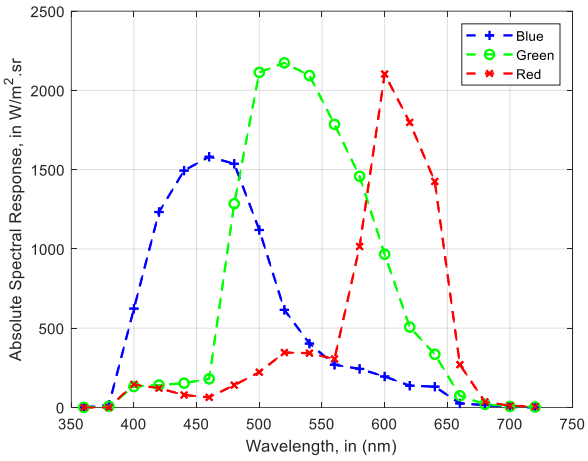

Figure 10 Absolute spectral response

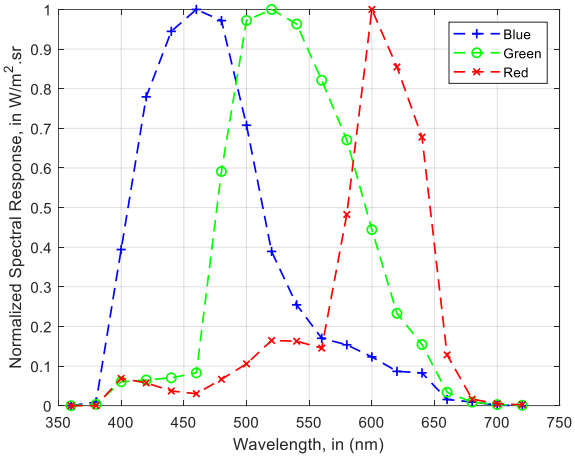

Figure 11 Relative spectral response

Furthermore, results obtained from dark frame rate analysis experiment are shown in Table 1.

Table 1 Dark frame rate test results

SS (µs)	**R** (number)	**G** (number)	**B** (number)
898	63.96	63.97	63.84
2391	64.04	63.88	63.89
4887	63.90	63.94	63.89
7401	63.95	63.93	63.90
9896	63.94	63.96	63.92
14887	63.92	63.93	63.94
19896	63.99	63.91	63.89
Average	**63.96**	**63.93**	**63.90**

As shown in Table 1, there is a very close resemblance between the r, g and b channels. Therefore, the dark frame values are consistent and very close to 64 data number values. This implies that, these values should be deducted from the raw Bayer values before further analysis. Additionally, it should be noted that it is not possible to obtain raw Bayer data values lower than the dark frame rates at any given time while attempting to calibrate the Raspberry Pi v2.1 camera as an absolute luminance meter.

3.2. Absolute luminance meter calibration

The Raspberry Pi v2.1 camera was made to be excited via OLED light source luminaire, with different shutter speeds and luminance level values in this work. By putting the OLED at the center of the camera Field of View (FoV), R, G, B to luminance mapping was computed as a function of SS, r, g and b raw data Bayer values. The calibration was done based on the principle of converting digital image raw data to luminance level. Knowing that the camera response is linear with the luminance scene functions, a 3X1 linear transformation matrix from RGB to Luminance level estimation was computed via a linear regression model. Please note that the central 80 × 80 Bayer data were used for this scrutiny.

Therefore, the final task of calibrating the Raspberry Pi v2.1 camera raw data to absolute luminance level was carried successfully in Matlab. Hence, the Raspberry Pi v2.1 camera was made read and measure absolute luminance levels. The transformation matrix is given in equation4.

$$L = (0.0046 \times r + 0.0064 \times g + 0.008 \times b)/SS \quad (4)$$

where:

SS is the shutter speed given in second and r, g and b are Bayer data values after the dark frame correction.

Results obtained showed an average of 1.6 cd/m^2 difference from the real luminance value measured using Konica Minolta Luminance Meter and 5.1 cd/m^2 and 0.1 cd/m^2 maximum and minimum deviations respectively, under different light sources.

Therefore, via activating raw Bayer data of Raspberry Pi v2.1 camera and deploying vignetting correction and absolute luminance transformation matrix, given in equations 1-4, the device can be used as a simple, compact, affordable and efficient absolute luminance meter for different absolute luminance measurement applications.

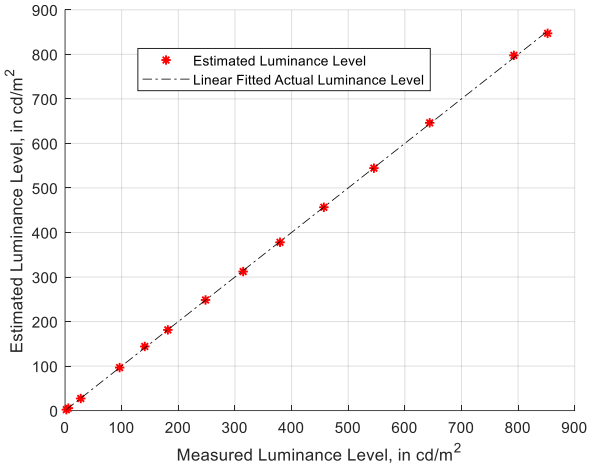

Figure 12 Measured vs estimated luminance

3.3. Absolute Luminance Meter Validation

Different luminance levels, from 3 to 850 cd/m^2, with a variety of light sources with different spectral properties including day light, Philips Hue LED lamp, incandescent lamp, florescent lamp, halogen lamp and combination of the above-mentioned light sources were used to assess the raw Bayer data-based absolute luminance level estimation accuracy. Results obtained from the validation assessments yielded an average deviation of less than 2 cd/m^2 from actual measurements with mean square error of 8.18, root mean square error of 2.86 and 97.48 % accuracy. Further, the device exhibited a capability of providing quick response compared with the traditional actual luminance meters. Figure 13 and Figure 14 show the validation results.

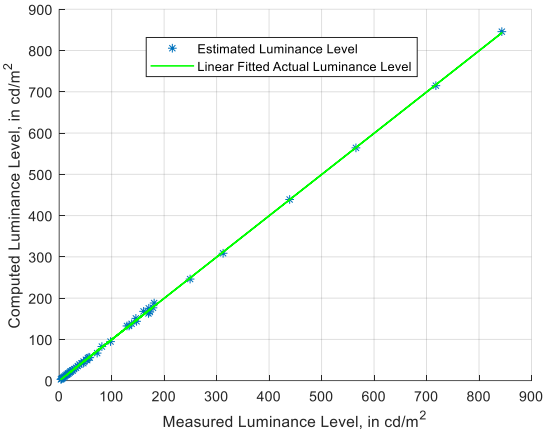

Figure 13 Validation for 0 – 900 cd/m^2 range

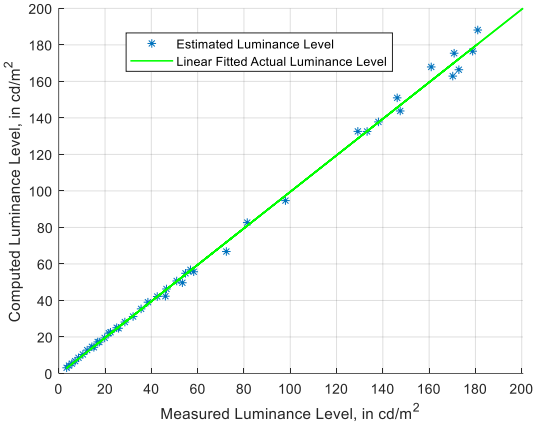

Figure 14 Validation for 0 – 200 cd/m^2 range

4. CONCLUSIONS

Results obtained from this work showed that, Raspberry Pi v2.1 camera can be calibrated to be used as a simple, compact, affordable and efficient absolute luminance meter. Using this device, a smart artificial luminaire system which does not only target power consumptions minimization but also

user comfort, humans' psychological boost, and illumination level adjustment can be realized. This in turn, will have positive effects in humans' productivity and quality of indoor lighting environment. This luminance meter can also be used in embedded systems, which deal with real-time absolute luminance level measurements for analysis and decision making. Hence, there is no doubt that the proposed calibrated absolute luminance level measuring device usage will be tremendous and can be readily used as a focal part of the measuring unit in typical smart luminaire systems and other similar applications.

CONFLICT OF INTEREST

The authors declare that there is no conflict of interest.

ACKNOWLEDGMENTS

This study was undertaken in the School of Electrical and Computer Engineering, Addis Ababa Institute of Technology. The authors are grateful to Addis Ababa University for its financial support and KU Leuven University for availing its laboratory facility.

REFERENCES

[1] Çakir, A., "*Human factors in lighting*", Behaviour and Information Technology, Taylor & Francis Journals, vol. 33, no. 10, 2014, pp.1111-1113.

[2] Tout, K., "*Automatic vision system for surface inspection and monitoring: Application to wheel inspection*", Doctoral dissertation, Université de Technologie de Troyes-UTT, 2018.

[3] Hiscocks, P.D. and Eng, P., "*Measuring Luminance with a digital camera*", Syscomp electronic design limited, Advanced Test Equipment Corporation, Datasheet,vol. 2, 2011.

[4] Rosinsky, R. D., "*A Lexicon for Camera Obscura*", Doctoral dissertation, Massachusetts Institute of Technology, 1984.

[5] Razavi, B., "*Design of analog CMOS integrated circuits*", New York, McGraw-Hill, 2001.

[6] Maschal, Jr, R.A., Young, S.S., Reynolds, J., Krapels, K., Fanning, J. and Corbin, T., "*Review of Bayer pattern CFA demosaicing with new quality assessment algorithms*", In Infrared Imaging Systems: Design, Analysis, Modeling, and Testing, XXI, SPIE, vol. 7662, 2010, pp. 363–374.

[7] Nice, K., and Gurevich, G. J., "*How Digital Cameras Work Understanding the Basics A Filmless Camera*", How Stuff Works, 2012. https://electronics.howstuffworks.com/cameras-photography/digital/digital-camera.htm, (accessed on: March 08, 2021)

[8] Jones, D., "*Picamera 31.13 Documentation Release 1.1*", Picamera documentation, 2020.

[9] Pagnutti, M. A., Ryan R.E., Gold M. J., Harlan R., Leggett E., and Pagnutti J. F., "*Laying the foundation to use Raspberry Pi 3 V2 camera module imagery for scientific and engineering purposes*", Journal of Electronic Imaging, vol. 26, no. 1, 2017, pp. 013014-1–013014-13.

[10] Mead, A. R. and Mosalam, K. M., "*Ubiquitous luminance sensing using the Raspberry Pi and Camera Module system*", Lighting Research &Technology, vol. 49, no. 7, 2017, pp. 904–921.

[11] Chun, S., Lee, C. S., and Jang, J. S., "*Real-time smart lighting control using human motion tracking from depth camera*", Journal of Real-Time Image Processing, vol. 10, 2015, pp. 805–820.

[12] Wu, Y., Shi, C., Zhang, X., and Yang, W., "*Design of new intelligent street light control system*", In IEEE ICCA 2010, IEEE, 2010, pp. 1423–1427.

[13] Chen, K. L., Chan, H. P., Hung, Y. C., & Shieh, S. H., "*A smart LED lighting with multiple dimming and temperature automatic protection capabilities*", 2016 International Symposium on Computer, Consumer and Control (IS3C), IEEE, 2016, pp. 614–617.

[14] Magno, M., Polonelli, T., Benini, L., and Popovici, E., "*A Low-cost, Highly Scalable Wireless Sensor Network Solution to Achieve Smart LED Light Control for Green Buildings*", IEEE Sensors Journal, vol. 15, no. 5, 2014, pp. 2963-2973.

[15] Amin, S. M. and Wollenberg, B. F., "*Toward a smart grid: power delivery for the 21st century*", IEEE power and energy magazine, vol. 3, no. 5, 2005, pp. 34–41.

[16] Li, S., Tan, S. C., Lee, C. K., Waffenschmidt E., Hui S. Y., and Tse C. K., "*A Survey, Classification, and Critical Review of Light-Emitting Diode Drivers*", IEEE Transactions on Power Electronics, vol. 31, no. 2, 2015, pp. 1503–1516.

[17] Inanici, M.N., "*Evaluation of high dynamic range photography as a luminance data acquisition system*", Lighting Research & Technology, vol. 38, no. 2, 2006, pp. 123-134.

[18] Kruisselbrink, T., Aries, M., and Rosemann, A., "*A practical device for measuring the luminance distribution*", International Journal of Sustainable Lighting, vol. 19, no. 1, 2017, pp. 75–90.

[19] Hiscocks, P. D. and Eng, P., "*Measuring luminance with a digital camera: case history*", Syscomp Electronic Design Limited, 2013.

[20] Ismail, A. H., Azmi, M. S. M., Hashim, M. A., Ayob M. N., Hashim M. M., and Hassrizal, H. B., "*Development of a webcam-based lux meter*", In 2013 IEEE Symposium on Computers & Informatics (ISCI), IEEE, 2013, pp. 70–74.

[21] Wüller, D. and Gabele, H., "*The usage of digital cameras as luminance meters*", Digital Photography III., vol. 6502, 2007, pp. 281-291.

[22] Cai, H., "*High Dynamic Range Photogrammetry for Light and Geometry Measurement*", AEI 2013: Building Solutions for Architectural Engineering, 2013, pp. 544–553.

[23] Theuwissen, A. J., "*Image processing chain in digital still cameras*", 2004 Symposium on VLSI Circuits, Digest of Technical Papers (IEEE Cat. No. 04CH37525), 2004, IEEE, pp. 2–5.

[24] Yu, W., Chung, Y., and Soh, J., "*Vignetting distortion correction method for high quality digital imaging*", Proceedings of the 17th International Conference on Pattern Recognition, ICPR 2004, vol. 3, 2004, pp. 666-669.

[25] Anaokar, S. and Moeck, M., "*Validation of high dynamic range imaging to luminance measurement*", Leukos, vol. 2, no. 2, 2005, pp. 133–144.

Amharic Speech Recognition Using Joint Transformer and Connectionist Temporal Classification with Character-Based and Sub-word-Based Acoustic and Language Models

Alemayehu Yilma Demisse[1] and Bisrat Derebssa Dufera[1,*]

[1] School of Electrical and Computer Engineering, Addis Ababa Institute of Technology, Addis Ababa University, Addis Ababa, Ethiopia
** Corresponding author's Email address: bisrat@aait.edu.et bisrat@aait.edu.et*

DOI: https://doi.org/10.20372/zede.v42i.10187

ABSTRACT

Sequence-to-sequence attention-based models have gained considerable attention in recent times for automatic speech recognition (ASR). The transformer architecture has been extensively employed for a variety of sequence-to-sequence transformation problems, including machine translation and ASR. This architecture avoids sequential computation that is used in recurrent neural networks and leads to improved iteration rate during the training phase. Connectionist temporal classification, on the other hand, is widely employed to accelerate the convergence of the sequence-to-sequence model by explicitly learning a better alignment between the input speech feature and output label sequences. Amharic language, a Semitic language spoken by 57.5 million people in Ethiopia, is a morphologically rich language that poses a challenge for continuous speech recognition as a root word can be conjugated and inflected into thousands of words to reflect subject, object, tense and quantity. In this research, the connectionist temporal classification is integrated with the transformer for continuous Amharic speech recognition. A suitable acoustic modeling unit for Amharic speech recognition system is also investigated by utilizing character-based and sub word-based models. The results show that a best character error rate of 8.04 % for the character-based model with character-level language model (LM) and a best word error rate of 22.31 % for the sub word-based model with sub word-level LM.

Keywords: Amharic, ASR, CTC**,** LMs, RNNs, Transformer,

1. INTRODUCTION

ASR has a wide range of applications including security, e-health, education, and transport systems, making it an important and active research domain. Research on Amharic ASR has been conducted using various methods. However, the development of ASR for Amharic, like other under-resourced languages, remains a challenging task due to the lack of high-quality language resources. Despite the challenges, ongoing research continues to improve the performance of Amharic ASR systems [1].

In recent years, ASR systems have undergone a significant transition from a hybrid HMM modeling approach [2] to an end-to-end or all neural networks modeling approaches [3, 4]. In contrast to the traditional models, which comprise a number of independent components, the end-to-end structure portrays the system as a single neural network [5].

End-to-end systems are exemplified by models such as the connectionist temporal classification (CTC) [6] and the attention-based encoder-decoder [7]. The CTC based acoustic model (AM) training does not need the frame level alignments between characters in the transcript and the observed input speech [6]. This is due to CTC

introducing a "blank label" which determines the start and end of one character [6]. In the attention-based encoder-decoder models, the encoder is analogous to AM that transforms input speech into higher-level representation, and also to LM that predicts each output token as a function of the prior prediction. The attention mechanism on the other hand is an alignment model to determine frames to predict the next token [8].

Recurrent neural networks (RNNs) are the basis of the end-to-end ASR models. RNN based models produce a sequence of hidden layers based on the network's prior hidden layer by performing computations on the character positions of the received and resulting data. Because this sequential procedure prevents parallel computation, training the model with a longer input sequence takes much more time. In order to reduce sequential processes, the transformer has been proposed [9]. This architecture eliminates recurrence and relies on its internal attention (self-attention) mechanism without using RNNs to determine dependencies between input and output data, which allows parallelization of the training process. The fast rate of learning due to the absence of sequential execution, as with RNN, is the major benefit of this architecture.

Several research studies [1, 10-12] have been done to develop a continuous speech recognition system for Amharic language using traditional HMM [10-12] and DNN [13-15] approaches. HMM-GMM paradigm with intermediate components [1, 10-12] has been employed to come up with an ASR system for Amharic language. Although they produced relatively acceptable results in the past [15], the complexity of the HMM-GMM approach has substantially reduced the effectiveness of using these systems. The complexity is a result of the separate training of the language, pronunciation, and AMs. In addition, the HMM model for speech has some inherent limitations. HMM is unable to represent contextual information, which could lead to misidentification in long sentences with complex structures. This is because the transitions between each state depend only on the current state and not on any information from previous states. HMMs are based on the assumption that the observations are independent, however speech signals are interdependent and highly non-linear in nature, which means HMM have difficulty in capturing these complex relationships between the observation sequences.

Consequently, few Amharic ASR research have concentrated on end-to-end modeling techniques such as CNN and RNN [14, 15], which seek to instantly simulate the translation between speech and labels without the need of intermediary components. Hybrid CTC and attention model with grapheme to phoneme conversion algorithms was proposed [13] to model sub-word level Amharic language units to address the problem of out-of-vocabulary words. Attention-based models are usually composed of encoder and decoder, which both consist of RNNs. However, in RNNs, the input is reliant on previous time steps, and hence calculations can only be done in sequence.

Transformer and RNN based ASR were combined by Syoun et. al. [16] to develop a faster and more accurate ASR system. A CTC with transformer is utilized for co-learning and decoding to develop the model. This strategy expedites learning and assists with LM integration. Significant advancements in many ASR tasks are implemented by the suggested ASR system. For instance, it reduced WER for the Wall Street Journal from 11.1 % to 4.5 % and for TED-LIUM from 16.1 % to 11.6 % while integrating CTC and LM into the transformer baseline. Transformer based paradigm for online streaming ASR that needs a

continuous speech as input was presented in a study [17]. In this work, an output is generated promptly after each utterance. They employed time-restricted self-attention for the encoder and triggered attention for the encoder-decoder attention mechanism. Their model resulted of WER 2.8 % and 7.3 % for the "clean" and "other" Libri Speech test data, respectively.

In this paper, we propose joint CTC and attention-based model with transformer architecture for Amharic continuous speech recognition. This architecture removes recurrence and relies on self-attention mechanism to determine relationships between input and output, which allows for parallelization. This research presents two significant contributions that aim to improve the accuracy of ASR for Amharic language. Firstly, it proposes the integration of two cutting-edge ASR techniques, namely CTC and transformer joint training, which enables modeling of different Amharic language units (characters and subwords) to achieve better ASR accuracy. Secondly, this research evaluates and analyzes the performance of various Amharic language modeling units, including character RNNLM and subword RNNLM.

As far as we can tell from our reading, no work has been published that employs the transformer-based end-to-end architecture for Amharic ASR tasks.

2. METHODS

The proposed model shown in Figure 1 consists of five pivotal stages, namely feature extraction, sub-sampling, AM, LM and joint decoding.

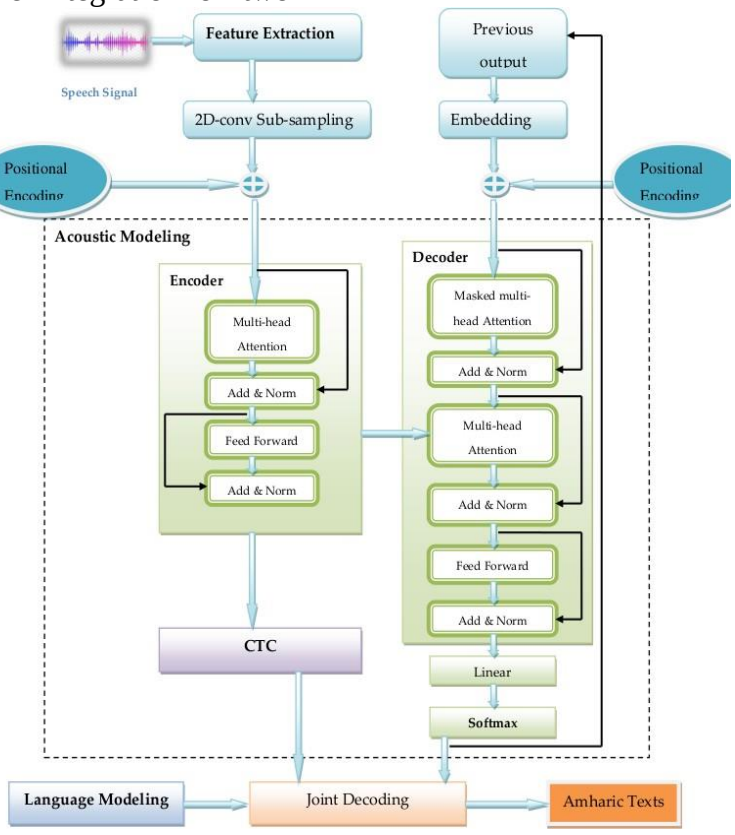

(a)

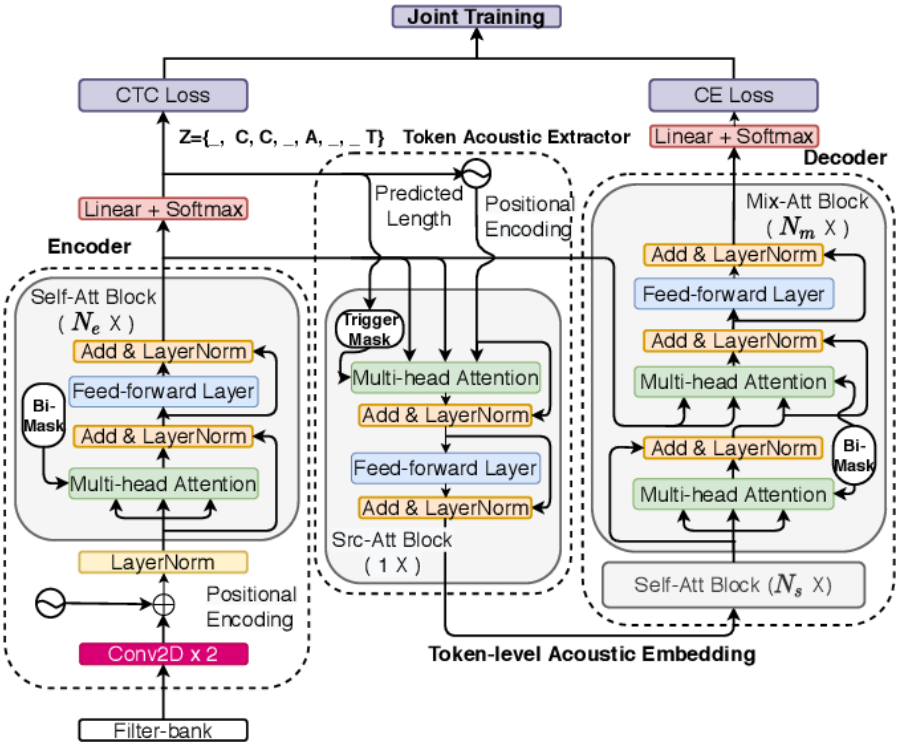

(b)

Figure 1 (a) The proposed model architecture for Amharic ASR and (b) CTC architecture.

2.1. Feature extraction

Feature extraction is a critical step in the process of ASR, as it helps to transform the raw audio data into manageable, relevant, and informative features. In this study, the log-Mel filter bank features are utilized to provide a compact representation of the input signal by computing a series of feature vectors.

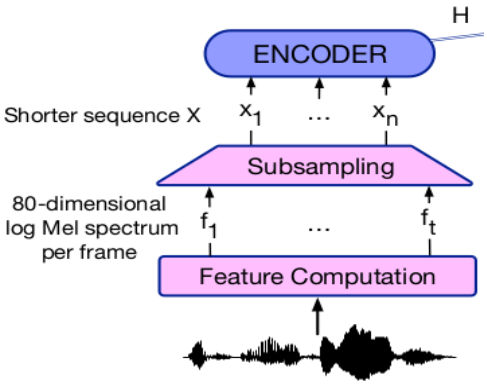

Figure 2 Schematic architecture showing pre-encoder stages.

2.2. Sub sampling

The encoder-decoder architecture ideally suits scenarios where input and output sequences have similar lengths. A single word could consist of five letters and go on for around 2 seconds, equating to approximately 200 acoustic frames (at 10ms per frame). Due to this significant length disparity, speech-based encoder-decoder architectures require to employ a compression stage. This stage pre-processes the speech features, typically shortening their sequence length before feeding them into the encoder.

One popular method is using 2D-conv subsampling [5], which involves reducing the size of the input while preserving essential features. After subsampling, the feature frames F are transformed into sub-sampled sequence $X \in R^{d^{sub} x\, d^{model}}$ with 2D-CNN sampling layer as shown in Figure 2.

2.3. Acoustic Modeling

In speech recognition, acoustic modeling involves creating statistical models that represent how sounds in speech relate to linguistic units. The joint transformer-CTC model is considered as an AM. This framework utilizes a shared transformer encoder to generate a high-level representation $h = (h_1,h_2,...,h_L)$ for the input sequence $x = (x_1,x_2,...,x_t)$ and subsequently applies both CTC model and transformer decoder to simultaneously generate targets based on the high-level representation h.

2.3.1. Transformer Architecture

Transformer uses sinusoidal position information and a self-attention mechanism to completely do away with repetitions in typical RNNs [18, 19]. It is made-up of one large block, which itself is made up of blocks of encoders and decoders.

The encoder's core function is to transform the input sequence into a high-level representation using a combination of two techniques: multi-head self-attention and a fully-connected network with positional encoding. Each sub-layer produces an output, which is then passed through a layer normalization process. Additionally, the sub-layer input is directly connected to the output via a residual connection. The first encoder block receives the subsampled sequence input X. Through the self-attention sub-layer, the X sequence is transformed into queries ($Q = X \times W^q$), keys ($K=X \times W^k$) and values ($V=X\times W^v$). This transformation occurs using learnable weights, W^v, W^q and $W^k \in R^{d^{model}\times d^k}$, where d^{model} represents the dimension of the output of the previous attention layer. Moreover, $d^q = d^k$, d^v, symbolize the dimensions of queries, keys and values, respectively. A normalized weighted similarity Z is obtained from self-attention using softmax, which is shown in Eq. (1).

$$\text{SelfAttention}(Q, K, V) = \text{softmax}\left(\frac{Q \times K^T}{\sqrt{d^k}}\right) \times V \quad (1)$$

Multi-head attention (MHA) tackles the challenge of attending to different aspects of the input simultaneously. It achieves this by applying multiple, parallel attention sub-layers, each focusing on different features or relationships within the data. MHA comprises concatenating all self-attention heads at a specific layer (see Eqs (2) and (3)).

$$MHA(Q,K,V)=[Z_1,Z_2,...,Z_h]\ W^h \quad (2)$$

$$Z_i=SelfAttention(Q_i,K_i,V_i) \quad (3)$$

After passing through the multi-head attention layer, the resulting representation is normalized and fed into a fully-connected neural network layer known as the feed-forward sub-layer, Eq. (4).

$$FF(z[t])=max(0,z[t]\times W_1+b_1)W_2+b_2 \quad (4)$$

where:

$z[t]$represents the t^{th} position of the input Z.

The decoder generates predictions in an auto-regressive manner. At each time step, it utilizes the high-level representation from the encoder and previous predictions from the decoder as inputs for the current prediction. At each time step, the decoder generates a prediction $\hat{Y}[t]$that hinges on the final encoder representation H_e andthe prior target sequence $Y[1: t-1]$. To achieve such conditional dependence, the decoder deploys multi head attention, enabling it to calculate attention between encoder high-level features and previously decoded sequences. Similar to the encoder, the decoder comes complete with layer normalizations and residual connections focused around every sub-layer.

The transformer employs two fundamental mechanisms, namely Positional Encoding (PE) and Embeddings. These crucial techniques are responsible for encoding the

positional information of the input sequence and learning representations for each token, respectively. PE is added to the token embeddings to indicate their position in the sequence, as self-attention does not have any notion of order or position. It provides valuable indication regarding the order of the words in the sequence to the model. On the other hand, Embeddings are a way to represent each token as a dense vector. In transformers, the initial vector representation starts as one hot encoding, but it is transformed into a dense vector through a trainable weight matrix before being passed through the network. This embedding method allows for the model to learn semantic relationships between the tokens, allowing it to generalize better by understanding the context of each token in the sequence.

2.3.2 Connectionist Temporal Classification

CTC: is a novel method that has revolutionized the way in which transformers are trained. CTC leverages a unique approach that does not require any previous alignment among input and output sequences of varying lengths [28]. Instead, it presents a high-level variable, known as the CTC path $\pi = (\pi_1, \pi_2,...,\pi_L)$ for the input sequence as a frame-level label.

One of the most significant advantages of CTC over other methods is its ability to identify different paths that lead to a particular label sequence. By removing repetitions of the same label and blank symbols, CTC expands its mapping capabilities, providing richer and more accurate results. Once the transformer encoder processes the input, it generates a high-level representation capturing the essential information. This representation is then utilized for subsequent processing stages in the speech recognition system [6]. The probability of a CTC path can be computed by using Eq. (5).

$$p\left(\frac{\pi}{x}\right) = \prod_{l=1}^{L} q_l^{\pi_l} \tag{5}$$

The likelihood of the label sequence is the sum of probabilities of all compatible CTC paths (see Eq. (6)).

$$p\left(\frac{y}{x}\right) = \sum_{\pi \in \Phi(y)} p\left(\frac{\pi}{x}\right) \tag{6}$$

where:

$\Phi(y)$ denotes the set of all CTC paths which can be mapped to the label sequence y.

A forward-backward algorithm can be employed to efficiently sum over all the possible paths. The likelihood of y can then be computed with the forward variable α^u and the backward variable β^u as shown in Eq. (7).

$$p\left(\frac{y}{x}\right) = \sum_{u} \frac{\alpha_l^u \beta_l^u}{q_l^{\pi_l}} \tag{7}$$

where:

u is the label index.

The CTC loss is defined as the negative log likelihood of the output label sequence, (Eq. (8)).

$$L_{CTC} = -\ln\left(p\left(\frac{y}{x}\right)\right) \tag{8}$$

The CTC loss can be used to train the transformer Encoder by using the back-propagation algorithm by derivation of the CTC loss.

2.3.3. Joint Transformer and CTC

Aiming to leverage the strengths of both models, an approach can be taken to combine the CTC loss and transformer loss. Although CTC and transformer- based methods possess distinct benefits, they also exhibit their own limitations. While CTC assumes conditional independence between labels, transformer attention mechanism uses a weighted sum over all inputs without constraints from alignments, resulting in difficulties when training the transformer-

based decoder.

The joint CTC-transformer objective function is the weighted sum of the transformer loss and CTC loss (Eq. (9)).

$$L_{joint} = \lambda L_{CTC} + (1-\lambda) L_{Transformer} \quad (9)$$

where:

$\lambda \in (0,1)$ is a tunable hyper-parameter.

2.4. Language Modeling

Language modeling refers to the process of predicting the likelihood of a sequence of tokens in a given language. Given that a transformer model is fundamentally a conditional LM, it implicitly learns a LM for the intended output domain via its training data.

Character level and subword level LMs for Amharic speech recognition were developed using LSTM. LSTMs are a type of re-current neural network that can learn long-term relationships in sequential data. They are particularly useful for language modeling because they can capture the context of a token and its impact on the following tokens in a sentence. In language modeling, the model receives a sequence of words or symbols as input, and predicts the likelihood of the next one in the sequence. The LSTM takes one token at a time as the input and based on previous state and current token it updates its internal state. The hidden state of the LSTM effectively captures the context of the sentence up to that point, allowing the model to predict the most likely next token.

2.1.5 Joint Decoding

In the decoding process, a LM is employed to distinguish and clarify between the expected sentences that are produced by the transformer decoder. By utilizing beam search, we obtain the final selection of hypothesized sentences in the form of an n-best list. These hypotheses are then rescored using a LM, whereby each hypothesis scored on the beam is recalculated. As can be seen in Eq. (10), this score is calculated by joining the score obtained from the LM with the CTC score.

$$\hat{y} = argmax(\lambda \log \rho_{s2s}\left(\frac{y}{x}\right) + (1-\lambda) \log \rho_{ctc}\left(\frac{y}{x}\right) + \gamma \log \rho_{lm}(y) \quad (10)$$

where:

$\rho_{s2s}\left(\frac{y}{x}\right)$ is the transformer decoder probability of the output sequence given theencoding feature sequence,

$\rho_{ctc}\left(\frac{y}{x}\right)$ is the CTC probability of the output sequence given the encoding feature sequence,

$\rho_{lm}(y)$is the LM probability of the output sequence,

λ and γ are hyper parameters named "CTC weight" and "LM weight", respectively.

2.2 EXPERIMENTAL EVALUATION

2.2.1 Dataset

In this study, the Amharic speech corpus prepared Solomon Abate et al. [21], which comprises approximately 110hours of speech obtained from 214 speakers (male and female in equal proportion) who read a total of 32,901 sentences were used. The sentences were obtained from the archive of Ethio Zena website which focuses on news related sentences. The dataset was split into training, validation and test set, which contains 29, 221 sentences, 500 sentences and 3180 sentences, respectively. All the dataset has both character-based and syllable-based transcription for each utterance.

2.2.2 ASR Evaluation Metrics

Character error rate (CER) and word error rate (WER) were taken as evaluation metrics of the proposed method.

CER is a metric used to assess the performance of systems that deal with text, like ASR and Optical Character Recognition

(OCR). It is the percentage of characters that were incorrectly processed by the system. A lower CER indicates better performance, with 0% being a perfect score.CER is useful because it focuses on individual characters, providing a more granular view of errors compared to metrics that look at entire words. This can be helpful in identifying specific issues with pronunciation or recognition. CER was evaluated using Equation 11.

$$CER = (S + D + I) / N \quad (11)$$

where:

CER is Character Error Rate (percentage)
S is Number of substitutions (incorrect characters)
D is Number of deletions (missing characters)
I is Number of insertions (extra characters)
N is Total number of characters in the reference text (ground truth)

WER were another common metric used to evaluate the performance of speech recognition and machine translation systems. It focuses on errors at the word level, rather than individual characters like CER. It is defined similar to CER except word is used instead of character.

2.2.3 Experiment Setup

The training and testing experiments were conducted using Google Colab, a convenient cloud-based service courtesy of Google. The transformer model consists of twelve encoder layers and six decoder layers that form a 2048-dimensional feed-forward network. Eight attention heads were used, each with 512 dimensions, to provide our system with increased attentiveness.

To implement the joint training method, a multi-task loss weight of 0.3 for CTC was used. To avoid risk of over fitting several regularization techniques were incorporated, including 10% dropout on every attention matrix and weight in feed forward (FF), layer normalization before every MHA and FF, as well as a penalty of 0.1 as label smoothing, effectively preventing over fitting. Training was conducted with over 100 epochs using Pytorch modeling and a batch size of 8. Further, the Noam optimizer with warm up steps, label smoothing, gradient clipping, and accumulating gradients were utilized to train the proposed speech recognition system.

A sampling rate of 16 kHz, audio frames of 25ms duration intervals separated by an interval of 10ms, leading to the extraction of 80-dimensional log mel-filter bank features, were used for both training and decoding.

Two distinct types of LMs were explored, namely sub-word units, and character units. In order to achieve optimal results with sub-word LM, a 2-layer LSTM architecture that consisted of 1024 hidden units supplemented with Noam optimization, a batch size of 64, and a maximum sequencelengthof55 was used. The sub word LM was found to be particularly useful for modeling the complex structure of words and phrases that do not appear in their entirety in the training data. Alternatively, character LM employed a 4-layered LSTM architecture, with each layer containing 512 hidden units. Similar to the sub-word model, the character LM also utilized Noam optimization to enhance performance. This model's batch size was increased to 256 batch size because character-level modeling often has longer sequences. The maximum sequence length was set at 400 characters. The character LM is particularly valuable when focusing on morphology or spelling patterns across diverse languages.

3. RESULTS AND DISCUSSIONS

Training on both transformer model and joint transformer-CTC model is shown in Figure 3

for character-level tokenization. The results in Figure 3 shows that the transformer model failed to converge even after increasing the number of epochs. On the other hand, the transformer-CTC joint training achieved faster convergence. The reason for such significant differences between the two models lies in the fact that CTC explicitly aligned speech features and transcriptions, which allowed the sequence-to-sequence model to learn monotonous attention for ASR. This in turn, allowed the framework to converge much more effectively and efficiently. These results not only provide valuable insights into the limitations of transformer models but also highlight the importance of using CTC joint training in ASR tasks.

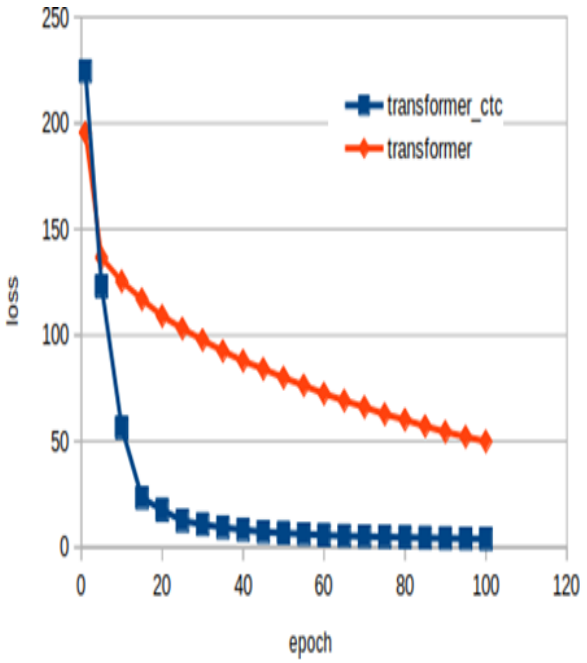

Figure 3 Training losses in character-based recognition

3.1 LM Training Results

As can be seen in Figure 4 and Figure 5 the perplexity is 6.35 and 10.24 for character-level and subword-level LMs, respectively for the validation dataset. The decrease in validation perplexity over epochs suggests that both models did not over fit on the training data and thus should generalize better on unseen test data.

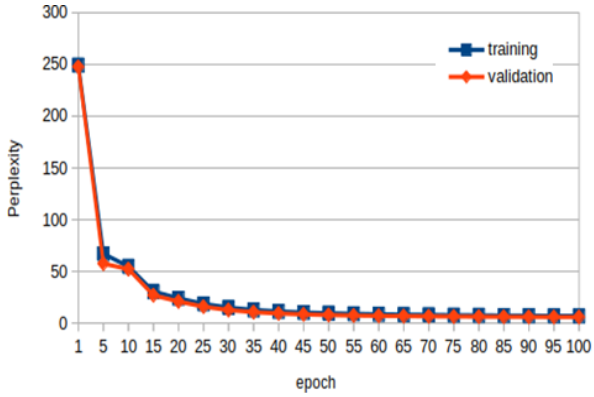

Figure 4 Training and validation perplexities of character-level LM

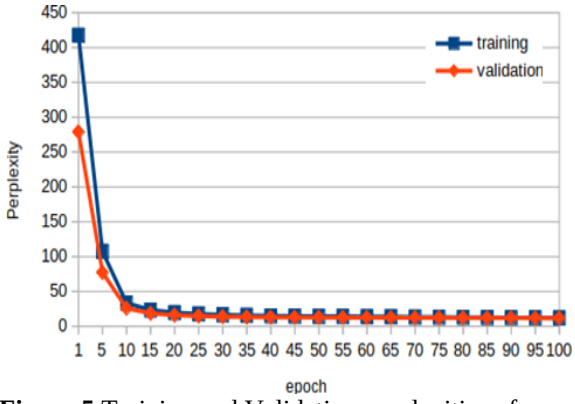

Figure 5 Training and Validation perplexities of subword-level LM

3.2 Joint Decoding

The results of the proposed joint transformer-CTC decoding have been categorized into two main categories: character-based AM with both character-level and subword-level L M, and subword-based AM with both character-level and subword-level LM. The models have been evaluated for their ability to decode an unseen test data, with the ultimate goal of achieving maximum transcription accuracy.

1) Character-based AM:

Table 1 depicts the performance of the character-based AM model. The initial results reveal a CER of 8.53% and a WER of 26.39 %, without the incorporation of LM.In order to enhance the performance of the model, distinct LMs such as a character-level

LM and a sub word-level LM were integrated into the decoding process.

Upon incorporating the character-level LM, both the CER and WER improved to 8.04% and 24.71% respectively. In contrast, the use of the sub-word-level LM resulted in a higher CER of 8.89% but a lower WER of 23.56%. This observation shows that even though character-level LM improves character recognition, in terms of word recognition sub-word-level LM is superior. The difference in performance between the character-level and subword-level LMs can be attributed to their inherent characteristics. Specifically, a sub-word-level LM is better suited to capturing the most probable sequence of characters that makeup a word, which can improve overall WER.

2) Sub-word-based AM:

Table 2 illustrates the performance subword-based joint transformer and model on unseen test data. The first result of the study showed that a model with 600 subword units achieved a CER of 9.21 % and a WER of 25.07 %. When a model with 2000 subword units is used, the CER increased significantly to 23.42 %, and the WER also increased to 42.3 %. This suggested that the high level of complexity resulting from more subword units creates over fitting. Additionally, increasing the number of subword units leads to sparser unit occurrences in the text corpus.

Table 1 Decoding results of joint transformer and CTC model using character as recognition unit

LM	CER		WER	
	Greedy decoding	Beam search decoding (width=3)	Greedy decoding	Beam search decoding (width=3)
No LM	9.43 %	8.53 %	28.2 %	26.39 %
Character -level	-	8.04 %	-	24.71 %
Subword -level	-	8.89 %	-	23.56 %

Table 2 Decoding results of joint transformer and CTC model using subword as recognition unit

Number of subwords	LM	CER		WER	
		Greedy decoding	Beam search decoding (width=3)	Greedy decoding	Beam search decoding (width=3)
600	No LM	10.71 %	9.21 %	26.53 %	25.07 %
2000	No LM	27.21 %	23.42 %	46.6 %	42.3 %
600	Character-level	-	8.85 %	-	24.02 %
600	Subword -level	-	9.20 %	-	22.31 %

To improve the model's performance, character-level and subword-level LMs were incorporated. The results demonstrated a significant improvement in accuracy when the character-level LM was utilized, with CER reduced to 8.85 % and WER to 24.02 % when using 600 subword units. On the other hand, incorporating a subword-level LM achieving a CER of 9.2 % and a WER of 22.31 %. Even though the character-level LM improved the character recognition, the subword-level LM achieved better WER as it captured the complex patterns of subwords present in the text and provided context to the model for more accurate predictions. This demonstrated that subword-based joint transformer and CTC models do not necessarily perform better with increasing subword units. Therefore, an optimal number of subword units is crucial to avoid having a model that is overly complex, leading to over fitting, as previously discussed. It is also worth noting that in this application beam search decoding outperformed greedy

decoding in all experiments, indicating that it is superior in decoding sequence of speech recognition hypothesis

4. CONCLUSIONS

In this study, we sought to investigate joint transformer and CTC in enhancing the accuracy of speech recognition. To assess the effectiveness of this approach, we employed two decoding techniques: greedy decoding and beam search decoding. Our findings revealed that beam search decoding outperformed greedy decoding in all experiments, indicating that it is superior in decoding sequences of speech recognition hypotheses. Specifically, our results demonstrate that beam search is a more viable strategy than greedy decoding for improving upon speech recognition accuracy utilizing joint transformer and CTC. The results of the evaluation demonstrated that subword-based models perform better than character-based models. Based on the findings, it can be concluded that using a joint transformer and CTC represents a promising method to achieve faster convergence of the transformer model. Additionally, selecting the appropriate language unit (character or subword) when developing Amharic speech recognition systems, is crucial and dependent on the end objective: higher word accuracy or lower character error rates.

CONFLICTS OF INTEREST

The authors have no conflict of interests related to this publication.

ACKNOWLEDGMENTS

The researchers would like to acknowledge School of Electrical and Computer Engineering, Addis Ababa Institute of Technology, Addis Ababa University for providing the computational facility to undertake this research.

REFERENCES

[1] Eshete Emiru, Yaxing, L., Awet Fesseha, and Moussa, D. "*Improving Amharic speech recognition system using connectionist temporal classification with attention model and phoneme-based byte-pair-encodings*", Information, vol. 12, February 2021. doi: https://doi.org/10.3390/info12020062.

[2] Amir, H., Shinji, W., and Ahmed, A. "*Arabic speech recognition by end-to-end, modular systems and human, Computer Speech & Language*", Computer Speech & Language, vol. 71, 2022.

[3] Geoffrey, H., Li,D., Dong, Y., George, D., Abdelrahman, M., Navdeep, J., Andrew, S., Vincent, V, Phuongtrang, N., Tara, S., and Brian, K."*Deep neural networks for acoustic modeling in speech recognition: The shared views of four research groups*", Signal Processing Magazine, IEEE, vol. 29, pp. 82–97, November 2012, doi:10.1109/MSP.2012.2205597.

[4] Rohit, P., Tara, S., Bo, L., Kanishka, R., and Navdeep, J., "*Analysis of "attention" in sequence-to-sequence models*" In proceeding of 18th Annual Conference of the International Speech Communication Association (Interspeech), Stockholm, Sweden, August 20-24, 2017

[5] Dong, W., Xiaodong, W., and Shaohe, L. "*An overview of end-to-end automatic speech recognition*". Symmetry, vol. 11, no. 8, 2019. doi: 10. 3390/sym11081018.

[6] Yanzhang, H., Tara, S., Rohit, P., Ian, M., et. al., "*Streaming end-to-end speech recognition for mobile devices*", International Conference on Acoustics, Speech, & Signal Processing (ICASSP), 12-17 May, 2019, Brighton, England, doi: 10. 1109/ICASSP.

[7] Chan, W., Jaitly, N., Le, Q. and Vinyals, O., *"Listen, attend and spell: A neural network for large vocabulary conversational speech recognition*", 2016 IEEE International Conference on Acoustics, Speech and Signal Processing (ICASSP), Shanghai, China, 2016, pp. 4960-4964, doi: 10.1109/ICASSP.2016.7472621.

[8] Martha Yifru Tachbelie, Solomon Abate, and Laurent, B., *"Using different acoustic, lexical and language modeling units for ASR of an under-resourced language – Amharic"*, Speech Communication, vol. 56 pp. 181–194, 2014, doi:10.1016/j.specom.2013.01.008

[9] Fergus, R., Vishwanathan, S., and Garnett, R., "*Advances in Neural Information Processing System,"*, MIT Press, volume 30. Curran Associates, Inc., 2017.

[10] Solomon Abate and Wolfgang, M., "*Syllable-based speech recognition for Amharic"*, In Proceedings of the 2007 Workshop on Computational Approaches to Semitic Languages: Common Issues and Resources, June 2007. doi:10.3115/1654576.1654583.

[11] Martha Yifiru Tachbelie, Solomon Teferra Abate, and Wolfgang, M., "*Morpheme-based automatic speech recognition for a morphologically rich language–Amharic",* In Workshop on Spoken Language Technologies for Under-resourced Languages, Penang, Malaysia, 2010.

[12] Ashish, V., Noam, S., Niki, P., Jakob, U., Llion, J., Aidan, N. Go., Łukasz, K., and Illia, P., "*All you need is attention",* Neural Information Processing Systems, 2017

[13] Nirayo Gebreegziabher N. and Sebsibe Hailemariam, "*Modeling improved syllabification algorithm for Amharic"*, In Proceedings of the International Conference on Management of Emergent Digital Eco Systems (MEDES '12). Association for Computing Machinery, New York, NY, USA, 16–21, 2012.

[14] Gebreegziabher, N., and Nürnberger, A., "*Sub-word Based End-to-End Speech Recognition for an Under-Resourced Language: Amharic*", 2020 IEEE International Conference on Systems, Man, and Cybernetics (SMC), Toronto, ON, Canada, 2020, pp. 3466-3470, doi:10.1109/SMC42975.2020.9283401.

[15] Alex, G., Santiago, F., Faustino, G., and Jürgen, S., "*Connectionist temporal classification: labeling unsegmented sequence data with recurrent neural networks*", In Proceedings of the 23rd international conference on Machine learning (ICML '06). Association for Computing Machinery, New York, NY, USA, 369–376. doi.org/10.1145/1143844.1143891.

[16] Suyoun, K., Takaaki, H., and Shinji, W., "*Joint ctc-attention based end- to-end speech recognition using multi-task learning",* ICASSP-2017, pages4835–4839, 03 2017. doi:10.1109/ICASSP.2017.7953075.

[17] Rohit, P., Kanishka, R., Tara, S., Bo,L., Leif, J., and Navdeep, J., "*A comparison of sequence-to-sequence models for speech recognition",* Interspeech, 2017, pages 939–943

[18] Zhou, S., Dong, L., Xu, S., & Xu, B.,"*A Comparison of Modeling Units in Sequence-to-Sequence Speech Recognition with the Transformer on Mandarin Chinese"*, in proceeding of International Conference on Neural Information Processing, 13-16 December, 2018 Siem Reap, Cambodia ArXiv, abs/1805.06239.

[19] Shiyu, Z., Linhao, D., Shuang, X., and Bo, X., "*Syllable-based sequence-to-sequence speech recognition with the transformer in mandarin Chinese",* Interspeech 2018, September 2-6, Hyderabad, India, pp. 791–795, 2018.

[20] Solomon Abate, Wolfgang M., and Bairu, T., "An Amharic speech corpus for large vocabulary continuous speech recognition", Interspeech-2005, 4-8 September 2005, Lisbon, Portugal, pp. 1601–1604, doi:10.21437/Interspeech.2005-467.